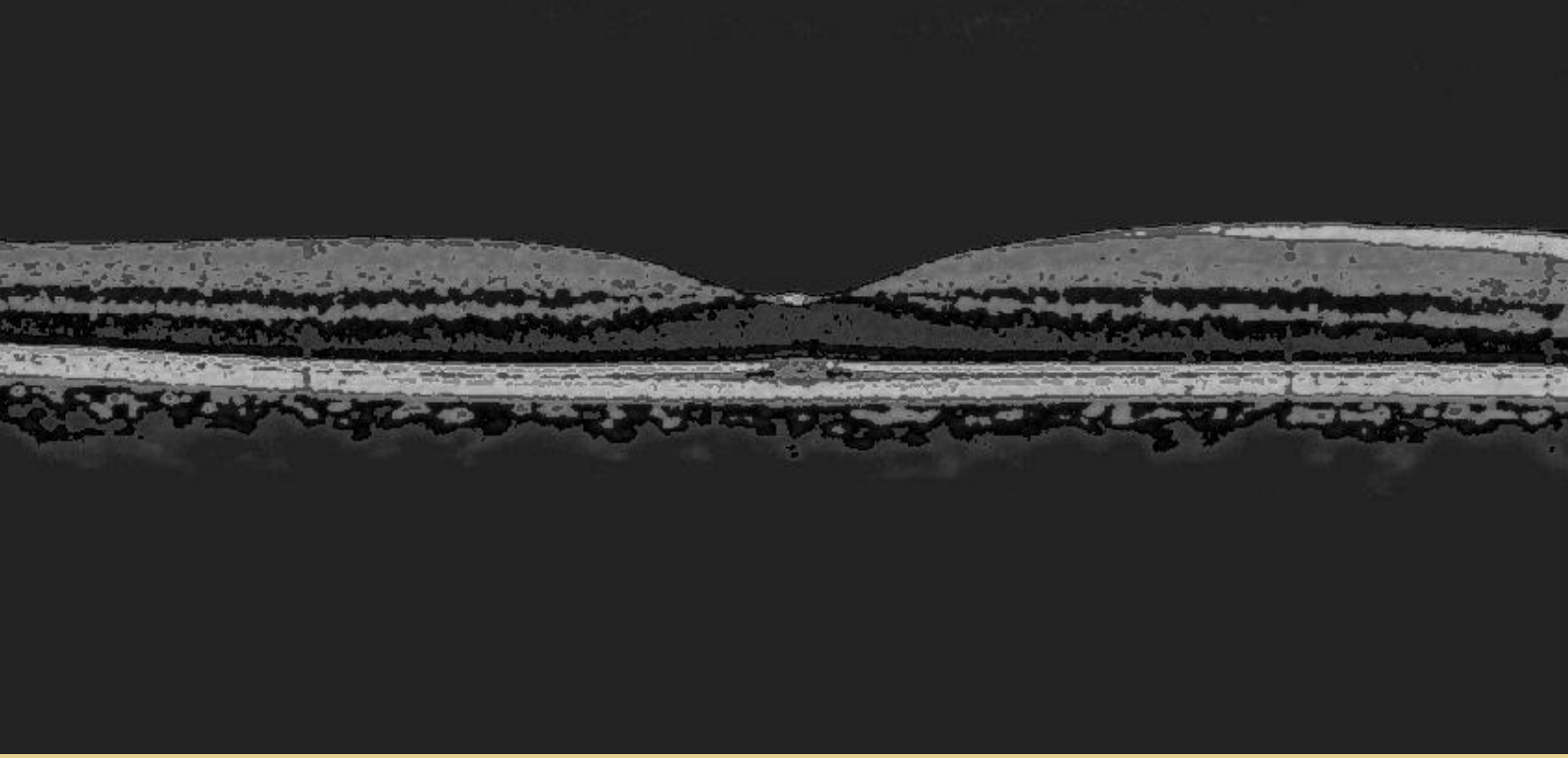

CATARINA ANDREIA DOMINGUES MATEUS

NOVOS BIOMARCADORES NO GLAUCOMA E NEUROPATIAS ÓPTICAS HEREDITÁRIAS: IMPLICAÇÕES PARA O DIAGNÓSTICO PRECOCE E MONITORIZAÇÃO DA EVOLUÇÃO CLÍNICA

PATHOPHYSIOLOGICAL MECHANISMS AND NOVEL BIOMARKERS IN ACQUIRED AND GENETIC DISEASES OF THE RETINAL GANGLION CELL

Tese de Doutoramento em Ciências da Saúde - ramo Tecnologias da Saúde, orientada por Professor Doutor Miguel de Sá e Sousa de Castelo-Branco e apresentada à Faculdade de Medicina da Universidade de Coimbra.

2014

· U C ·

UNIVERSIDADE DE COIMBRA

Novos Biomarcadores no Glaucoma e Neuropatias Ópticas Hereditárias: Implicações para o Diagnóstico Precoce e Monitorização da Evolução Clínica

Pathophysiological Mechanisms and Novel Biomarkers in Acquired and Genetic Diseases of the Retinal Ganglion Cell

Catarina Andreia Domingues Mateus

Novos Biomarcadores no Glaucoma e Neuropatias Ópticas Hereditárias: Implicações para o Diagnóstico Precoce e Monitorização da Evolução Clínica

Pathophysiological Mechanisms and Novel Biomarkers in Acquired and Genetic Diseases of the Retinal Ganglion Cell

2014

· U C ·

Universidade de Coimbra

Dissertação de Doutoramento apresentada à
Faculdade de Medicina da Universidade de Coimbra,
para prestação de provas de Doutoramento em Ciências da Saúde

A Faculdade de Medicina de Coimbra não aceita qualquer responsabilidade
em relação à doutrina e à forma desta dissertação.
(Reg. da Facudade de Medicina de Coimbra, 1931, artº 108, § único)

Este trabalho foi realizado no Laboratório de Neurociências da Visão, no Instituto Biomédico de Investigação da Luz e Imagem (IBILI) da Faculdade de Medicina da Universidade de Coimbra, sob a orientação do Prof. Doutor Miguel Castelo-Branco e ao abrigo de uma bolsa de doutoramento atribuída pela Fundação para a Ciência e a Tecnologia (SFRH/BD/64306/2009).

Aos meus filhos,

Dinis e Duarte

ACKNOWLEDGMENTS

Aos meus colegas e amigos que colaboraram nas diferentes etapas deste trabalho, não só pela transmissão de conhecimentos e disponibilidade manifestada, como também pelo espírito de entreajuda e companheirismo. A todos, o meu sincero obrigado.

Um agradecimento especial à Doutora Aldina Reis pelo seu contributo fundamental durante estes anos de investigação, ao Dr. Pedro Faria e ao Prof. Doutor Eduardo Silva pela ajuda na seleção dos pacientes e na avaliação clínica dos mesmos, à Engª Otília d'Almeida pelo envolvimento direto no processamento dos dados de ressonância magnética, à Dra. Bárbara Oliveiros pela ajuda na análise estatística dos dados, e por fim, aos Engos João Meneses, Eduardo Domingues e Manuel Vítor pela ajuda no desenvolvimento dos novos testes psicofísicos de discriminação do movimento e de sensibilidade ao contraste cromático e acromático.

Ao Professor Doutor Miguel Castelo-Branco deixo um agradecimento sincero, pois a conclusão deste trabalho não teria sido possível sem a sua orientação, espírito crítico, contributo científico e disponibilidade permanente.

Por fim, uma palavra de agradecimento à minha família pela constante motivação, apoio incondicional e ajuda inegável ao longo destes anos.

PUBLICATION LIST

1. Silva MF, Maia-Lopes S, Mateus C, Guerreiro M, Sampaio J, Faria P, Castelo-Branco M. Retinal and cortical patterns of spatial anisotropy in contrast sensitivity tasks. Vision Res. **2008**, 48(1): 127-135.

2. Maia-Lopes S, Silva ED, Reis A, Silva MF, Mateus C, Castelo-Branco M. Retinal function in Best Macular Dystrophy: relationship between electrophysiological, psychophysical and structural measures of damage. Invest Ophthalmol Vis Sci. **2008**, 49(12): 5553-5560.

3. Silva MF, Mateus C, Reis A, Nunes S, Fonseca P, Castelo-Branco M. Asymmetry of visual sensory mechanisms: electrophysiological, structural and psychophysical evidences. J Vis. **2010**, 10(6): 26, 1-11.

4. Reis A, Mateus C, Macário MC, de Abreu JR, Castelo-Branco M. Independent patterns of damage to retinocortical pathways in multiple sclerosis without a previous episode of optic neuritis. J Neurol. **2011**, 258: 1695-1704.

5. Reis A, Mateus C, Viegas T, Florijn R, Bergen A, Silva E, Castelo-Branco M. Physiological evidence for impairment in autosomal dominant optic atrophy at the pre ganglion level. Graefes Arch Clin Exp Ophthalmol. **2013**, 251: 221-234.

6. Mateus C, Lemos R, Silva MF, Reis A, Fonseca P, Oliveiros B, Castelo-Branco M. Aging of low and high level vision: from chromatic and achromatic contrast sensitivity to local and 3D object motion perception. PLoS One. **2013**, 8: e55348.

7. Laguna A, Barallobre MJ, Marchena MA, Mateus C, Ramírez E, Martínez-Cue C, Delabar JM, Castelo-Branco M, de la Villa P, Arbonés ML. Triplication of DYRK1A causes structural and functional retina alterations in Down syndrome. Hum Mol Genet. **2013**, 22: 2775-2784.

8. d'Almeida OC, Mateus C, Reis A, Grazina MM, Castelo-Branco M. Long term cortical plasticity in visual retinotopic areas in humans with silent retinal ganglion cell loss. Neuroimage. **2013**, 81: 222-230.

9. Reis A, Mateus C, Melo P, Figueira J, Cunha-Vaz J, Castelo-Branco M. Neuroretinal dysfunction with intact blood-retinal barrier and absent vasculopathy in Diabetes type 1. Diabetes. **2014**, 63: 1-12.

10. Mateus C, d'Almeida OC, Reis A, Silva E, Castelo-Branco M. Genetically induced diffuse impairment of retinal ganglion cells is linked to extrastriate cortical plasticity. Brain Struct Funct *[Submitted]*

11. Mateus C, Raimundo M, Oliveiros B, Faria P, Reis A, Castelo-Branco M. A new approach to assess early progressive loss across multiple visual channels in the natural history of glaucoma. JAMA Ophthalmol *[Submitted]*

12. Silva MF, d'Almeida OC, Oliveiros B, Mateus C, Castelo-Branco M. Development and aging of visual hemifield asymmetries in contrast sensitivity. J Vis *[Submitted]*

LIST OF CONTENTS

LIST OF ABBREVIATIONS

2AFC Two-alternative forced choice

ATP Adenosine triphosphate

AUC Area under the curve

C Control

CCT Cambridge color test

C/D Cup-to-disc

CI Confidence interval

cpd Cycles per degree

CRT Cathode-ray-tube

CS Contrast sensitivity

CT Cortical thickness

DS Down syndrome

EPI Echo planar imaging

ERG Electroretinogram

FA Flip angle

FDT Frequency doubling technology

FI Fixed interval

FoV Field of view

G Glaucoma

GCL Ganglion cell layer

GS Glaucoma suspect

HT Ocular hypertension

IN Inferior nasal

INL Inner nuclear layer

IOP Intraocular pressure

IPL Inner plexiform layer

IRL Inner retinal layer

ISCEV International society for clinical electrophysiology of vision

ISF Intermediate spatial frequency

IT Inferior temporal

K Koniocellular

L-cone Long wavelength sensitive or red cone

LE Left eye

LGN Lateral geniculate nucleus

LHON Leber hereditary optic neuropathy

LSD Least significant difference

LV Loss variance

M Magnocellular

M-cell Retinal parasol ganglion cell projecting to the magnocellular pathway

M-cone Medium wavelength sensitive or green cone

MD Mean deviation

MDf Mean defect

Mo Motion

MOBS Modified binary search

MPRAGE Magnetization prepared rapid acquisition gradient echo

MR Magnetic resonance

MRI Magnetic resonance imaging

MS Mean sensitivity

MT Middle temporal area

mtDNA mitochondrial DNA

n.s. Not significant

OCT Optical coherence tomography

ON Optic neuropathies

ONL Outer nuclear layer

OPL Outer plexiform layer

ORL Outer retinal layer

P Parvocellular

P-cell Retinal midget ganglion cell projecting to the parvocellular pathway

POAG Primary open-angle glaucoma

PSD Pattern standard deviation

PERG Pattern electroretinogram

RDK Random dots kinetograms

RE Right eye

RGC Retinal ganglion cells

RNFL Retinal nerve fiber layer

ROC Receiver operating characteristic

ROIs Regions-of-interest

RPE Retinal pigment epithelium

RT Retinal thickness

$\mathbf{R_a^2}$ Adjusted coefficient of determination

SAP Standard Automated perimetry

S-cone Short wavelength sensitive or blue cone

SD Standard deviation

SD-OCT Spectral domain optical coherence tomography

SEM Standard error of the mean

SFM Structure from motion

SN Superior nasal

ST Superior temporal

SWAP Short wavelength automated perimetry

TE Echo time

TOP Tendency oriented perimetry

TR Repetition time

UR Until response

VA Visual acuity

VMB Voxel-based morphometry

V1 Primary visual cortex

V2, V3, V4 Cortical visual areas

$\boldsymbol{\eta_p^2}$ Partial eta-squared

RESUMO

As células ganglionares da retina (CG) têm um papel fundamental no processamento da informação até ao córtex visual, conforme evidenciam as suas características específicas morfológicas e funcionais. A lesão das CG constitui a base da patogénese de algumas doenças da retina e do nervo óptico. Assim, esta tese centra-se na identificação de novos biomarcadores de lesão em doenças adquiridas e genéticas das CG, nomeadamente na Neuropatia Óptica Glaucomatosa e na Neuropatia Óptica Hereditária de Leber (NOHL).

Deste modo, aplicámos um conjunto de métodos funcionais e estruturais, inovadores e convencionais, com o objectivo de comparar mecanismos patofisiológicos de lesão em dois grupos diferentes de pacientes, correspondendo a dois modelos de doença das CG: 1) modelo de neuropatia óptica hereditária, 15 portadores assintomáticos de NOHL com mutação mtDNA 11778G>A, pertencentes a duas gerações do mesmo *pedigree*; 2) modelo de neuropatia óptica adquirida, 52 participantes provindos da consulta de Glaucoma, divididos nos seguintes grupos: hipertensão ocular (n=18 olhos), suspeitos de glaucoma (n=15 olhos) e glaucoma primário de ângulo aberto (n=19 olhos). Os dados obtidos foram comparados com dois grupos de controlos ajustados à idade e ao género.

Relativamente aos portadores assintomáticos de NOHL, fenotipámos a lesão subclínica em termos psicofísicos, neurofisiológicos e estruturais, através da sensibilidade ao contraste cromático (Cambridge Color Test, CCT), do electroretinograma *pattern* (ERG *pattern*, para medição da função das CG) e da tomografia de coerência óptica (OCT, para registo das espessuras da zona macular, da camada de fibras nervosas da retina e das camadas interna/externa da retina), respectivamente. Com o intuito de estabelecer uma relação entre as características do dano das CG e a reorganização cortical das áreas visuais corticais mapeadas retinotopicamente, foi usada a ressonância magnética estrutural em regiões de interesse mapeadas através da ressonância magnética funcional retinotópica.

Observou-se que a espessura da camada de fibras nervosas macular é predictiva de um mecanismo compensatório de plasticidade cortical nas áreas visuais corticais extraestriadas. Este foi também o parâmetro mais discriminativo entre portadores de NOHL e controlos, evidenciado pela análise da curva *ROC*. Assim, concluímos que a

patologia dos axónios da CG pode desencadear plasticidade cortical compensatória nas áreas visuais extraestriadas V2/V3.

No que respeita aos indivíduos com Glaucoma, utilizámos métodos quantitativos psicofísicos, como a perimetria de dupla frequência (FDT) e CCT, para caracterizar o desempenhos das vias magno, parvo e coniocelulares. A função das CG foi registada pelo ERG *pattern* e a espessura da camada de fibras nervosas foi obtida através do OCT. Foram desenvolvidos três testes psicofísicos utilizando uma estratégia de resposta forçada com duas alternativas (variáveis independentes: movimento, sensibilidade ao contraste acromático e sensibilidade ao contraste cromático das três populações de cones L, M e S) tendo sido aplicados num subgrupo destes pacientes (16 com hipertensão ocular, 15 suspeitos de glaucoma e 12 com glaucoma primário de ângulo aberto).

Encontrámos disfunção relativa das vias retinocorticais magno, parvo e coniocelulares, desde o estadio inicial da doença. A sensibilidade ao contraste acromático encontrava-se alterada em pacientes com hipertensão ocular e as sensibilidades cromáticas estavam significativamente aumentadas nos eixos protan, deutan e tritan. A cerca de 80% de especificidade, o FDT foi o teste que apresentou a melhor sensibilidade para detectar o dano funcional precoce. Não obstante, a sensibilidade dos testes comerciais foi inferior quando comparada com os resultados dos nossos novos métodos psicofísicos, sugerindo que um teste com um menor grau de redundância apresenta uma maior capacidade para detectar precocemente danos glaucomatosos. Por fim, todos estes testes podem ser usados combinadamente como potenciais biomarcadores de progressão de doença, dado que os seus parâmetros se encontram moderadamente correlacionados com a história natural do glaucoma.

SUMMARY

Retinal ganglion cells (RGC) are key players in the processing of visual information to the visual cortex, as further illustrated by their specific morphological and functional features. Degeneration of RGC is currently thought to play a key role in the pathogenesis of some retinal and optic nerve pathologies. So, the major focus of this thesis concerns the identification of novel biomarkers of impairment in acquired and genetic diseases of the RGC, namely glaucomatous optic neuropathy and Leber hereditary optic neuropathy (LHON).

For this purpose we applied a range of novel and conventional functional and structural methods in order to compare pathophysiological mechanisms of damage in two different groups of patients, corresponding to two different models of the RGC impairment: 1) inherited optic neuropathy model, 15 asymptomatic LHON carriers (mtDNA 11778G>A point mutation) from two generations of the same pedigree; 2) acquired optic neuropathy model, 52 participants recruited from the glaucoma consultation, which were divided into different groups: ocular hypertension (HT, n=18 eyes), glaucoma suspects (n=15 eyes) and primary open-angle glaucoma (n=19 eyes). Obtained data were compared with two distinct gender and age-matched groups of controls.

Concerning asymptomatic LHON carriers, we phenotyped pre-clinical silent degeneration from the psychophysical, neurophysiological and structural points of view, using chromatic contrast sensitivity test (Cambridge Color Test, CCT), pattern electroretinogram (PERG; to measure RGC function) and optical coherence tomography (OCT; assessing macular, retinal nerve fiber layer/RNFL and inner/outer retinal layer thicknesses), respectively. In order to establish a link between features of RGC impairment and cortical reorganization of retinotopically mapped visual cortical areas, we also used structural magnetic resonance in regions of interest mapped using retinotopic functional magnetic resonance imaging (fMRI).

We found that compensatory cortical plasticity occurring in extrastriate visual cortical areas is predicted by macular RNFL thickness. This was also the most discriminative measure between LHON carriers and controls, as revealed by Receiver Operating Characteristic (ROC) curve analysis. We conclude that pathology in RGC axons may trigger cortical compensatory plasticity in extrastriate visual areas V2/V3.

Concerning glaucoma patients, quantitative psychophysical methods, as Frequency Doubling Technology (FDT) and CCT, were used to assess magno, parvo and koniocellular pathways. RGC function was assessed by PERG and RNFL thickness was obtained using OCT. Three novel two-alternative-forced-choice (2AFC) psychophysical discrimination tests (independent variables: motion, achromatic and chromatic L, M and S cone contrast sensitivities) were developed by our group, implemented in relatively standard hardware and then applied to a subgroup of glaucoma patients (16 ocular hypertension, 15 glaucoma suspects and 12 primary open-angle glaucoma).

We found a relative damage of magno, parvo and koniocellular retinocortical pathways since the initial stage of the disease. Mean achromatic contrast sensitivity (FDT) was impaired in patients with HT and chromatic thresholds were significantly increased for protan, deutan and tritan axes. At approximately 80% specificity, the FDT showed the highest sensitivity to detect early functional damage. Interestingly, the sensitivity of the currently available tests used is this study is lower comparing with our novel psychophysical discrimination tools, suggesting that a smaller degree of test redundancy leads to a great ability to detect early glaucomatous damage. Finally, all these tests can be used in combination as potential markers of disease progression, since their measures correlate moderately with the natural course of glaucoma.

AIMS

This thesis is focused on the identification of novel biomarkers of pathophysiological impairment in acquired and genetic diseases of the retinal ganglion cells (RGC), namely glaucomatous optic neuropathy and Leber hereditary optic neuropathy (LHON).

According to this global aim, we developed three novel psychophysical discrimination tests in order to functionally isolate specific and sparse RGC populations, without the redundancy afforded by the neighboring cells and possibly allowing an early diagnosis. Thus, we used two separated small and peripheral moving dots to probe motion sensitivity, achromatic and chromatic L, M and S cone contrast sensitivities. These tests were applied across several disease stages with the goal of obtaining new insights about the natural history of glaucoma.

This strategy arose from the evidence that the conventional perimetry used in the clinical practice seems to be not sensitive enough to detect early RGC dysfunction. We argue that this is due to the fact that the stimulation approach (white targets) is simultaneously detected by all neurophysiological sub-systems in the retina.

We also aimed to evaluate the potential ability of these novel tests to probe disease progression.

In glaucomatous patients, and for comparison purposes, we also applied a broad range of psychophysical and electrophysiological tests. This further allowed to study independent visual information processing within magno, parvo and koniocellular pathways. We compared the diagnostic accuracy of the three novel psychophysical tools with some currently available tests described as sensitive to detect glaucoma at an early stage.

Another goal of this work was to phenotype pre-clinical retinal degeneration of LHON mutation carriers from the psychophysical, electrophysiological and structural points of view. This allowed to compare phenotypic measures in another model of RGC degeneration. Using functional magnetic resonance imaging (fMRI), we further aimed to establish a link between features of RGC impairment and cortical reorganization in genotyped LHON carriers, as assessed by cortical thickness measures in retinotopically mapped visual cortical areas.

The first part of this thesis starts with a theoretical background in Chapter 1, which covers relevant basic topics that are important within the goals of this thesis, such as parallel information processing in vision, namely within the retina, the organization of subcortical (magno, parvo and koniocellular) and cortical (dorsal and ventral) visual pathways, and also aging of the visual pathway.

Chapter 2 presents a specific introduction to the clinical models of RGC dysfunction addressed in this thesis. The first section refers to LHON and the second one refers to glaucomatous optic neuropathy.

Chapter 3 describes the psychophysical, electrophysiological and structural methods used in the experimental work.

The results obtained from the analysis of data are presented in Chapter 4, 5 and 6, wherein the first data corresponds to the LHON model and the data of the last two chapters corresponds to the glaucoma model.

Chapter 7 presents the discussion and final conclusions of the thesis.

PART I

THEORETICAL BACKGROUND

CHAPTER 1

PARALLEL PROCESSING IN VISION

1.1. BIOLOGY OF THE RETINA

The first comprehensive anatomic description of the neural cell types that constitute the retina was revealed in the 19th century by Ramon y Cajal (Ramon y Cajal, 1892) and still remains largely correct. More recent applications of intracellular recording and staining techniques provided a detailed account of the neural architecture of the retina (Werblin and Dowling, 1969), which is organized in ten distinct layers of cells and their synapses, namely:

1) Inner limiting membrane (vitreoretinal interface; basement membrane composed by Müller cells);
2) Nerve fiber layer (ganglion cell axons);
3) Ganglion cell layer (nuclei of ganglion cells);
4) Inner plexiform layer (synapses between bipolar cell axons and dendrites of ganglion cells and amacrine cells);
5) Inner nuclear layer (nuclei of bipolar cells);
6) Outer plexiform layer (synapses between photoreceptors axons and dendrites of bipolar cells);
7) Outer nuclear layer (nuclei of rods and cones);
8) Outer limiting membrane (layer that separates the inner segment of the photoreceptors from their cell nucleus);
9) Photoreceptors layer (rods and cones);
10) Retinal pigment epithelium (single layer of cuboidal cells).

These can be simplified into 3 main processing stages. In fact, the neural architecture comprises a three-neuron excitatory pathway composed of 1) photoreceptors that transduce the light stimulus and 2) bipolar interneurons that relay the photoreceptor signals to 3) ganglion cells, the output neurons of the retina. Added to

this pathway are two sets of inhibitory interneurons: the horizontal cells that modify transfer at the photoreceptor-bipolar synapse and the amacrine cells that modulate information processing at the bipolar-ganglion cell synapse (Dacey, 2000) (Figure 1.1).

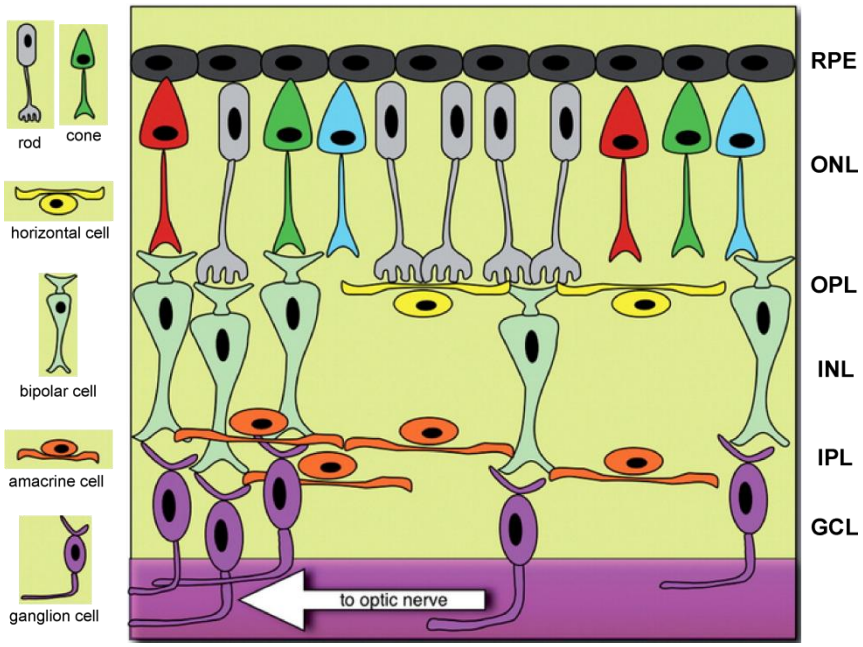

Figure 1.1. Vertical cross-section of the retina. Note the principal cell types involved in visual information processing. RPE – retinal pigment epithelium; ONL – outer nuclear layer; OPL – outer plexiform layer; INL – inner nuclear layer; IPL – inner plexiform layer; GCL – ganglion cell layer (Adapted from Archibald et al., 2009).

The human retina contains, on average, 128 million photoreceptors (Sekuler and Blake, 1994): 120 million of them are rods and the other 8 million are three types of cones, which are classified based on the peak wavelength within the visible spectrum to which their photopigment is highly sensitive [L-cones or sensitive to long-wavelengths (peak sensitivity at ~565 nm); M-cones or sensitive to middle-wavelengths (~535 nm); and S-cones or sensitive to short-wavelengths (~440 nm)] (Gegenfurtner and Kiper, 2003). The cones respond to bright-light (photopic vision) and mediate high-resolution color vision. On the other hand, at low levels of light (scotopic vision), only the rods are activated. Thus, rods are important to monochromatic, low-resolution vision under very low levels of illumination. Under mesopic levels of light, both rods and cones are activated (Archibald et al., 2009).

The spatial arrangement of the photoreceptors is called 'photoreceptor mosaic'. These neurons do not have a homogenous distribution across the retina (Curcio et al., 1990; Ahnelt, 1998). In the center of the fovea (foveal pit), there are only cones (Figure 1.2). In fact, this is the region of the retina with the highest density of cones. These cones are thinner and longer than cones of the surrounding retina, possibly because (in evolutionary terms) they need to absorb the incident photons of light more efficiently, contributing for a higher performance in visual acuity. The number of cones per area falls rapidly outside the fovea to a fairly even density into the peripheral retina (Curcio et al., 1987). Concerning rods, the first ones emerge at about 0.13 mm from the center of the fovea and their number increases rapidly, reaching a peak in a ring around the fovea at about 4.5 mm (18 degrees) from the foveal pit. In more peripheral regions the number of rods decreases, being always higher than the number of cones. Interestingly, the optic nerve is composed of about one million axons and since there are no photoreceptors, visual stimulation cannot occur ("blind spot").

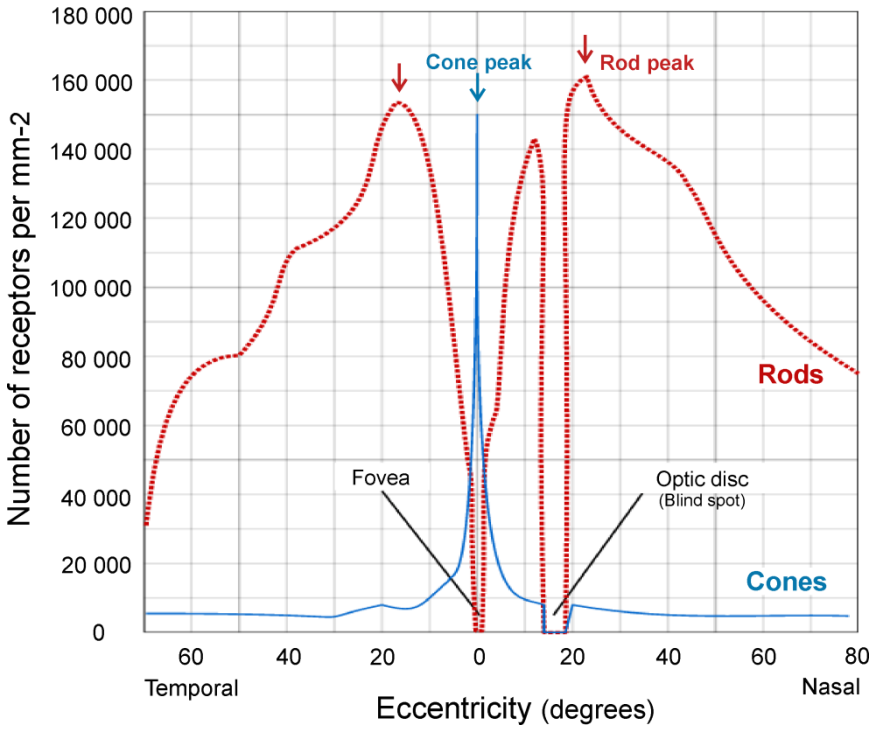

Figure 1.2. The photoreceptors (rods and cones) distribution within the human retina (Adapted from Osterberg, 1935; Source: http://webvision.med.utah.edu/).

In summary, the light photons pass through the whole retina and are detected by photoreceptors. In the photoreceptors layer visual processing sets off with the transduction of light into bioelectrical signals. Then, photoreceptors transmit information to bipolar cells that in turn connect to ganglion cells. Finally, ganglion cells project their axons to form the optic nerve and convey visual information to the brain.

1.1.1 THE RETINAL GANGLION CELL

Ganglion cell axons travel from the retina to the lateral geniculate nucleus (LGN) and then to different parts of the visual cortex. The primate retina contains 20 or more types of morphologically and functionally distinct ganglion cells (Kolb et al., 1992; Shabana et al., 2003). Nevertheless, *in vitro* preparations of primate retina provided information about three major types of ganglion cells that project to the LGN (Dacey, 1994; Kaplan, 2004): the parasol (Pα), midget (Pβ) and small bistratified cells.

The parasol cells (about 10% of the ganglion cells) have larger dendritic fields and the corresponding axons are thicker (with more myelin) and have faster conduction time than the midget cells (about 80% of the ganglion cells) at any given eccentricity (Shabana et al., 2003; Yoonessi and Yoonessi, 2011) (Figure 1.3). The small bistratified ganglion cells tend to have larger dendritic field than the midget cells and smaller than the parasol cells (Yamada et al., 1996). For all types of cells, the RGC size correlates with the eccentricity (Perry et al., 1984; Shabana et al., 2003).

The distribution of ganglion cells is very non-linear. In the perifoveal macula these cells are concentrated, becoming relatively sparse in the periphery. On the other hand, ganglion cells near the fovea tend to be smaller with smaller dendritic fields and axons, whereas some larger ganglion cells are mainly found peripherally (Carelli et al., 2004).

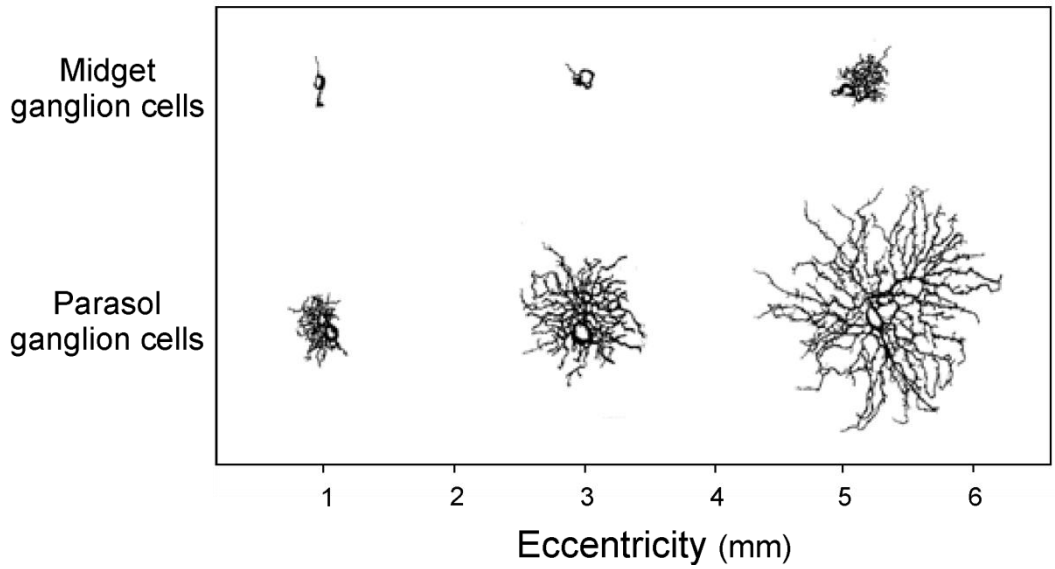

Figure 1.3. The major ganglion cell types of a primate retina. At approximately the same eccentricity within the retina, the dendritic tree of the midget ganglion cell is smaller and denser than the parasol cell. Note that for both types of cells, the absolute size of the dendritic field increases with eccentricity (Adapted from Watanabe and Rodieck, 1989; Source: https://www.stanford.edu/group/vista/cgi-bin/FOV/).

Perry et al. (1984), using retrograde horseradish peroxidase labeling, found that the majority of Pα cells in the retina project to the magnocellular layers of the LGN (first two layers), whereas the majority of Pβ cells in the retina project to the parvocellular layers of the LGN (layers 3 to 6). Thus, it has become a common practice to refer to the RGC by their connections to the LGN, namely, parasol as magnocellular (M) cells and midget as parvocellular (P) cells (Shabana et al., 2003). In addition, there is some evidence that the small bistratified cells, project to interlaminar layers - koniocellular (K) layers, in parallel with the parasol and midget cells in the LGN (Kaplan, 2004; Yoonessi and Yoonessi, 2011).

There are considerable differences in the physiological properties of M and P cells. The M cells have higher contrast sensitivity (CS) than P cells. Furthermore, the conduction time of the M pathway is faster than the P pathway (Yoonessi and Yoonessi, 2011) and the time of response in the M cell tends to be transient, whereas the P cells respond in a sustained mode (Hicks et al., 1983).

1.2. MAGNO, PARVO AND KONIOCELLULAR SUBCORTICAL VISUAL PATHWAYS

Anatomical and physiological measurements suggest that magno, parvo and koniocellular pathways carry different types of information to the brain.

The M cells collect information from all types of cones, thus process no specific information about color and therefore detect "luminance". These cells can also signal motion and are sensitive to high temporal/ low spatial frequency stimuli (Yoonessi and Yoonessi, 2011). On the other hand, the P cells are sensitive to low temporal and high spatial frequencies (Derrington and Lennie, 1984) and also mediate visual acuity, pattern and texture discrimination, besides chromatic information (P cells are sensitive to red-green opponency) (Schiller et al., 1991; Lynch et al., 1992; Kaplan, 2004). However, blue-yellow opponency is mediated by the small-bistratified ganglion cells (Dacey and Lee, 1994; Dacey, 2000).

Some behavioral studies of monkeys developed by Schiller et al. (1990) showed that lesions of the P layers of LGN result in marked decreases in spatial CS, fine stereopsis, and pattern, color, texture and shape discrimination. These functions were unaffected by lesions of the M layers. In comparison, lesions of the M layers caused specific decreases in flicker (especially at high temporal frequencies) and motion sensitivity.

1.3. DORSAL AND VENTRAL CORTICAL VISUAL PATHWAYS

The axons from the M layers of the LGN project to the lamina 4C-α of the primary (striate) visual cortex (V1), while the axons from P layers project to layer 4C-β (Perry et al., 1984). Thus, the M and P visual pathways from the retina to the LGN remain clearly separated up to the level of V1 (Shabana et al., 2003). At the cortical level, two pathways dominate the complex network of connections in the visual cortex: the dorsal and ventral visual pathways. The dorsal pathway, which receives a major contribution from the M pathway, proceeds from V1 to the thick stripe regions of V2, mainly to the middle temporal (MT) area (specialized in motion processing) and to

areas in the posterior parietal cortex. On the other hand, the ventral pathway, which receives a major contribution from the P pathway, proceeds from V1 to the thin and interstripe regions of V2, mainly to V4 (specialized in color processing) and to areas of the inferotemporal cortex (Merigan and Maunsell, 1993; Shabana et al., 2003) (Figure 1.4).

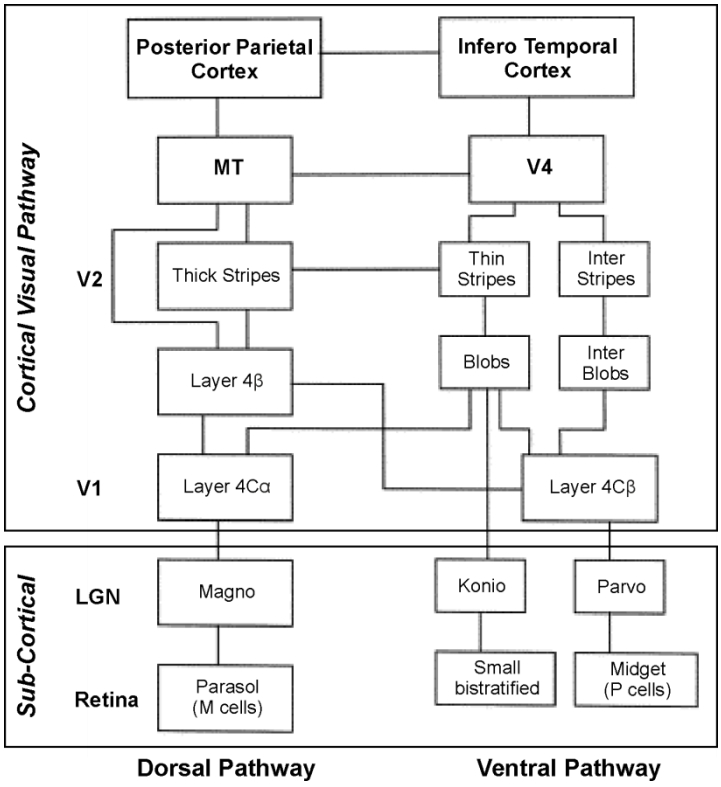

Figure 1.4. Schematic diagram of visual pathways. The main subcortical visual pathways (Magno, Parvo and Koniocellular) proceed from the respective RGC and show a clean separation up to the LGN of the thalamus. From the LGN, signals are projected to the primary visual cortex (V1). At the cortical level, the dorsal visual pathway ends in the parietal cortex, whereas the ventral pathway ends in the temporal cortex. Note that between dorsal and ventral pathways, there are, at least, three hundred known connections (Adapted from Shabana et al., 2003).

In summary, M cell information is processed through the "where" (dorsal) pathway (important for motion perception and spatial location) to the posterior parietal cortex, while information from P cells is mostly processed through the "what" (ventral) pathway (important for object recognition, and their neurons respond to properties, such as shape, colors and patterns) to the inferotemporal cortex (Goodale and Milner, 1992;

Ungerleider and Haxby, 1994; Callaway, 2005; Yoonessi and Yoonessi, 2011). The dorsal and ventral pathways are grossly parallel, however there are a complex pattern of connections between them (Merigan and Maunsell, 1993).

1.4. AGING OF THE VISUAL PATHWAY

Gradual decline of visual function is a feature of normal aging. This partly results from the combination of optical factors, retinal neural factors such as photoreceptor and ganglion cell degeneration and cortical factors (Lam, 2005; Owsley, 2011). In particular at photopic light levels, spatial CS deficits may also be affected by optical characteristics (Owsley, 2011). Aging of the lens is particularly relevant in which concerns color vision: lens yellowing might indeed affect the interpretation of changes in blue-yellow discrimination tests (Castelo-Branco et al., 2004; Silva et al., 2005).

Many visual functions are expected to be impaired in people in the last aging decades, which is a rising problem due to changes in demographic structure of western populations. Since, the process in healthy and pathological aging is distinct (Graewe et al., 2013), it is important perform a hierarchical analysis of low- and high-level visual function within multiple visual channels in healthy aging (from early adulthood up to old age cohorts), to better understand visual function in pathological aging.

The influence of normal aging in early, intermediate and high-level visual processing is still poorly understood. By other words, a hierarchical approach of visual function analysis has not been used before to access aging across the life span. Here we attempted to address this issue using a hierarchical approach from the point of view of visual processing and stimulus construction. In this way we used chromatic and achromatic CS tasks with simple gratings and patches, motion discrimination tasks with simple random dots kinetograms (RDK), and high-level object integration tasks using the same type of dots. The rationale of this study tackles the principles of the organization of the visual system: in the early part of the visual system, information is transmitted from the retina to the visual cortex through three parallel and physiologically distinct pathways - Parvo, Magno and Koniocellular.

We have addressed this important issue in a large cohort of 653 subjects divided into five distinct age groups, [20;30[, [30;40[, [40;50[, [50;60[and [60;[. We applied a broad range of psychophysical tests, testing distinct levels of the visual hierarchy, from local processing to global integration, using simple gratings [spatial CS using high temporal/ low spatial frequency (FDT) or intermediate spatial frequency (ISF) static gratings], color CS using Landolt patches (CCT), moving dot stimuli (Local Speed Discrimination) and dot patterns defining 3D objects (3D Structure from Motion, 3D SFM). 3D tasks (requiring the detection of complex SFM targets) involve high-level dorsal stream function and dorso-ventral integration for object recognition (Lemos et al., 2012; Graewe et al., 2013). On the other hand, local speed signals are mainly processed in early human visual cortex, in particular V1 and V2 (Castelo-Branco et al., 2002). Finally, chromatic and achromatic CS tests require the integrity of low-level retinal or retinocortical visual pathways (Castelo-Branco et al., 2004; Maia-Lopes et al., 2008; Reis et al., 2011).

Aging data were fitted with linear or quadratic regression models, using the adjusted coefficient of determination (R^2_a) to quantify the effect of aging. A significant effect of age was found on all visual channels tested, except for the chromatic channel. In our study, red-green and blue-yellow CS testing showed only significant age effects in the latter. This seems to be consistent with the relatively stable anatomical cone distribution during aging (Curcio et al., 1993) and also with evidence that optical factors (yellowing of the crystalline lens) contribute for the gradual decline of color vision function with aging, only for stimuli modulated along the tritan axis (Pokorny et al., 1987).

The high temporal/ low spatial frequency CS channel showed a mean sensitivity loss of 0.75dB per decade (R^2_a=0.17, p<0.001) (see Figure 1.5 for representative examples of age-related CS decline obtained with FDT perimetry for each age group), while the lower intermediate spatial frequency channel showed a more pronounced decrease, around 2.35dB per decade (R^2_a=0.55, p<0.001) (see Figure 1.6 for representative examples obtained with ISF perimetry). Concerning low-level motion perception, speed discrimination decreased 2.71º/s (R^2_a=0.18, p<0.001) and 3.15º/s per decade (R^2_a=0.13, p<0.001) only for short presentations for horizontal and oblique meridians, respectively.

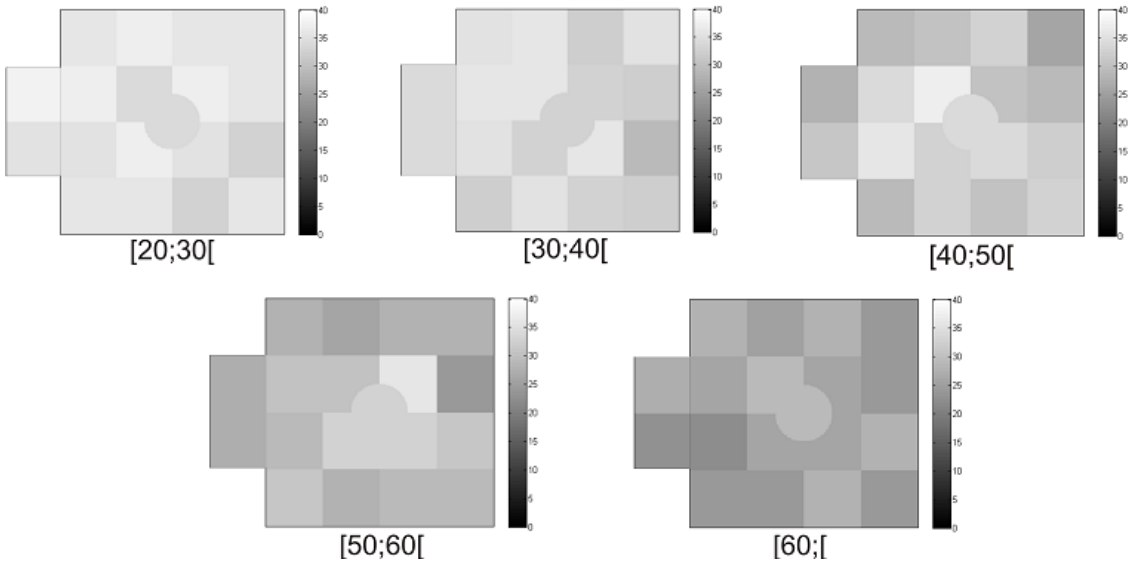

Figure 1.5. Illustration of gradual decline in achromatic CS over age groups observed with FDT perimetry using representative cases for each age group. Greyscale bar depicts contrast sensitivity in decibels. Darker regions correspond to worse CS.

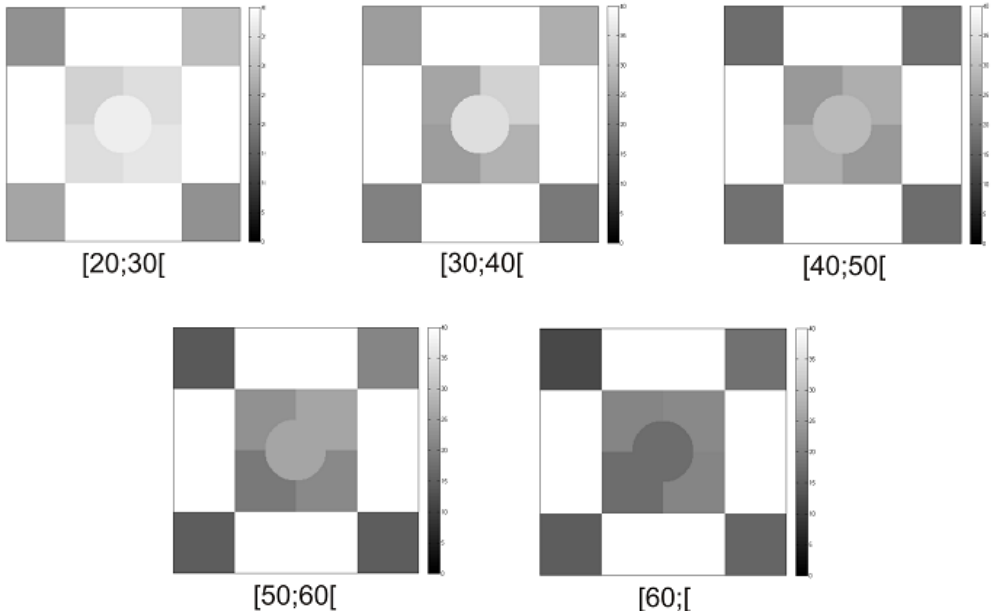

Figure 1.6. Illustration of progressive sensitivity loss in achromatic CS over age groups assessed by ISF perimetry, using representative cases for each age group. Greyscale bar depicts contrast sensitivity in decibels. Darker regions correspond to worse CS.

The 3D SFM task showed the strongest (quadratic) decrease of motion coherence perception with age, especially when the task was temporally constrained (R^2_a=0.54, p<0.001) (Figure 1.7).

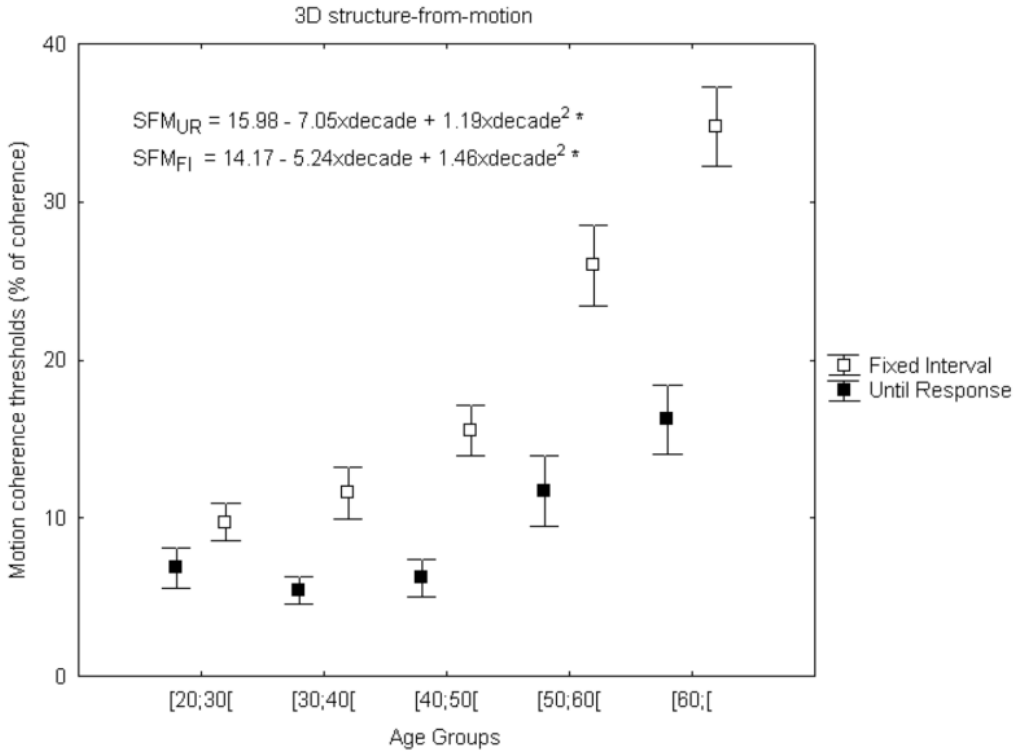

Figure 1.7. Visual dorsal/ventral streams performance during normal aging. High-level functions showed a fast deterioration with an accelerating pattern. Error bars depict standard error of the mean (SEM). The dependent measure is % of coherence (percentage of signal dots that are necessary for the subject to report the presence of a sphere) (*p<0.001). UR, until response; FI, Fixed Presentation Interval.

In summary, the mainly affected level of processing that was tested was high-level visual dorsal-ventral integration using the 3D SFM task. The stimulus used in SFM induces the perception of a 3D rotating sphere, in other words, one perceives a form or structure based on motion information, so an interaction between motion processing areas and brain areas involved in form processing is required (van der Boomen et al., 2012).

These findings show that visual channels are influenced by aging into different extents. The hierarchical age-related decline of visual functions is further substantiated by the fact that high-level mechanisms showed a quadratic profile of loss, unlike low-level mechanisms which in general showed a linear pattern of decay. Only the low-level achromatic intermediate frequency CS channel showed comparatively high loss, but with a still linear pattern.

CHAPTER 2

CLINICAL MODELS OF GANGLION CELL DYSFUNCTION

2.1 OPTIC NEUROPATHIES - OVERVIEW

Optic neuropathies (ON) comprise a group of disorders that share the hallmark of optic nerve dysfunction. In fact, ganglion cell axonal damage is clinically manifested by pathological changes in optic nerve appearance associated with visual acuity loss, visual field defects, decreased brightness sensation and color vision impairment (Newman, 1996).

How RGC degeneration (with associated visual loss) occurs is important to understand the etiology of the optic neuropathy. In other words, rapid pathophysiological processes are characteristic of optic neuritis, ischemic optic neuropathy, inflammatory (non-demyelinating) and traumatic optic neuropathy. On the other hand, a gradual process is typical of toxic/nutritional optic neuropathy, compressive and hereditary optic neuropathies (Behbehani, 2007). Glaucomatous optic neuropathy (open-angle glaucoma) is distinguished from other optic neuropathies by slow progressive degeneration of RGC and their axons over months to years (Weinreb and Khaw, 2004; Quigley, 2011).

In the inherited forms, the classification of the hereditary ON is based on the study of typical clinical features (eventually symmetric and bilateral visual loss with concomitant central/cecocentral scotomas due to papillomacular nerve fiber bundle damage) and classic patterns of familial transmission. However, genetic analysis is important, allowing to diagnose some of these neuropathies even in the absence of family history (family members may be subclinically affected) or in the presence of unusual clinical presentations (Votruba et al., 2003; Newman and Biousse, 2004; Newman, 2005).

Therefore, this chapter will address one of the most frequent mitochondrial hereditary optic neuropathies (Carelli et al., 2009; Yu-Wai-Man et al., 2009), namely LHON and also address the most commonly acquired optic neuropathy found in clinical

practice, glaucomatous optic neuropathy (O'Neil et al., 2011). These two entities can exhibit similar topographical changes at the optic nerve head, particularly in late-stage disease, making difficult to differentiate between LHON and open-angle glaucoma only based on optic disc assessment (O'Neil et al., 2011). Some clinical features overlap in these two optic neuropathies, but there are retinal differences as first manifestations, namely on the type of the RGC involved in each disease model: in LHON, the smallest RGC are first and preferentially affected (in particular the central thin axons – papillomacular bundle) (Sadun et al., 2000; Carelli et al., 2004), while in glaucoma, the peripheral large RGC axons are the firstly affected. Interestingly, some histological evidence has suggested that damage to larger RGC axons firstly occurs in the natural course of glaucoma (Quigley et al., 1987; Quigley et al., 1988). However, 'larger RGC axons' does not necessarily mean 'magnocellular axons'. In fact, larger diameter optic nerve fibers are not exclusively magnocellular fibers. The size of the fibers is dependent on retinal eccentricity as well as ganglion cell type, so some eccentric parvocellular RGC axons may be larger than more central magnocellular RGC axons (Perry et al., 1984; Shabana et al., 2003).

2.2 LEBER HEREDITARY OPTIC NEUROPATHY

Leber hereditary optic neuropathy (LHON) is a maternally inherited disease, which occurs due to mutations in mitochondrial DNA (mtDNA) (Harding et al., 1995; Yu-Wai-Man et al., 2009).

2.2.1 GENETICS

This hereditary optic neuropathy is transmitted by non-Mendelian (mitochondrial) inheritance and, since mitochondria are maternally inherited, there is no male to male transmission in a LHON pedigree (Votruba, 2004).

Over 90% of LHON pedigrees are known to harbor one of these three mtDNA point mutations (so-called "primary" LHON mutations): 3460G>A (13% of the cases),

11778G>A (69%) and 14484T>C (14%). All mutations involve genes encoding complex I subunits of the mitochondrial respiratory chain and are pathogenic in the large majority of patients (Mackey et al., 1996; Man et al., 2002; Carelli et al., 2004). Molecular genetic testing on a blood DNA sample is the diagnostic gold standard and identifies the primary mtDNA mutation of the patient. In most LHON pedigrees, the primary mutation is homoplasmic (100% of the mtDNA molecules is mutant), but 10-15% of LHON carriers are thought to be heteroplasmic (if the mutational load is <60%, the risk of blindness is minimal) (Chinnery et al., 2001).

2.2.2 CLINICAL FEATURES

LHON is the most common of the primary mtDNA diseases (Chinnery et al., 2000). The onset of visual loss typically occurs between the ages of 15 and 35 years (Newman et al., 1991; Nikoskelainen et al., 1996) and visual failure in 95% of carriers will occur before the age of 50 years (Newman, 2005). However, visual deterioration can be manifested anytime during the first to the seventh decade of life and it is generally accepted that neither gender nor mutational status significantly influences the timing and severity of the initial visual loss (Yu-Wai-Man et al., 2009).

In a pre-symptomatic phase, some asymptomatic carriers present telangiectatic vessels around the optic discs and swelling of the peripapillary RNFL (pseudoedema) (Newman, 2005; Yu-Wai-Man et al., 2009). Using optical coherence tomography (OCT) imaging, a swelling of the papillomacular bundle in temporal and inferior quadrants can be observed (Savini et al., 2005). On psychophysical testing, some individuals exhibited subtle impairment of optic nerve function, namely loss of color vision affecting mostly the red-green system and also reduced CS (Quiros et al., 2006; Sadun et al., 2006; Ventura et al., 2007). In fact, there is an early involvement of the axons that form the papillomacular bundle (small caliber fibers), which is the anatomical substrate for central and color vision (Sadun et al., 2000; Carelli et al., 2004).

LHON carriers remain asymptomatic until they experience rapid and painless loss of central vision in one eye (acute phase - first six months). In the majority of cases, visual dysfunction is bilateral, the fellow eye becoming affected simultaneously (25%)

or sequentially (75%), with a median inter-eye delay of 6-8 weeks (Harding et al., 1995). Visual acuity reaches its lowest value 4-6 weeks after disease onset and it is severely reduced to 6/60 or less (Yu-Wai-Man et al., 2009). Patients present characteristic large central or centro-cecal absolute scotomas on visual field and also impairment of color vision perception (Newman et al., 1991; Nikoskelainen et al., 1996). The characteristic signs at fundus examination include vascular tortuosity of the central retinal vessels, circumpapillary telangiectatic microangiopathy, swelling of the RNFL around the disc (pseudoedema) (OCT shows swelling of RNFL in the superior/inferior quadrant, but also loss of the papillomacular bundle temporal fibers; Barboni et al., 2005) and absence of leakage from the disc or papillary region on fluorescein angiography (in contrast to the true disc edema) (Smith et al., 1973; Carelli et al., 2004). However, the optic disc may look entirely normal in the acute phase in about 20% of LHON cases.

The optic disc appears hyperemic initially, though the axonal loss in the papillomacular bundle leads to severe temporal atrophy of the optic disc (Carelli et al., 2009). The RNFL gradually degenerates (OCT shows severe loss of fibers in all quadrants in chronic phase, the nasal being the most spared; Barboni et al., 2005) and, after 6 months, optic disc turns completely atrophic (Yu-Wai-Man et al., 2009).

As expected, some magnetic resonance imaging (MRI) studies have demonstrated signs of atrophy and increased T2-weighted signal in optic nerves of LHON patients (Kermode et al., 1989; Morrisey et al., 1995). MR spectroscopy studies have found a non selective and isolated involvement of the optic nerve, reporting an abnormal mitochondrial energy metabolism in the occipital lobe from these patients (Cortelli et al., 1991; Barbiroli et al., 1995; Lodi et al., 2002). Using MRI and voxel-based morphometry (VMB), Barcella et al. (2010) have described a significant reduced grey matter volume in bilateral primary visual cortex, as well as reduced white matter volume in optic chiasm, optic tract and optic radiations, in LHON patients.

Optic atrophy with permanent severe loss of central vision but with relative preservation of papillary light responses is the usual endpoint of the disease (Carelli et al., 2004). However, in some patients, even years after disease onset, spontaneous recovery is occasionally observed (Newman et al., 1991; Stone et al., 1992; Nikoskelainen et al., 1996; Pezzi et al., 1998). The recovery is not only restricted to visual acuity, including the development of small islands of normal field within the central scotoma or a reversal of color vision impairment (Stone et al., 1992). An early

age of disease onset (<20 years) is not necessarily an unfavorable prognostic factor and the rate of visual recovery seems to be closely related to the type of pathogenic mutation (changes of visual recovery are highest in the presence of 14484T>C mutation, lowest in 11778G>A mutation and intermediate in 3460G>A mutation) (Oostra et al., 1994; Carelli et al., 2004; Yu-Wai-Man et al., 2009). However, the majority of patients show no functional improvement. Respiratory dysfunction may lead to axoplasmic stasis and swelling, with evidence of demyelination, and if mitochondrial apoptotic pathway is activated, RGC are permanently lost (Votruba, 2004).

2.2.3 PATHOPHYSIOLOGY

Mitochondria play an essential role in the life and death of cells, including neurons. All mitochondria are produced in the RGC somata and must be transported to the axonal terminal by axoplasmic transport, which is very energy-demanding, and distributed along strategic locations in the optic nerve (Sadun, 1998; Carelli et al., 2004). Among other factors, efficient transportation of mitochondria depends on their own energy production and adequate myelination of the axons.

The human optic nerve is comprised of approximately 1.2 million unmyelinated RGC axons. These axons, originate at the RGC cell bodies, travel within the nerve fiber layer toward the optic nerve head, and then turn sharply at the disc through the lamina cribrosa to form the optic nerve, gaining their myelin sheath in the process (Yu Wai Man et al., 2005; Carelli et al., 2009). Asymmetric patterns of myelination may have functional implications on energy dependence and distribution of mitochondrial populations in the different sections of the optic nerve. Once RCG axons achieve myelination, their energy dependence decreases drastically (Carelli et al., 2009). Accordingly, histological and histochemical techniques have shown a non-homogeneous distribution of mitochondria along the optic nerve axons (Carelli et al., 2002). As expected, the mitochondrial density is higher in the prelaminar region but drastically decreases in the postlaminar section (Yu Wai Man et al., 2005). Thus, the prelaminar portion of optic nerve may be particularly vulnerable to mitochondrial dysfunction (Newman and Biousse, 2004).

Histopathological studies in LHON patients with long-standing visual loss show axonal degeneration in the optic nerve and loss of myelin, and evidence that the small/ thinly fibers, mostly belonging to the papillomacular bundle (centrally in the optic nerve) are particularly vulnerable (Sadun et al., 2000; Votruba, 2004).

Small diameter fibers present the lowest volume to surface area ratio, having the least margin for error in the setting of energy depletion (the energy expenditure of an axon is related to its surface area, while the content of mitochondria is constrained by the cell's volume) (Sadun, 1998; Sadun et al., 2000). They also have a thinner myelin sheath and a rapid rate of firing. Thus, these fibers have the most disadvantageous condition in terms of energy dependence for maintaining efficient axoplasmic transport (Sadun, 1998). Considering the energy depletion (impairment of ATP production by the mitochondria), possibly induced by the LHON pathogenic mtDNA mutations (Sadun et al., 2000), the most vulnerable component of the optic nerve would be the papillomacular bundle, particularly at the prelaminar (unmyelinated) portion of the optic nerve head (Carelli et al., 2002).

Energy depletion and impairment in axoplasmic transport with compensatory increase of mitochondrial biogenesis may initially result in swelling of the most vulnerable smaller axons (Barboni et al., 2010) and possibly lead to signaling that activates the apoptotic cascade and the subsequent preferential death of RGC with smallest-caliber axons (Sadun et al., 2000)

2.3 GLAUCOMATOUS OPTIC NEUROPATHY

Glaucoma is an optic neuropathy that is characterized by a slow progressive degeneration of RGC and their axons, resulting in changes in the optic disc and retinal nerve fiber layer (RNFL) with a concomitant pattern of progressive visual loss and visual field defect (Weinreb and Khaw, 2004; Quigley, 2011). In fact, vision loss caused by glaucoma is irreversible, making this disease the second leading cause of blindness in the world (Kingman, 2004; Resnikoff et al., 2004). It was estimated that, in 2010, 60.5 million people had glaucoma and this number is expected to increase up to 79.6 million in 2020 (Quigley and Broman, 2006). However, the scope of the problem is probably larger, since several epidemiological studies have shown that at least half of glaucoma patients are undiagnosed (Burr et al., 2007).

The glaucoma is classified by the appearance of the iridocorneal angle. There are open-angle, closed-angle and developmental categories, which are further divided into primary and secondary forms (Kwon et al., 2009). Primary open-angle glaucoma (POAG) is the most common type of glaucoma. In POAG the iridocorneal angle is unobstructed and with normal appearance but aqueous humour outflow is diminished. Although elevated intraocular pressure (IOP) is not part of the clinical definition because POAG can occur when it is normal (normal-tension glaucoma), elevated IOP is a prominent risk factor for developing optic nerve glaucomatous damage (Bahrami, 2006; Kwon et al., 2009). Besides an elevated IOP, a thin central corneal thickness could be associated with a major risk for the development and progression of the disease (Chauhan et al., 2005; European Glaucoma Prevention Study Group, 2007). There is also a good evidence that black race (high prevalence of POAG in Africans as compared with European or Asian people), older age (the mean age of onset is typically after the age of 40 years and the frequency of this disease rises with age), family history of POAG (first-degree relatives have up to ten times increased risk for developing the disease compared with the general population) and a high myopia are risk factors for POAG (Tielsch et al., 1991; Wolfs et al., 1998; Leske et al., 2001; Weinreb and Khaw, 2004; Falkenber and Bex, 2007).

2.3.1 GENETICS

Details about the inheritance of the POAG remain unclear. No single Mendelian mode of inheritance can adequately describe this disease.

Myocilin is a secreted, glycosylated protein of 504 amino acids with two major domains: a coiled coil domain near the amino terminus, and an olfactomedin-like domain near the carboxy terminus (Liu and Vollrath, 2004). This protein is produced in many tissues, including the ciliary body and trabecular meshwork - the two ocular tissues that regulate IOP (Kwon et al., 2009). In fact, myocilin is expressed in many ocular and non-ocular tissues and it is found in both intracellular and extracellular spaces. However, the normal/physiologic function of this protein is unknown and how changes in myocilin expression or presence of myocilin mutations may lead to glaucoma have yet to be identified (Fingert et al., 2002; Resch and Fautsch, 2009).

The *MYOC* gene (at *GLC1A* locus), which encodes the protein myocilin, was identified as the first gene linked to early and late-onset POAG (Stone et al., 1997; Alward et al., 1998; Fingert et al., 1999). The vast majority (more than 90%) of glaucoma associated *MYOC* mutations was found within the large segment of myocilin protein (exon 3) that is homologous to the olfactomedin proteins (Resch and Fautsch, 2009; Kwon et al., 2009).

Some *MYOC* mutations have been detected in a sufficient number of patients to allow identification of some mutation-specific glaucoma phenotypes, including age at onset and maximum IOP: individuals with the T377M mutation are generally diagnosed in their 4^{th} life decade, later than the P370L mutation (1^{st} and 2^{nd}) and Y437H (2^{nd} decade; 44 mmHg mean maximal IOP), but earlier than the most common disease-associated mutation in Caucasians, Q368X (average onset in 5^{th} and 6^{th} decades; 30 mmHg mean maximal IOP) (Alward et al., 1998; Fingert et al., 1999; Shimizu et al., 2000; Fingert et al., 2002). In fact, mutations associated with early-onset POAG lead to the greatest elevations in IOP (about 40 mmHg), whereas mutations associated with late-onset typically cause maximum pressures of 25 to 40 mmHg (Kwon et al., 2009).

Some studies indicate that myocilin is possibly secreted from ocular tissues that may include the trabecular meshwork or ciliary body (Jacobson et al., 2001). Patients with glaucoma-associated MYOC mutations showed dramatic decrease in secretion of myocilin in trabecular meshwork cells and reduced quantity of myocilin into the

aqueous humor, suggesting that failure to secrete myocilin is a central feature in the pathogenesis of myocilin-associated glaucoma (Jacobson et al., 2001). There is also evidence that mutant myocilin may be retained within the intracellular space by means of an anormal association with other proteins (Shepard et al., 2007). Mutant myocilin accumulated in the intracellular space may be toxic to trabecular-meshwork cells, initiating a cascade of events that begins with loss of function in these cells (Kwon et al., 2009). The retention of mutant myocilin potentially cause a stiffer, less-pliable trabecular meshwork, possibly increasing resistance to aqueous outflow and elevating IOP (Wentz-Hunter et al., 2004; Resch and Fautsch, 2009). Regardless of the retention mechanism, decreased secretion and increased accumulation of intracellular myocilin appear to be the first steps in the pathogenesis of myocilin-associated glaucoma (Kwon et al., 2009).

Several large studies suggested that myocilin mutations have been found in 2-4% of cases of adult-onset POAG and more than 10% in juvenile-onset cases (Stone et al., 1997; Fingert et al., 1999). Perhaps due to the low prevalence of myocilin-associated glaucoma in the general population, screening tests of whole populations for myocilin defects are not especially useful.

2.3.2 CLINICAL FEATURES

POAG is a chronic asymptomatic disease, generally bilateral, but often asymmetrical, that is characterized by progressive dysfunction or death of the RGC axons as shown by changes in the optic disc, thinning of retinal nerve fiber layer and visual field loss (Weinreb and Khaw, 2004; Anderson, 2006). Many glaucomatous patients present an elevated IOP, although it is extremely important to evaluate the central corneal thickness, since this measure can mask the real IOP (European Glaucoma Society, 2008).

It is known that, in normal subjects, the convergence of the RGC axons forms a central physiological depression in the optic disc (so called “cup”) and the neuroretinal rim of the optic nerve head surrounds this cup. In the case of glaucomatous neuropathy, as more RGC and their axons are affected and lost, more the width of the neuroretinal rim decreases, as well as the thickness of the RNFL surrounding the disc.

Concomitantly, there is a deepening and widening of the cup (cup-to-disc ratio progressively increases) - see Figure 2.1. The optic disc excavation occurs not only due to the loss of RGC axons, but also due to deformation of connective tissues supporting the optic disc (Weinreb and Khaw, 2004). In summary, evidence of glaucomatous optic disc damage is defined by the presence of excavation, neuroretinal rim thinning or notching and/or retinal nerve fiber defects (Johnson et al., 2003).

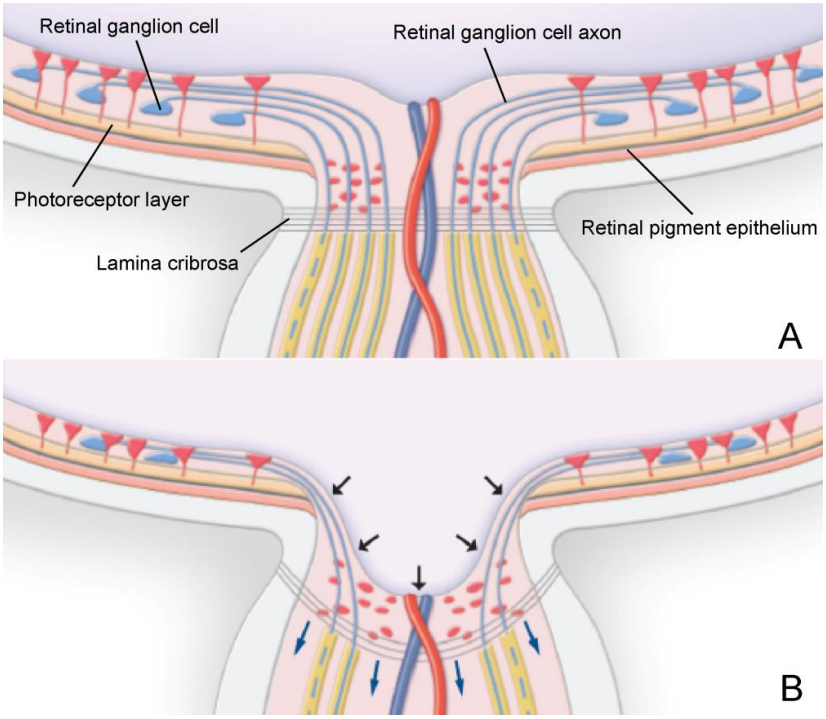

Figure 2.1. Longitudinal cross-section of normal (A) and glaucomatous optic nerve head (B). The lamina cribrosa undergoes deformation (blue arrows), leading to a significant loss of RGC and their axons with concomitant thinning of RNFL, decrease of the neuroretinal rim and an increased cupping of the optic nerve disc (black arrows) (Adapted from Kwon et al., 2009).

Thus, examination of the optic disc is an important and valuable method for diagnosing early glaucoma, because changes in the optic nerve appearance often occur before overt visual field loss (Sommer et al., 1991; Artes and Chauhan, 2005; Sharma et al., 2008). Some objective and quantitative methods have emerged to assess the structural changes of the optic disc and RNFL, namely scanning laser polarimetry (to assess the RNFL thickness), confocal scanning laser ophthalmoscopy (to measure the topography of the optic disc and to quantify the area of the optic disc cup and the

neuroretinal rim) and OCT (to measure RNFL thickness and to visualize the optic disc topography) (Sharma et al., 2008).

The functional loss is traditionally assessed by quantifying light sensitivity at specific visual field locations within the central 30 degrees, using a white-on-white standard automated perimetry (SAP) - *golden standard* (Anderson, 2006; Sharma et al., 2008). The characteristic visual field defects include a nasal step scotoma that respects the horizontal raphe, inferior or superior arcuate scotoma, paracentral scotoma or generalized depression (Weinreb and Khaw, 2004) (Figure 2.2). Since peripheral vision is most susceptible to glaucomatous damage, loss of central visual acuity typically occurs only in the end stage of disease.

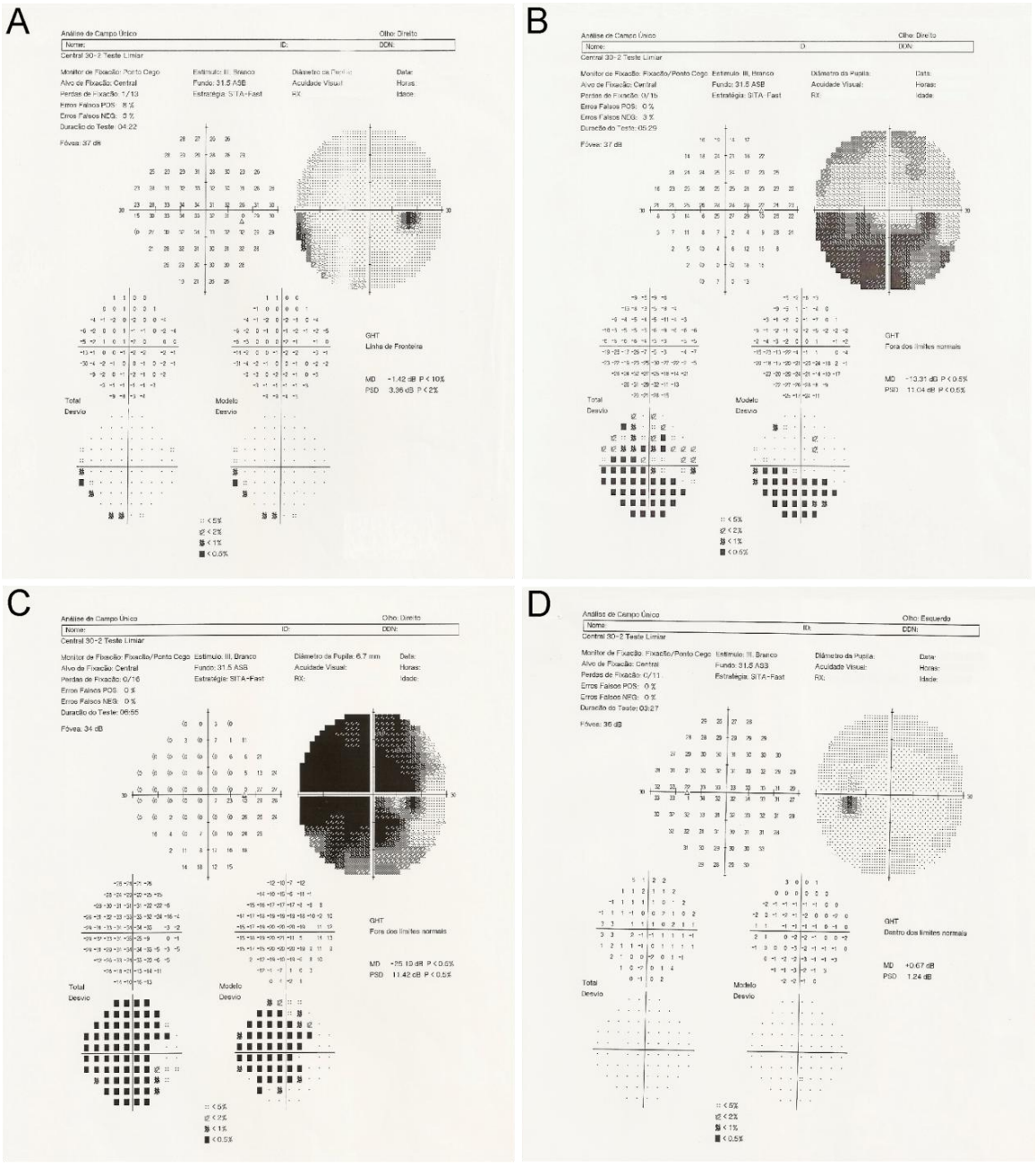

Figure 2.2. Visual field results across different stages of glaucoma (A, B, C): Damage usually starts in the nasal field (upper or lower half quadrant) (A); Mid-stage disease shows pronounced loss in the initial hemifield, which can be extended to the opposite hemifield (B); At an end-stage disease, before the entire visual field becomes affected, only an island of vision remains (C). Representative example of a normal visual field (D).

It is known that SAP does not test selectively a particular RGC type, being insensitive to early RGC dysfunction. Under the current conditions of SAP, the white stimulus is detected by all sub-systems in the retina and, if a few cells of a specific subtype become dysfunctional, the stimulus can still be detected by different types of

functional cell populations, which 'fill the gap' (Anderson, 2006). In fact, a significant fraction of RGC may be permanently lost when a visual defect becomes apparent in visual field testing (Quigley et al., 1989; Harwerth et al., 1999; Kerrigan-Baumrind et al., 2000). In this sense, selective functional visual tests, which aim to isolate specific RGC populations, losing the redundancy afforded by the other cell types, might potentially be better suited to identify glaucomatous defects earlier than standard visual field testing (Johnson et al., 1993; Maddess et al., 1999; Castelo-Branco et al., 2004; Spry et al., 2005; Bagga et al., 2006). For instance, frequency doubling technology perimetry (FDT), which uses a vertical sinusoidal grating of low spatial frequency that undergoes counterphase flickering at a high temporal frequency, producing an illusory double spatial frequency (Turpin et al., 2002a; Silva et al., 2008), predominately stimulates the magnocellular RGC pathway (My-subtype) (Sample et al., 2000) and can reveal early losses before they can be found using conventional clinical test procedures (Johnson and Samuels, 1997; Brusini and Brusatto, 1998; Landers et al., 2000; Cello et al., 2000; Cellini et al., 2012). On the other hand, short-wavelength automated perimetry (SWAP), which uses a blue stimulus over a yellow background and selectively tests the koniocellular ganglion cell pathway (Sample et al., 2000), consistently shows visual field defects even at a pre-SAP loss stage, suggesting that magnocellular axons are not the only ones affected in the early disease stages and that the pathological process does probably affect several subsets of RGC (Johnson et al., 1993; Casson et al., 1993).

Color vision impairment is also observed in glaucoma patients, not only in the later stages of the disease, but also in the ocular hypertension stage (Castelo-Branco et al., 2004). It is widely believed that glaucoma is predominantly associated with tritan-like defects (Johnson et al., 1993; Heron et al., 1994; Felius et al., 1995; Gray et al., 1995; Sample et al., 1997). Although most studies imply a predominant involvement of the koniocellular pathway, an important parvocellular dysfunction has also been reported (Greenstein et al., 1996; Alvarez et al., 1997; Castelo-Branco et al., 2004).

Interestingly, there is evidence (neuroimaging studies) that glaucomatous damage extends from RGC to neurons in all structures along the visual pathway, including the optic nerve, optic chiasm, lateral geniculate nucleus and primary visual cortex (Yücel et al., 2003; Duncan et al., 2007a; Duncan et al., 2007b; Qing et al., 2010; Hernowo et al., 2011; Dai et al., 2013).

Since the disease progression can frequently be arrested or slowed with medical and surgical treatment and the visual impairment caused by glaucoma is irreversible, early detection is critical (Sharma et al., 2008). Early diagnosis of POAG typically relies on examination of structural damage of the optic nerve combined with measurements of visual function. New imaging and psychophysical tests can certainly improve both early detection and monitoring of disease progression.

2.3.3 PATHOPHYSIOLOGY

Retinal ganglion cell death or dysfunction is the pathological hallmark of glaucoma, albeit the pathophysiology of the progressive impairment of RGC is not fully understood (Weinreb and Khaw, 2004; Anderson, 2006). Most of the theories concerning the pathogenesis of glaucoma can be grouped in two broad categories: mechanical (IOP-related) and vasogenic (Fechtner and Weinreb, 1994).

The level of IOP is unquestionably related to the death of RGC and optic nerve fibers in some, but not in all, patients with POAG. Although no obstruction can be observed with clinical examination, resistance to aqueous outflow through the trabecular meshwork is increased in patients with this type of glaucoma.

Clinical observations have indicated that the lamina cribrosa is the initial site of glaucomatous damage (Quigley, 1999). Lamina cribrosa consists of about ten lamellar sheets with pores which align to form about 400 to 500 channels through which pass the axons of the RGC grouped into optic nerve fiber bundles. The lamina cribrosa supports and separates unmyelinated prelaminar RGC axons from myelinated postlaminar RGC axons (Kwon et al., 2009). Within the collagenous beams of the lamina cribrosa are blood vessels and extracellular matrix components which contribute to the nourishment of the axons together with axonal transport (Fechtner and Weinreb, 1994).

Some studies *in vitro* have shown that high pressure can distort the lamina cribrosa (Levy et al., 1981; Zeimer and Ogura, 1989). In fact, when IOP increases above physiological levels, the pressure gradient across the lamina cribrosa and the RGC axons undergo deformation and mechanical stress (Bellezza et al., 2003). A structural change in the lamina cribrosa related with high pressure may result in changes in orientation or collapse of the laminar channels which could distort the alignment of the

axonal channels producing direct mechanical impingements on nerve fibers (Fechtner and Weinreb, 1994). These may cause damage of RGC axons not only by mechanical factors, but also by compromising blood flow and delivery of nutrients to the axons.

With this line of evidence, some experimental models postulate a blockade of RGC axonal transport due to IOP-induced compression of optic nerve axons at the lamina cribrosa, which can reduce retrograde axoplasmic flow, causing stress of the cells and their death by deprivation of neurotrophic factors (Quigley et al., 2000). On the other hand, if blood perfusion at the optic nerve head is persistently reduced (Mozaffarieh et al., 2008), tissue hypoxia can induce the formation and accumulation of reactive oxygen species in the retina, causing cellular stress and malfunction (Ko et al., 2005).

Interestingly, regional differences in the lamina cribrosa may also account for some of the characteristic patterns of damage seen in glaucoma (Figure 2.3). The lamina cribrosa septae is more closely packed and thicker along the horizontal meridian of the nerve, including areas corresponding to retinal nerve fibers subserving the central and temporal portion of the visual field, which are relatively spared (Quigley and Addicks, 1981). In these areas, the thick septae may be more resistant to mechanical deformation, sparing the nerve fibers from injury until a late stage in the course of the disease (Fechtner and Weinreb, 1994). In addition, the largest pores of the lamina cribrosa are typically arranged in an hourglass configuration at the superior and inferior poles of the optic nerve head. These areas are composed by a high proportion of large diameters fibers subserving the arcuate regions, suggesting an increased vulnerability of these fibers to pressure-related damage (Fechtner and Weinreb, 1994).

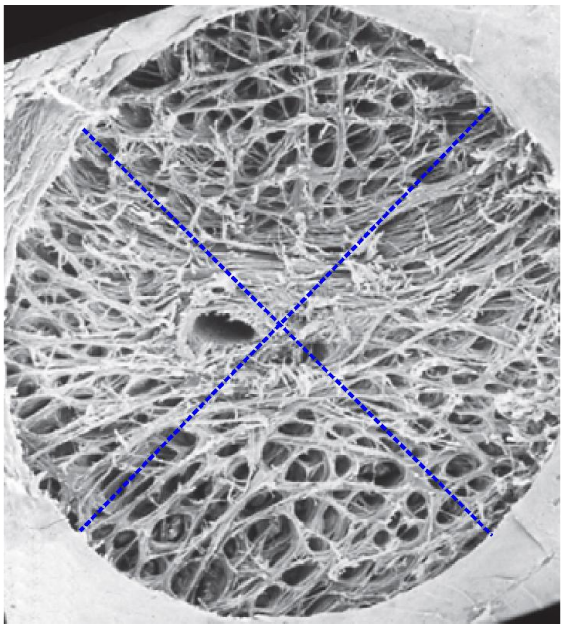

Figure 2.3. Human lamina cribrosa demonstrating pores through which pass RGC axons. Note schematic representation of typical hourglass arrangement of pores (blue lines) with the largest pores found in the superior and inferior poles (Adapted from Quigley, 2011).

Although elevated IOP is considered to be a prominent risk factor for POAG, this cannot explain the fact that some individuals with ocular hypertension do never develop glaucomatous damage, while others with normal IOP do. There are normal-tension glaucoma patients in whom optic nerve and visual field changes occur similarly to alterations in POAG patients. Thus, other factors must play an important role in glaucoma pathogenesis.

There is considerable evidence supporting the concept that changes within the microcirculation may be relevant to the POAG development. It was suggested by Ernest (1975) that a faulty autoregulation of ocular microcirculation may contribute to the pathogenesis of POAG (Ernest, 1975). The retina and optic nerve are dependent on their blood supply for satisfying the high metabolic needs, and local ischaemia-hypoxia, maybe due to dysfunction of blood-flow autoregulation, has been implicated as one of the possible factors that could cause POAG (Weinreb and Khaw, 2004).

PART II

METHODS

CHAPTER 3

METHODOLOGICAL OVERVIEW

3.1 FUNCTIONAL ASSESSMENT

3.1.1 PSYCHOPHYSICS

3.1.1.1 CHROMATIC CONTRAST SENSITIVITY

We have probed chromatic contrast sensitivities using a computer-controlled psychophysical method, a slightly modified version of Cambridge Color Test (CCT; Cambridge Research Systems Lda., CRS, Rochester, UK) (Silva et al., 2005; Mateus et al., 2013). This technique uses three parallel, randomly interleaved staircases, corresponding to simultaneous assessment of the three cone confusion axes (protan/red, deutan/green and tritan/blue) modulated in the CIE 1976 u'v' color space (Trivector version of the test). Each staircase was composed by 11 reversals and the mean of the last 7 reversals was taken as the threshold estimate. Subjects looked monocularly (the first eye tested was chosen in a random manner) at a screen (21-inch monitor; viewing distance - 180cm) with a static pattern of circles of various sizes and luminances with superimposed chromatic contrast defining a Landolt-like C-shaped ring (gap size: 1.6º; outer diameter: 7.6º; inner diameter: 3.81º), which forces the subject to use specific color cues (see Figure 3.1). These patches were randomly assigned six different luminance noise levels (8 to 18cd/m^2 in steps of two units). Subjects were instructed to indicate one out of four possible gap positions (up, down, left or right) of the Landolt C stimulus, by pressing one of four buttons of the response box. Psychophysical thresholds were expressed in CIE 1976 u'v' color space units. Note that high chromatic thresholds relate to low CS.

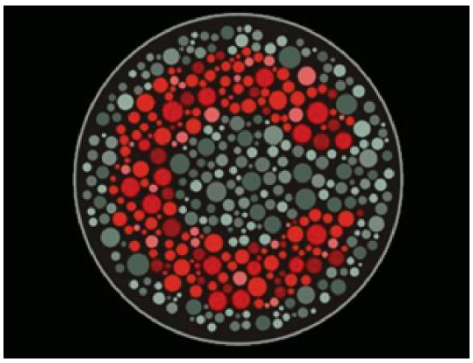

Figure 3.1. Schematic illustration of the stimuli used in the Cambridge Color Test, representing a luminance noise stimulus with superimposed chromatic target (Landolt C shape, colored in red).

3.1.1.2 ACHROMATIC CONTRAST SENSITIVITY

Frequency Doubling Technology (FDT) perimeter (Humphrey Matrix perimeter, Welch Allyn, Skaneateles, NY; Zeiss – Humphrey, Dublin, CA) determines CS measures for detection of sinusoidal gratings with spatial frequency of 0.25cpd undergoing counterphase flicker at 25Hz (Turpin et al., 2002b; Silva et al., 2008). We performed N-30-F FDT full threshold test, which uses a staircase threshold strategy known as a Modified Binary Search (MOBS) with a four-reversals rule for determining the threshold level. The range of possible threshold level values for the raw data is between 0 dB Maximum Contrast and 56 dB Minimum Contrast. Stimulus duration was 300 ms and background luminance was 100 cd/m^2. Stimuli (10º by 10º squares, except for a 5º radius central circular target) were presented at 17 locations, plus 2 nasal locations, testing 30º nasally and 20º temporally (Figure 3.2).

Performance reliability was assessed by monitoring fixation loss and computing false positive and negative errors (results with false positive and negative errors ≥ 33% and fixation loss ≥ 20% were excluded (Caprioli, 1991; Clement et al., 2009)). In this study, subjects were instructed to fixate the black square in the centre of the screen and report the presence of "striped" targets. All participants performed the test under monocular conditions.

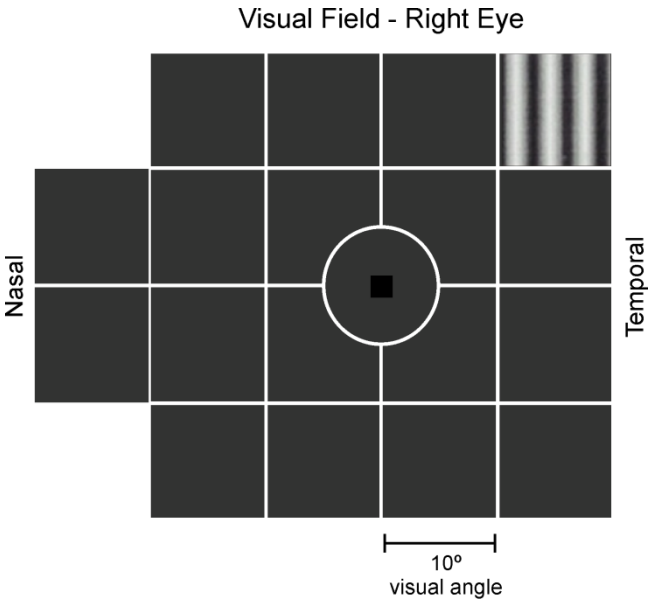

Figure 3.2. Schematic representation of the 17 visual field locations plus 2 nasal positions tested in FDT task. The black square in the middle of the figure represents the fixation square. Sinusoidal gratings were used as detection target stimuli.

Statistical analysis was performed considering both global indices, mean deviation (MD) and pattern standard deviation (PSD). For analysis purposes, 4 visual field quadrants (inferior nasal, IN; inferior temporal, IT; superior nasal, SN; superior temporal, ST) and 3 zones were defined: zone 1 corresponds to 5º of visual field, zone 2 contains locations between 5º and 10º eccentricity and zone 3 contains locations between 10º and 20º temporally or 30º nasally.

3.1.1.3 STANDARD AUTOMATED PERIMETRY

Octopus Perimeter

The LHON carriers group performed the SAP, using a commercially available system Octopus version 311 (Haag-Streit AG, Germany) (Reis et al., 2013). Patients were instructed to fixate the central point and report the presence of bright targets, which could appear in 76 different locations within 30º of visual field (program 32, stimulus size: Goldmann III; stimulus duration: 100 ms). Threshold data was obtained with the TOP (tendency oriented perimetry) strategy (Moraled et al., 2000), in which

every answer at a particular point is taken into account in the adjustments of the neighboring locations.

The test was performed under monocular conditions, being the first eye tested chosen in a random manner. Performance reliability was assessed by computing false positive and negative errors (results with false positive and negative errors ≥ 33% were excluded). Fixation loss was monitored during the examination, although an electronic eye fixation control system. This system interrupts the examination and notifies if patient is not fixating or is closing the eye. Global indices as mean sensitivity (MS), mean defect (MDf) and loss variance (LV) were analyzed. We also obtained the mean sensitivity of two rings (ring 1, central circle with 15º of radius; ring 2, 30º of radius). According to device manual, a normal visual field shows a MDf between -2 and +2 dB and a LV < 6 dB^2.

Humphrey Perimeter

Automated visual fields were performed on the Humphrey Field Analyzer (HFA II, Carl Zeiss Meditec, Dublin, CA) in the case of glaucomatous patients. They were instructed to report the presence of bright targets (white stimulus, size Goldmann III), which could appear in 76 different locations within 30º of visual field (SITA-Fast strategy, 30-2 standard program).

The test was performed under monocular conditions and the first eye tested was chosen in a random manner. Performance reliability was assessed by computing fixation loss and false positive/negative errors (results with false positive/ negative errors ≥ 33% and/or fixation loss ≥ 20% were excluded (Caprioli, 1991; Clement et al., 2009)). Global parameter as mean deviation (MD) was analyzed: MD more than -2 dB or > 5% of confidence interval is characteristic of a normal visual field.

3.1.1.4 NOVEL PSYCHOPHYSICAL MOTION, ACHROMATIC CONTRAST AND CHROMATIC CONTRAST DISCRIMINATION TESTS

Set-Up

Our experiments were setup in MATLAB® (MATLAB® 2011a, The Mathworks Inc, Natick, MA, USA), using the Psychophysics Toolbox (PTB-3) extensions (Brainard, 1997; Pelli, 1997; Kleiner et al., 2007). All stimuli were presented on a 24" LCD-IPS monitor (ColorEdge CG243W, Eizo®, Japan) with a native screen resolution of 1920x1200 pixels and a refresh rate of 60 Hz. It is important to point out that although our monitor has a resolution of 10 bits, we only accessed 8 bits, which was adequate for the purposes (detection task) of our experiment (see below). Monitor characterization was implemented as described by Brainard et al. (2002), and all spectral and luminance measurements were made using a calibrated spectroradiometer (PR-650 SpectraScan Colorimeter, Photo Research Inc., Chatsworth, PA, USA).

In terms of luminance response, we conducted an extensive channel independent characterization with 60 points per color channel. We found that this LCD-IPS monitor luminance response follows a power-law curve, with a nonlinearity similar to those found in CRT monitor models, which can be fitted with high correlation coefficient by the following power-type function: $l = a * (rgb)^{\wedge b} + c$ [where "l" stands for luminance in cd/m^2; rgb represents each channel (red, green, blue) digital number related to channel stimulation power - in the graphics this rgb value is normalized to the unit; and finally "a", "b" and "c" are curve fit parameters, "b" is also known as the Gamma power value]. This LCD-IPS monitor also presents low angular dependence, good channel constancy, and high spatial homogeneity. In order to check for channel spectrum constancy, each channel spectrum response was tested in different powers (20%, 40%, 60%, 80%, 100%). We found good spectrum stability at different stimulation powers, from which we can construct a linear model typical to those models for CRT monitors, where the monitor emission spectrum for each RGB combination can be obtained with negligible error by independent summation of independent color channel spectrum weighted by it stimulation power. Also, we tested this monitor color gamut, and found that it is superior to CRT typical models.

General Test Features

We developed three novel 2AFC (two-alternative forced choice) psychophysical tests that required the comparison and discrimination of a visual feature (motion, achromatic contrast and chromatic contrast) between two separated moving single dots (a reference dot and a target dot, which were presented in opposite hemifields).

The use of physically similar stimuli allows for better comparison, the reference and target dots only differ in the visual feature being measured. We used two squared dots measuring 0.3ºx0.3º for the motion discrimination test and 0.6ºx0.6º for both achromatic and chromatic contrast discrimination tests. Fixation on a black central cross (size of 1º) was present during all the tests and central fixation was monitored online using a camera. The grey background for all tests had a luminance of 25 cd/m^2. During 400 ms trials, the reference and target dots were simultaneously presented on randomly alternated visual hemifields, moving back and forth along a 2º pseudo-random linear trajectory (between 0º and 180º). The experiments took place in a darkened room where subjects executed the experiments monocularly (only the dominant eye was tested), with refraction corrected for distance and 50 cm away from the display system. Each test was repeated four times, corresponding to one of four different meridian/eccentricity pairs (the horizontal meridian, 0º, was tested at 7.5º of eccentricity; the vertical meridian, 90º, at 10º; the oblique meridians, 45º and 135º, at 15º) (see Figure 3.3, schematic illustration of the three tasks).

After each trial, the subject gave a verbal response (the instruction for each test is described below) which the experimenter stored by means of a standard keyboard (due to the subject's average age and to avoid motor errors). There was no time limit for this response.

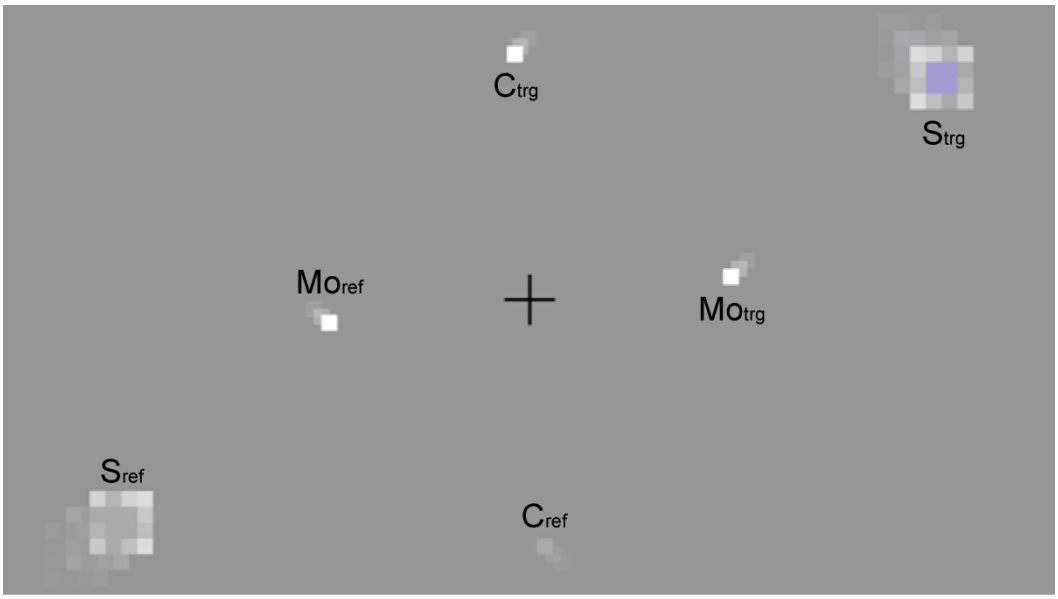

Figure 3.3. Schematic illustration of motion (Mo), achromatic contrast (C) and S-cone chromatic contrast test (S) stimuli, at 0º, 90º and 45º meridians with an eccentricity of 7.5º, 10º and 15º, respectively. The tests consist of the discriminative comparison of moving dots, a reference dot (ref) and a target dot (trg), which differ on a specific visual attribute being tested (in Mo, a motion/speed difference between dots; in C, a luminance difference and in S, a chrominance, S-cone selective, difference).

Staircase

Each visual feature being evaluated was estimated by using a non linear logarithmic staircase procedure. In this procedure, the tests ended after 6 reversals and a discrimination threshold was calculated using the arithmetic mean of the last 4 reversals. In each trial, the staircase feeds the display software with the visual feature estimation to be visually displayed on the target dot, then the display software computes the best match between what the display monitor can really show (based on monitor characterization), and the estimated value asked by the staircase. The best match value is then feedback to the staircase to substitute the asked value, and the trial is finally constructed around this best match value. In the end of each trial the software program feeds the staircase with the subject's response, and then calculates the next step based on subject's answer, restarting this cycle one more time.

Psychophysical tests

Motion discrimination test

In the motion discrimination test, the reference and target dots consisted of two white dots moving at different velocities. The reference dot velocity was always 5 deg/s (visual degrees per second), while the target dot velocity started at 24 deg/s (physically matched in luminance, 30 cd/m^2) and was then manipulated by the logarithmic staircase procedure (maximum step size of 1 dB and minimum of 0.05 dB). The subject was asked "Which dot is moving faster?" and answered either "Left/Right" (for the horizontal meridian) or "Up/Down" (for the vertical and oblique meridians).

Achromatic contrast discrimination test

In the achromatic contrast discrimination test (or, more precisely, achromatic *luminance* discrimination), both reference and target dots moved at the same velocity (5 deg/s), and a grey equal appearance with R=G=B, but their luminance was distinct. The reference dot had a fixed luminance of 30 cd/m^2, while the target dot had a variable luminance that started at 70 cd/m^2 and was then manipulated by the logarithmic staircase procedure (maximum step size of 1 dB and minimum of 0.3 dB). For better accuracy in calculating luminance stimulus, we made a characterization just in grey color (R=G=B), which culminates in the fitted power-law function with the following parameters a=72.2384, b=2.2095, c=0.1464, has described before.

Importantly, concerning the luminance tests, our monitor characterization data shows that step sizes are rather small at a global luminance around 30 cd/m^2, allowing for good luminance contrast steps in this range. The continuous working of the logarithmic staircase procedure if the subject can effectively spot the luminance differences between the two dots, brings the target dot toward this high resolution area, where we can find smaller luminance levels, even with an 8-bit channel graphics card. The subject was asked "Which dot is brighter?" and answered either "Left/Right" (for the horizontal meridian) or "Up/Down" (for the vertical and oblique meridians).

Chromatic contrast discrimination test

The chromatic contrast discrimination test was composed of three sub-tests in approximate isoluminance conditions concerning the masking surrounding pattern of squares with randomly varying luminance, and dots (reference and target) moved at the same velocity (5 deg/s). We computed all cone contrast relative coordinates at the selected luminance interval near 30 cd/m^2 with an error up to 2 cd/m^2 (transformed using human cone spectral sensitivities (Stockman and Sharpe, 2000) at 10º), possible in this monitor display (relative LMS coordinates assume that display's maximum white corresponds to LMS coordinate (1.0,1.0,1.0)). From this approximate isoluminance cone contrast relative coordinates selection we build one table, and from this table we select the same gray "colorless" coordinate to be our reference dot for all three tests, with an LMS cone contrast relative coordinate (0.4106,0.4108,0.4241). To further avoid the use of residual luminance cues, we adopted the noise luminance strategy (Regan et al., 1994; Barbur et al., 1994; Pacheco-Cutillas et al., 1999; Castelo-Branco et al., 2004). In short, the addition of luminance noise ensures that only chrominance cues can be used. Residual luminance cues were avoided by placing a matrix of luminance noise around each dot. This matrix was composed of twelve 0.3º squared dots, with six different luminance noise levels (30, 34, 38, 42, 46 or 48 cd/m^2), the luminance of each dot randomly changed during the trial (synchronized to the screen refresh rate). In summary, given the inherent limitations of conventional hardware, we aimed at the use of color cues using luminance noise, and computed all colors at a luminance near 30 cd/m^2 +/- 2 cd/m^2. We did not aim to go above 30 cd/m^2 to ensure adequate color output range across channels. This error was masked with squares with different luminances.

We then developed three (relatively) biased cone contrast relative coordinates stimulation tests. For example, concerning the L-cone test, its stimulation exceeds the M-cone stimulation and at the same time we fix the S-cone stimulation value; the reverse happens in M-cone test, where M-cone stimulation exceeds L-cone stimulation value, whereas the S-cone remains fixed (for instance, a variation of 15% in one cone produced a reciprocal variation of 2.5% in the other cone). In the S-cone test, we fix L-Cone and M-cone stimulation value, and vary only the S-cone relative contrast coordinate. The target dot starting point for each test was L-cone test (l=0.4732), M-cone test (m=0.5158), S-cone test (s=0.9). These appeared like a pale red, green and purple dot, respectively. Maximum and minimum step size in the staircase procedure

for the L, M, S-cone tests were 0.1 dB / 0.001 dB, 0.1 dB / 0.001 dB and 0.4 dB / 0.08 dB. The subject was asked "Which dot has color?" and answered either "Left/Right" (for the horizontal meridian) or "Up/Down" (for the vertical and oblique meridians).

3.1.2 ELECTROPHYSIOLOGY

3.1.2.1 PATTERN ELECTRORETINOGRAM

We recorded pattern electroretinogram (PERG; RETIport32, Roland Consult, Germany), which provides information about macular and ganglion cell function, following the ISCEV standards (Bach et al. 2013) and using DTL fiber as recording electrodes. The stimulus consisted in a reversal black and white checkerboard pattern (4.3 reversals per second, rps), with a contrast of 97% and a check size of 0.74º. The stimulus was presented binocularly at a 20-inch monitor (frame rate: 60 Hz), at a viewing distance of 1 meter. Observers were instructed to fixate a small red cross in the center of the screen and the fixation was checked by means of online video-monitoring during recording sessions. Refractive errors were corrected for the test distance, when applicable.

The active voltage range of bioelectrical signal was ±100 μV. Signals were amplified with a gain of 100,000 and bandpass filtered (1-100 Hz). We collected 200 artefact-free sweeps to obtain an average waveform (artifact rejection level of 5%). To confirm reproducibility, two PERG measurements were taken (Figure 3.4). Finally, the amplitudes (μV) and peak time values (ms) of responses for each P-50 and N-95 components and also the PERG ratio (N-95 amplitude divided by P-50 amplitude) were analyzed.

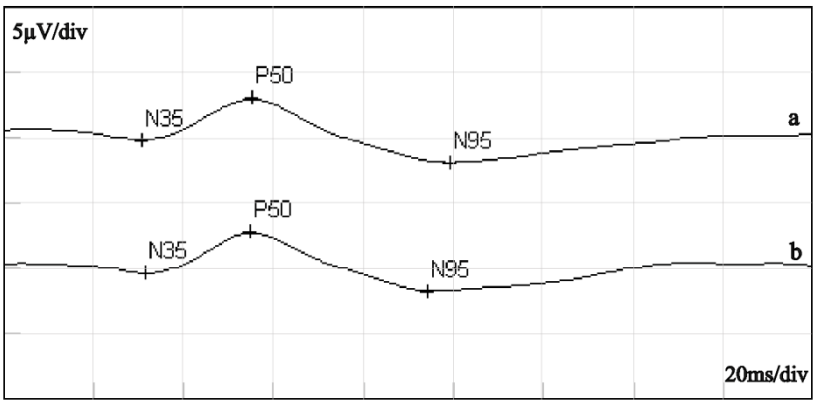

Figure 3.4. A Pattern ERG recorded in a healthy eye [a and b, first and second measurement].

3.2 STRUCTURAL ASSESSMENT

3.2.1 SPECTRAL-DOMAIN OPTICAL COHERENCE TOMOGRAPHY

OCT has histology-level resolution, given the optical accessibility of the retina. In this study, we have used Spectralis SD-OCT software version 5.3.2 (Heidelberg Engineering, Heidelberg, Germany) to obtain peripapillary RNFL and retinal thickness (RT) measurements (Laguna et al. 2013). Image acquisition was performed in high-speed mode, providing an axial resolution of 7 μm and a transversal resolution of 14 μm.

Peripapillary RNFL thickness

Concerning RNFL measurements, a circular 3.5 mm scan centered on the optic nerve head was used (768 A-scans) and a peripapillary RNFL thickness sectors were evaluated (temporal [315º - 45º], superior [45º - 135º], nasal [135º - 225º], and inferior quadrant [225º - 315º]).

Macular thickness

We also obtained cross-sectional images centered on the macula, scanning a 20ºx20º pattern, with 25 horizontal raster scans (distance between B-scans: 245 μm) and 512 A-scans (ART mode: 20 images averaged). Macular retinal thickness was calculated by computing the distance between the signal from vitreoretinal interface and the signal from basement membrane of the retinal pigment epithelium (RPE), Bruch's membrane complex. We used the RT map analysis protocol, which displays retinal thickness in nine ETDRS subfields. For analysis three rings were considered: ring 1 (central circle with 1 mm of diameter), ring 2 (3 mm) and ring 3 (6 mm).

IRL, ORL and macular RNFL thickness

Inner retinal layer (IRL) thickness measurements (including nerve fiber layer, ganglion cells layer, inner plexiform layer and inner nuclear layer) were also determined through manual segmentation (Aaker et al. 2010). This was accomplished using Heidelberg software by setting the inner limit of the IRL at the internal limiting membrane, and the outer limit at the outer border of the inner nuclear layer (see Figure 3.5). We also performed a manual segmentation of macular RNFL thickness (first layer of IRL). Subtracting IRL thickness from the global retinal thickness, we obtained Outer retinal layer (ORL) (including outer plexiform layer, outer nuclear layer, outer limiting membrane, layer of rods and cones and RPE). For IRL, ORL and macular RNFL analysis, we also considered the 3 rings described above.

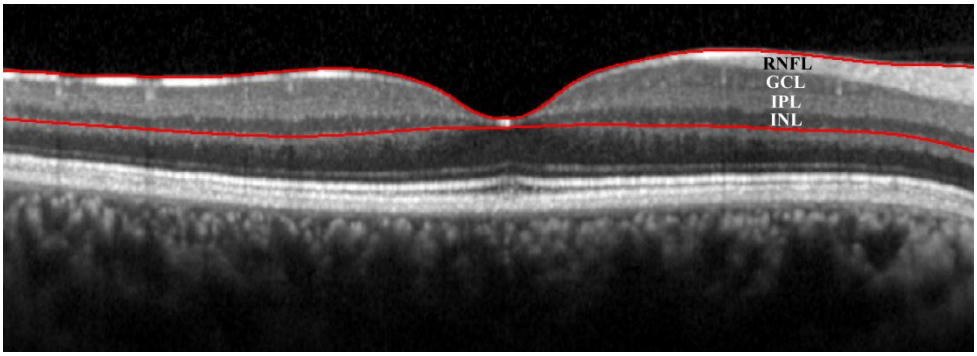

Figure 3.5. Spectral domain OCT image of a section through the fovea of the right eye of a control subject showing the segmented inner retinal layer (IRL) (red lines). The following layers of the IRL are shown: retinal nerve fiber layer (RNFL), ganglion cell layer (GCL), inner plexiform layer (IPL) and inner nuclear layer (INL).

3.2.2 MAGNETIC RESONANCE IMAGING

The magnetic resonance imaging (MRI) data was acquired in a 3T scanner (Siemens Magnetom TrioTim 3T, Erlangen, Germany) at the Portuguese Brain Imaging Network, with a 12 channel head coil (d'Almeida et al. 2013). For each participant we obtained two 9-minute long T1-weighted three-dimensional Magnetization Prepared Rapid Acquisition Gradient Echo (MPRAGE) sequences, repetition time (TR) 2.3 s, echo time (TE) 2.98 ms, flip angle (FA) 9º, field of view (FoV) 256x256 mm^2, yielding 160 slices with 1x1x1 mm^3 voxel size; and also four functional runs (three polar angle and one eccentricity stimuli) using single shot echo planar imaging (EPI) acquired in the axial plane orthogonal to the anterior commissure covering the occipital, temporal and frontal cortices, TR 2 s, TE 39 ms with a 128x128 imaging matrix, interslice time 76 ms, FA 90º, FoV 256x256 mm^2, yielding 26 slices with 2x2x2 mm^3 voxel size.

The stimuli presented consisted in a polar angle encoding paradigm comprised by a rotating (anticlockwise) black and white checkered wedge flickering at 8 Hz (48s full cycle, 4 cycles/scan, three scans per subject); and an eccentricity mapping paradigm, using an expanding black and white checkered ring flickering at 8 Hz (48s each full expansion, 4 expansions/scan, one scan per subject), while the subject was instructed to fix an orange-colored central point (Figure 3.6). The stimuli spanned 23ºx23º of visual angle (diameter).

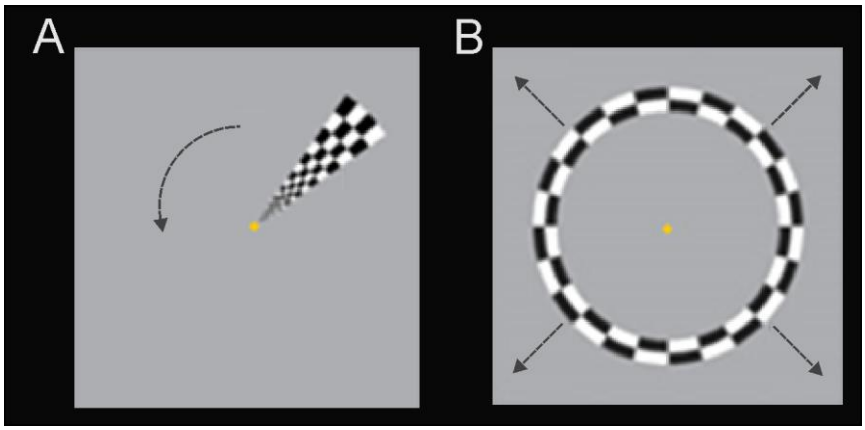

Figure 3.6. Schematic illustration of visual stimuli for functional MRI: (A) *polar angle* paradigm - rotating wedges revolving 360º anticlockwise around the fixation point and (B) *eccentricity* paradigm - expanding ring outward from the fixation point.

All image processing, cortical thickness and retinotopic mapping was performed with BrainVoyager QX 2.2 (Brain Innovation, Maastricht, The Netherlands). Thickness values of each visual area were extracted with BVQX toolbox for MATLAB (R2008a, v.7.6.0, The MathWorks, USA).

Basically, cortical thickness (CT) was measured through a process that involves four essential steps: 1) high-quality segmentation of the inner and outer cortex boundary of the preprocessed high quality T1-weighted anatomical 3D data sets. The two anatomical datasets were averaged to get a higher signal-to-noise ratio and then normalized to the Talairach coordinate space; 2) cortical thickness measurement in volume space by the Laplace method (Jones et al. 2000); 3) cortical thickness measurement in surface space in order to profit from cortical alignment, over inflated meshes; 4) cortical thickness analysis for regions-of-interest (ROIs) delineating patches-of-interest based on color coding of polar angle and eccentricity experiments (see Figure 3.7 for an example of cortical thickness map).

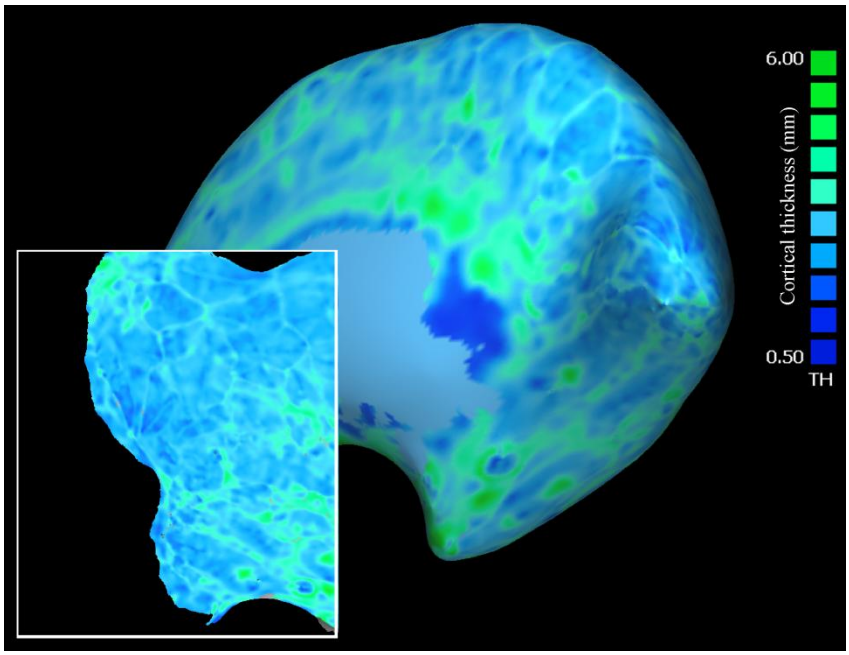

Figure 3.7. Thickness map over inflated and flattened meshes (right hemisphere of a control subject). The color-scale map ranges from 0.5 mm (dark blue) to 6 mm (green).

The eccentricity and polar angle gradients define visual field sign maps that reflect the mirrored representation of visual areas (Sereno et al. 1994). Hence, we obtained two-color code map that established the lateral boundaries of the cortical visual areas. Retinotopic areas V1, V2 and V3 were manually defined over flattened meshes for each subject in each hemisphere using Brainvoyager's surface drawing tools (Figure 3.8). Obtained ROIs were used as "masks" to the analysis of regional cortical thickness.

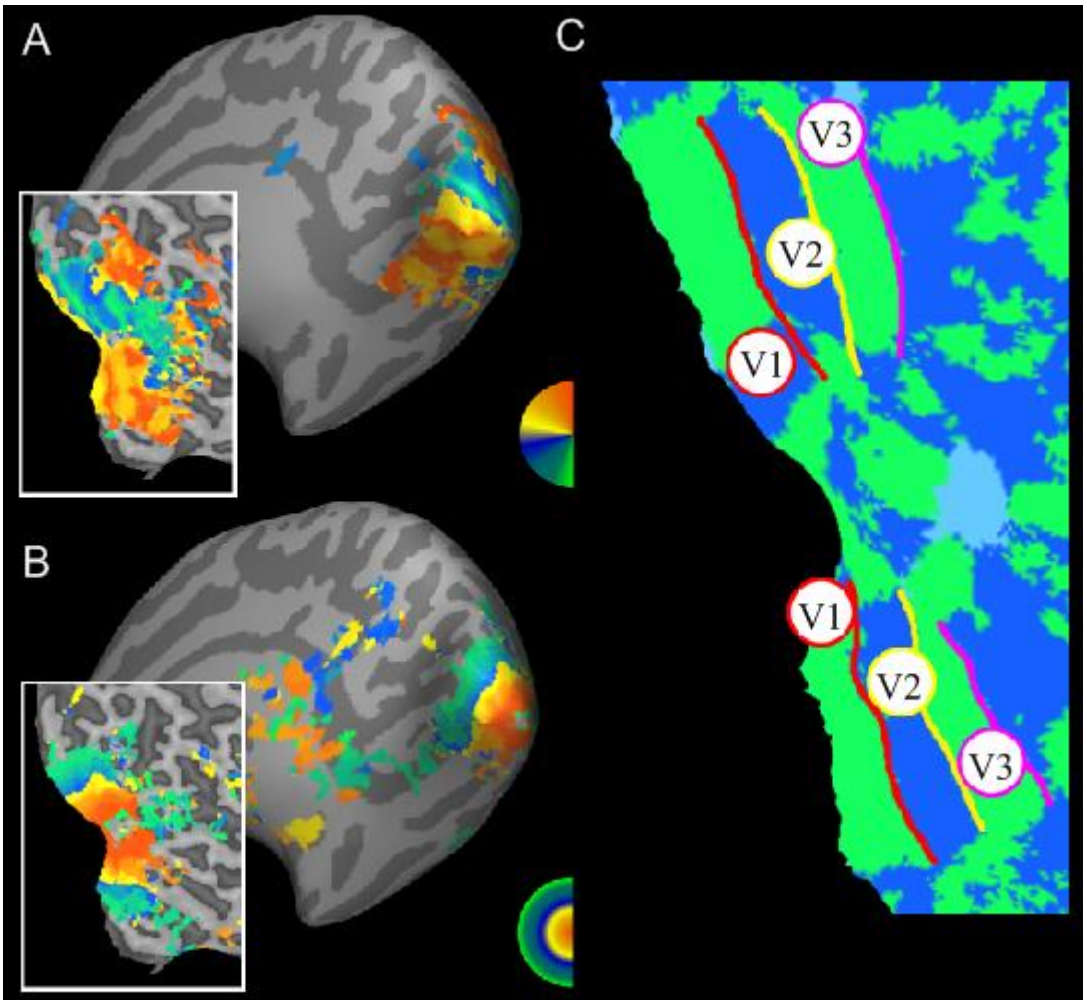

Figure 3.8. Retinotopic mapping on inflated and flattened meshes (right hemisphere of a control subject): (A) *polar angle* paradigm; (B) *eccentricity* paradigm and (C) Delineating early visual areas as regions-of-interest based on color coding of *polar angle* and *eccentricity* experiments.

PART III

RESULTS

CHAPTER 4

GENETICALLY INDUCED IMPAIRMENT OF RETINAL GANGLION CELLS IS LINKED TO EXTRASTRIATE CORTICAL PLASTICITY

4.1 SUMMARY

Leber hereditary optic neuropathy (LHON) is a maternally inherited mitochondrial disorder, which leads to initially silent visual loss due to RGC degeneration. The major aim of this study was to establish a link between features of silent retinal progressive impairment and cortical reorganization in a cohort of 15 asymptomatic patients harboring the 11778G>A mutation with preserved visual acuity and normal ocular examination (pre-clinical phase). Most of these patients showed a visual field with a constant pattern of a paracentral defect. To study plasticity evoked by clinically silent degeneration of RGC we only studied mutation carriers.

We phenotyped pre-clinical silent degeneration from the psychophysical, neurophysiological and structural points of view to understand whether retinal measures could be related to cortical reorganization, using pattern electrophysiology (RGC function was studied), chromatic CS along three chromatic axes and OCT to measure macular, RGC nerve fiber layer as well as inner and outer retinal layer thickness. We then performed correlation analysis of these measures with cortical reorganization as assessed by cortical magnetic resonance imaging (MRI) thickness measures in retinotopically mapped (using functional MRI) extrastriate visual cortex. We found that compensatory cortical plasticity occurring in V2 and V3 is predicted by thickness of macular RGC axonal layer. This was also the most discriminative measure between carriers and controls, as revealed by ROC curve analysis. Moreover we found that the substantial cortical reorganization that occurs in the carrier state can be used to provide statistical discrimination between carrier and normal groups to a level that is similar to measures of retinal dysfunction.

We conclude that cortical compensatory plasticity in visual areas V2 and V3 is triggered by pathology in RGC axons.

4.2 INTRODUCTION

Leber hereditary optic neuropathy (LHON) is a maternally inherited disease associated with mtDNA pathogenic point mutations (Carelli et al., 2007). This optic neuropathy is the most frequent mitochondrial disorder (Chinnery et al., 2002) and in over 90% of cases it is due to three mtDNA point mutations, respectively at position 11778G>A, 14484T>C and 3460G>A, affecting complex I subunit genes of the mitochondrial respiratory chain (Mackey et al., 1996; Man et al., 2002; Newman, 2005). LHON leads to degeneration of RGC and their axons in the optic nerve, with a selective loss of the smaller-caliber fibers of the papillomacular bundle in early disease stages (Sadun et al., 2000; Carelli et al., 2004).

In a pre-clinical phase, swelling of retinal nerve fiber layer (RNFL) may occur (Carelli et al., 2004; Yu-Wai-Man et al., 2009) as objectively documented by OCT. In this sense, unaffected carriers (pre-clinical phase) may show a thickened RNFL in temporal and inferior quadrants (Savini et al., 2005). On psychophysical testing, these also show evidence for subtle impairment of optic nerve function, as assessed by chromatic and achromatic CS (Quiros et al., 2006; Sadun et al., 2006; Ventura et al., 2007).

After clinical onset, the RNFL gradually degenerates and the endpoint is usually optic atrophy with permanent severe loss of central vision and relative sparing of papillary light responses (Carelli et al., 2004). A few studies using magnetic resonance (MR) spectroscopy have found a non selective and isolated involvement of the optic nerve and reported an abnormal mitochondrial energy metabolism in the occipital lobe of clinically affected patients (Cortelli et al., 1991; Barbiroli et al., 1995; Lodi et al., 2002). Using voxel-based morphometry (VMB), Barcella et al. (2010) have described a significant reduced grey matter volume in bilateral primary visual cortex, and reduced white matter volume in optic chiasm, optic tract and areas located in optic radiations, in LHON patients in well established retinal degeneration and clinical symptoms.

Interestingly, in the pre-symptomatic stage cortical thickness may actually be increased (d'Almeida et al., 2013), suggesting early compensatory plasticity that is lost when the disease becomes clinically established. Cortical plasticity is here defined as the capacity of the brain to adapt to changing demands by altering its structure (Lövdén et al., 2010; Lövdén et al., 2013). Recent studies have established a link between structural brain plasticity and changes in cortical thickness (Engvig et al., 2010; Lövdén et al., 2013). In that study, we used magnetic resonance imaging (MRI) to measure cortical thickness and functional MRI retinotopic mapping to define functionally cortical visual areas V1, V2 and V3 in unaffected mutation carriers (pre-clinical phase). We found that cortical thickness, in particular in extrastriate regions (V2, V3), was significantly higher in LHON carriers as compared to age-matched controls.

The major aim of this study was to test whether a link can be established between RGC impairment in Leber optic neuropathy and such cortical compensatory plasticity in extrastriate cortex. All our selected patients were mutation carriers (pre-clinical phase). Therefore, RGC degeneration is present, affecting their visual function, such as chromatic CS.

In summary, we analyzed the visual and cortical phenotype of asymptomatic genetically characterized LHON patients (unaffected carriers from the same pedigree) which also allowed to compare retinal and cortical markers in statistical classification of the LHON carrier status. We found that the RNFL status predicts cortical plasticity, as assessed by correlation analysis.

4.3 METHODS

4.3.1 PARTICIPANTS

A cohort of 15 asymptomatic LHON carriers from two generations of the same pedigree (mean age ± SD = 29.2 ± 13.4 years; age range [8-47]) was included in the study and was compared with a gender and age-matched control group (n = 24; mean age ± SD = 31.3 ± 13.5 years; age range [7-54]). Asymptomatic LHON patients underwent genetic analysis and the presence of mtDNA 11778G>A mutation was

confirmed in all family members (homoplasmic in eleven and heteroplasmic in four participants) (demographic characteristics are summarized in Table 4.1).

All participants were submitted to a complete ophthalmological examination, including best-corrected visual acuity (VA; decimal scale), slit lamp biomicroscopy, ocular tension measurement (Goldmann applanation tonometer) and fundus examination (Goldman lens). LHON carriers presented a normal ocular examination, good visual acuity (mean ± SD = 1.1 ± 0.1) and no fundus changes. In spite of the absence of a clinical diagnosis, visual field deficits were found. According to Octopus v311 normative database, we found 6 normal visual fields (20% of the total sample); the remaining 80% showed a mean defect (MDf) and/or a loss variance (LV) outside the normal range, with a constant pattern of paracentral defects (see Table 4.1 and Figure 4.1 for representative visual field defects).

Exclusion criteria included retinal and neurological diseases, diabetes even in the absence of retinopathy, significant media opacities, pseudophakic and aphakic eyes, and high ammetropies (sphere > ± 4D; cylinder > ± 2D).

This study and all procedures were reviewed and approved by the Ethics Commissions of the Faculty of Medicine of the University of Coimbra (*Comissão de Ética da Faculdade de Medicina da Universidade de Coimbra*) and were conducted in accordance with the Declaration of Helsinki. Written informed consent was obtained from participants older than 18 years of age and from parents/ guardians in the case of participants younger than 18 years of age and procedures of the study were fully explained.

Table 4.1. Demographic characteristics and clinical data of LHON carriers group.

Patient	mtDNA 11778G>A Mutation	Heteroplasmic mutational load (%)	Age (years)	Gender	Visual Acuity RE/LE		Visual Field MDf (dB) RE/LE		Visual Field LV (dB^2) RE/LE	
1	homoplasmic		47	M	1.2	1.2	-0.7	0.7	3.8	3.3
2	heteroplasmic	80.6	46	F	1.0	1.0	1.8	1.7	5.2	4.4
3	homoplasmic		43	F	1.0	1.0	2.8	3.8	4.9	10.3
4	homoplasmic		41	M	1.2	1.2	4.2	4.0	4.0	8.3
5	homoplasmic		40	F	1.0	1.0	4.0	4.4	3.1	6.6
6	homoplasmic		39	F	1.0	1.0	5.0	3.8	2.1	7.9
7	homoplasmic		37	F	1.2	1.2	1.8	0.9	5.2	5.1
8	heteroplasmic	78.8	30	F	1.2	1.2	7.0	7.8	10.8	9.1
9	heteroplasmic	78.0	21	M	1.2	1.2	5.5	7.8	32.3	40.4
10	homoplasmic		22	F	1.2	1.2	3.9	6.6	9.2	26.7
11	homoplasmic		17	M	1.2	1.2	3.3	5.0	10.9	24.1
12	homoplasmic		19	M	1.0	1.2	2.8	5.2	10.5	15.2
13	homoplasmic		10	M	1.0	1.0	4.1	6.9	6.3	13.7
14	heteroplasmic	67.0	18	F	1.2	1.2	7.8	7.6	9.2	6.7
15	homoplasmic		8	M	1.0	1.2	3.1	3.1	9.9	7.9

Note: M = male; F = female; RE = right eye; LE = left eye; MDf = mean defect; LV = loss variance

4.3.2 FUNCTIONAL ASSESSMENT

In this study, LHON carriers group and controls performed the following psychophysical and electrophysiological methods:

- Standard automated perimetry (Octopus version 311, Haag-Streit AG, Germany);
- Chromatic contrast sensitivity psychophysical test (CCT; Cambridge Research Systems Lda., CRS, Rochester, UK);
- Pattern electroretinogram (PERG; RETIport32, Roland Consult, Germany).

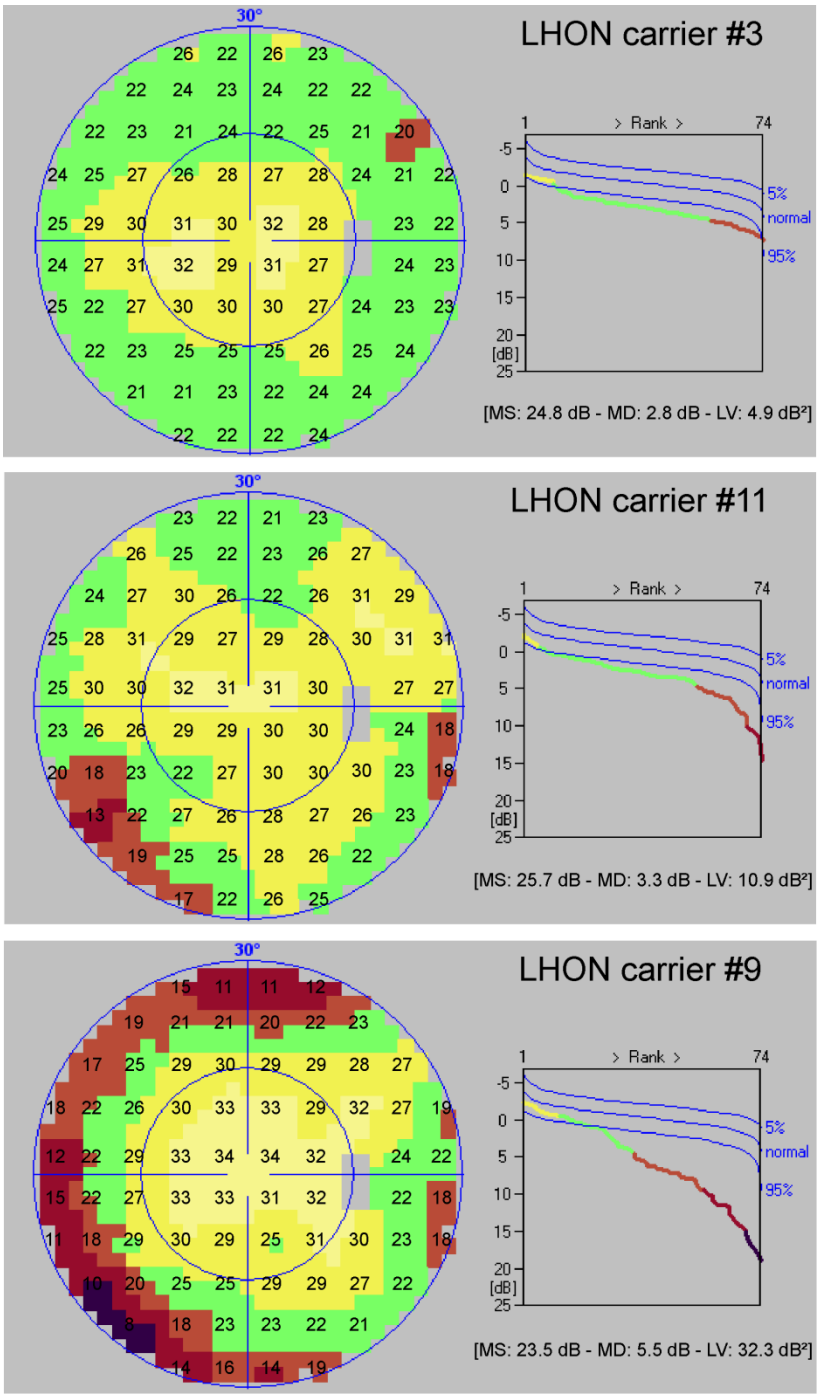

Figure 4.1. Representative visual field perimetric maps (color maps depict decibel scale) of LHON carriers. Note a constant pattern of a paracentral defect in visual fields with a relatively preserved sensitivity of central locations as illustrated in the cumulative defect curves.

4.3.3 STRUCTURAL ASSESSMENT

We have used a Spectralis SD-OCT software version 5.3.2 (Heidelberg Engineering, Heidelberg, Germany) to obtain peripapillary RNFL and macular thickness measurements. Through manual segmentation, we also determined the inner retinal layer (IRL), outer retinal layer (ORL) and macular RNFL thickness.

All patients and controls have also performed a Magnetic resonance imaging experience. The MRI data was acquired in a 3T scanner (Siemens Magnetom TrioTim 3T, Erlangen, Germany).

For detailed methods see Chapter 3 – Methodological overview.

4.3.4 STATISTICAL ANALYSIS

Statistical analysis was performed using statistical software packages (SPSS version 19.0 - SPSS Inc., Chicago, IL; and StatView - SAS, Cary, NC, USA). After verifying statistical assumptions using Shapiro-Wilk normality check and Levene homogeneity tests, comparisons between means were performed with multivariate General Linear Model based on Wilk's Lambda, with Sidak's adjustment for multiple comparisons. To prevent biases caused by violations of independence, we used the mean value of both eyes for all variables, since a significant interocular correlation was found (for control and LHON carrier groups). For cortical thickness analysis (each hemisphere was considered individually), age was setting as covariate (d'Almeida et al. 2013). Pearson coefficient was used for correlation analyses.

The Receiver Operating Characteristic (ROC) curve analyses were also performed using MedCalc version 12.2.1.0 (MedCalc Software, Mariakerke, Belgium) to determine sensitivities at a fixed specificity (approximatey 80%) for all tested parameters. The relative diagnostic accuracies of functional and structural tests were assessed by comparing areas under the ROC curves (AUC). Statistically significant differences between AUC were determined using the method of DeLong et al. (1988). Results with $p<0.05$ were considered statistically significant.

4.4 RESULTS

Evidence for impairment of Parvo and Koniocellular contrast sensitivity

We found a significant group effect on chromatic CS [$F_{(3,21)}$=3.876, p=0.024, η_p^2=0.356]. Chromatic thresholds were significantly higher in LHON carriers for protan (red) (p=0.008), deutan (green) (p=0.016) and tritan (blue) (p=0.010) axes, as compared to control participants (Figure 4.2).

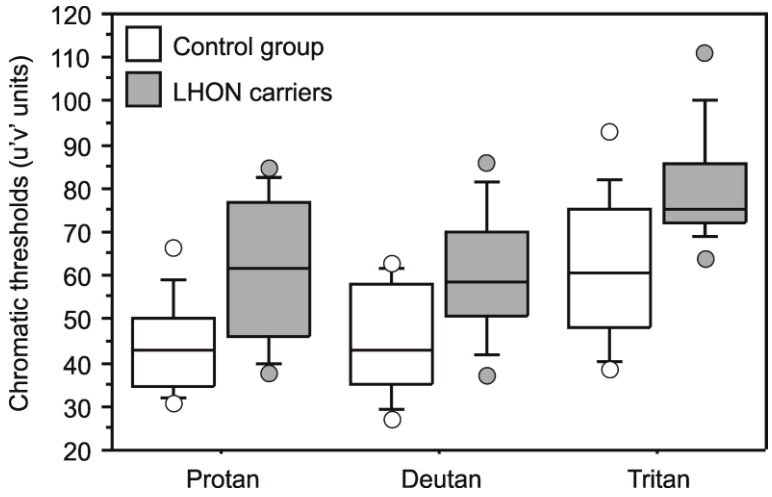

Figure 4.2. Chromatic contrast sensitivity thresholds. Significant impairment is observed for the three chromatic axes in patients. Note that higher chromatic thresholds are related to lower contrast sensitivity.

Assessment of RGC function using the pattern electroretinogram (PERG)

Surprisingly, we found a marginally significant group effect on PERG waves amplitude [$F_{(2,23)}$=3.200, p=0.059, η_p^2=0.218]. Higher amplitudes of P-50 (p=0.047) and N-95 (p=0.017) waves were found in LHON carriers, as compared to the control group (Figure 4.3; see also a representative example in Figure 4.4A). Implicit time of both waves was normal, as well as N-95/P-50 ratio.

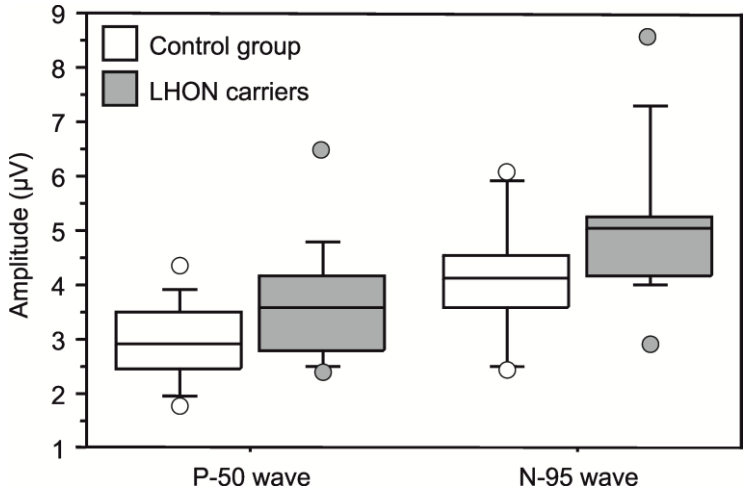

Figure 4.3. Ganglion cell function assessed by pattern ERG. LHON carriers show surprisingly higher amplitudes of P-50 and N-95 components of PERG than control group.

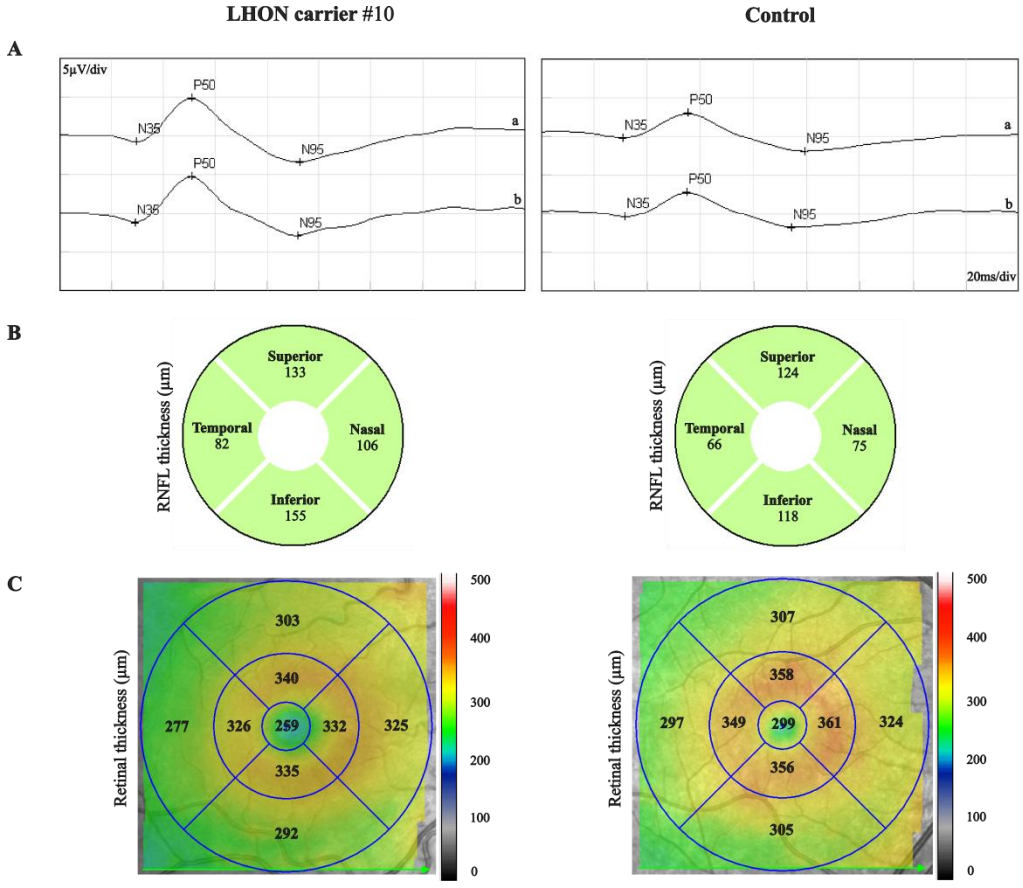

Figure 4.4. PERG plots (A), OCT – peripapillary RNFL (B) and OCT - retinal thickness (C) maps of a representative LHON carrier (#10) and a control subject. Note that carrier #10 presents an increase in amplitudes of both P-50 and N-95 waves [a and b, first and second measurement] (A), an increase in peripapillary RNFL thickness (B) and decreased retinal thickness (more evident in the most central rings) (C), as compared to the control.

Evidence for early swelling of papillomacular RNFL bundle

A significant group effect was not found on peripapillary RNFL thickness [$F_{(4,19)}$=2.364, p=0.090, η_p^2=0.332]. However, LHON carriers showed an increased RNFL thickness, which was significant for inferior (p=0.009) and temporal (p=0.027) quadrants (see Figure 4.5A and Figure 4.4B for a representative example of increased RNFL thickness in Leber carriers group).

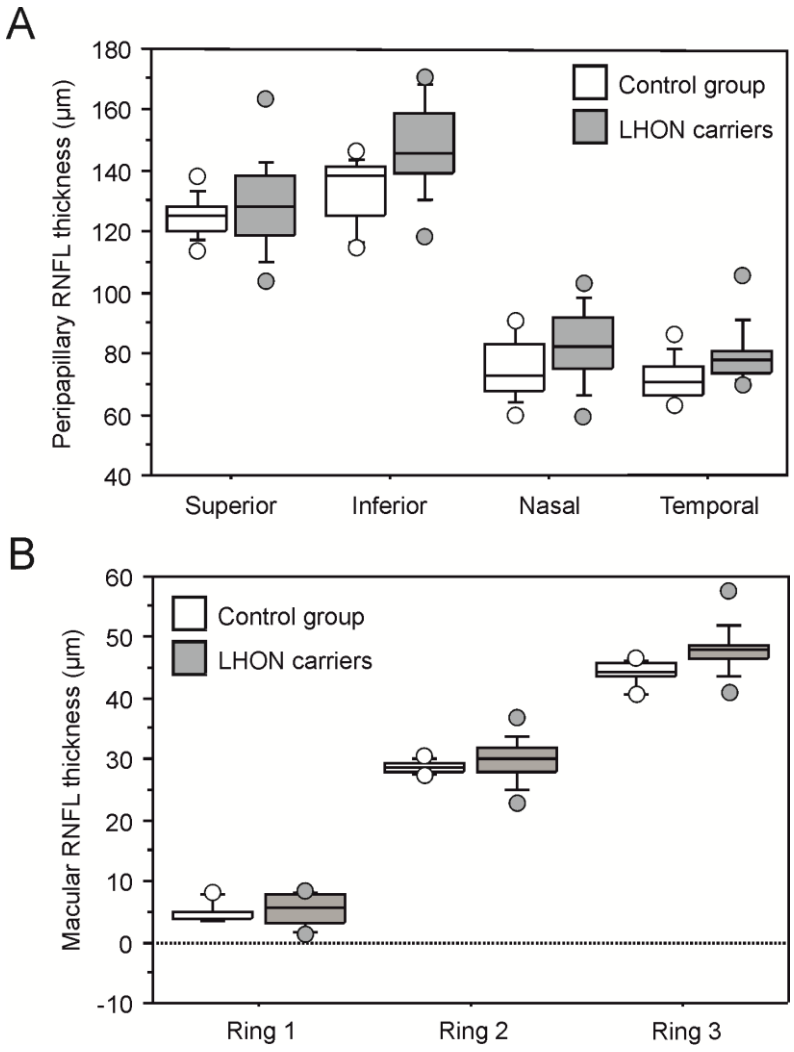

Figure 4.5. Pathophysiological RNFL swelling as an early change in LHON carriers. Peripapillary RNFL (inferior and temporal quadrants) (A) and macular RNFL thickness (ring 3) (B) are significantly increased in the LHON carrier group, comparing with controls.

Inner retinal layer, Macular retinal nerve fiber layer and Outer retinal layer thickness measured using Spectral Domain-OCT

We found a significant group effect on global macular thickness [$F_{(3,20)}$=9.066, p=0.001, η_p^2=0.576] and ORL thickness [$F_{(3,13)}$=3.246, p=0.057, η_p^2=0.428]. By the other hand, a group effect was not found for IRL and macular RNFL thickness.

Analysis by rings showed a significant decrease in global macular thickness for the most central rings [ring 1: p=0.013; ring 2: p=0.017] (Figure 4.6; Figure 4.4C, representative example of retinal thickness of LHON carrier and control groups).

We also found a decrease in outer retinal layer thickness for the most central rings [ring 1: p=0.005; ring 2: p=0.017], unlike the inner retinal layer that showed no differences between carriers and controls. On the other hand, we found the expected increase (due to the known pathophysiological swelling) in macular RNFL thickness (most peripheric ring) in Leber carriers [ring 3: p=0.044] (Figure 4.5B).

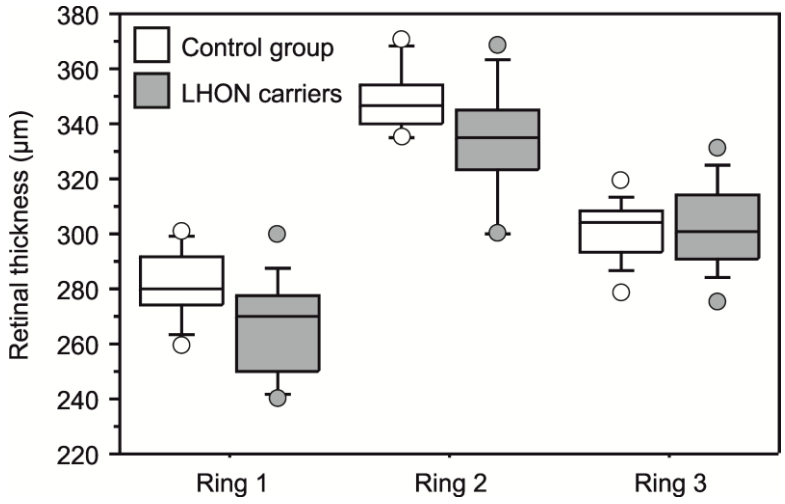

Figure 4.6. Retinal thickness assessed by SD-OCT. Macular thickness (most central rings) are significantly decreased in Leber carriers.

Cortical thickness of retinotopically defined visual areas using functional magnetic resonance imaging

Mean cortical thickness was calculated as the average of all vertices inside each functionally defined visual area V1, V2 and V3 from each subject hemispheres (d'Almeida et al., 2013).

We found a significant group effect on mean cortical thickness [$F_{(3,47)}$=3.156, p=0.0335, η_p^2=0.213]. LHON carriers had higher values of visual cortical thickness than controls, significant for V2 (p=0.0038) and V3 (p=0.0211) (age was setting as covariate) (Figure 4.7; see also Figure 4.8 for a representative example of cortical thickness of both groups). Figure 4.9 shows preserved functional retinotopic data confirming that we were indeed studying the cortical impact of subtle RGC functional and structural loss.

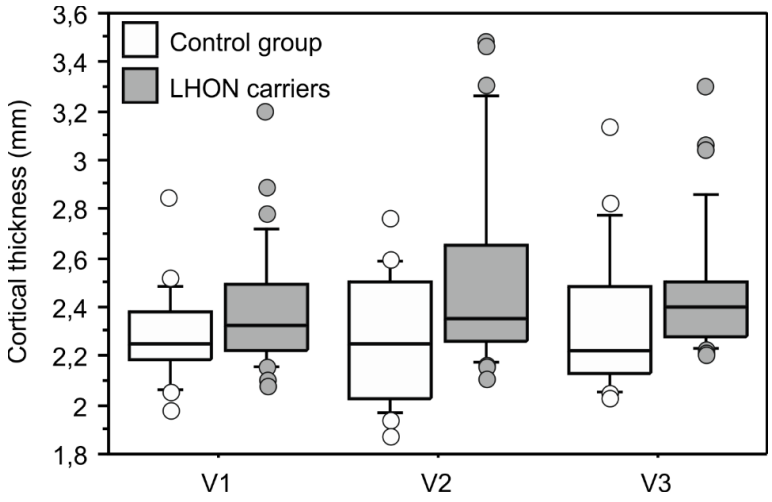

Figure 4.7. LHON carriers show an increased cortical visual areas thickness, being significant for V2 and V3.

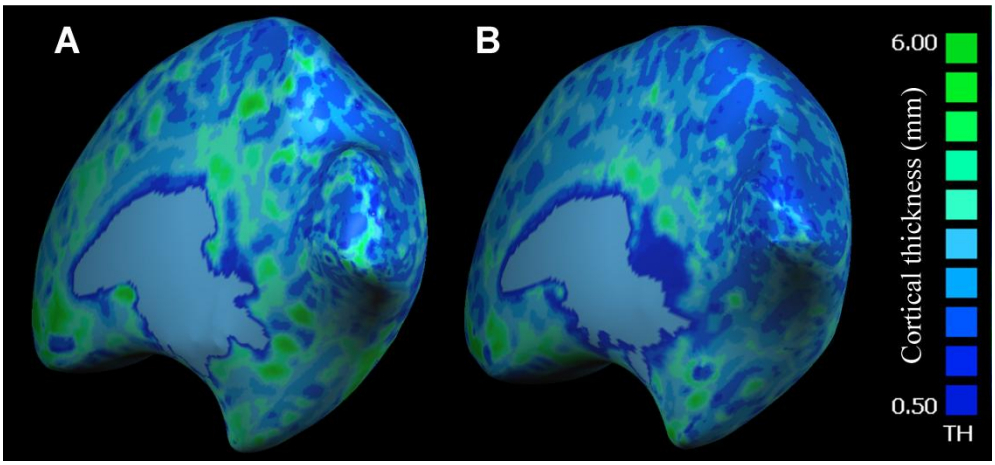

Figure 4.8. Representative cortical thickness map (in mm) of a LHON carrier #10 (A) and a control subject (B) as assessed by Magnetic Resonance Imaging. Note the higher cortical thickness values observed in Leber carrier patients in visual cortex.

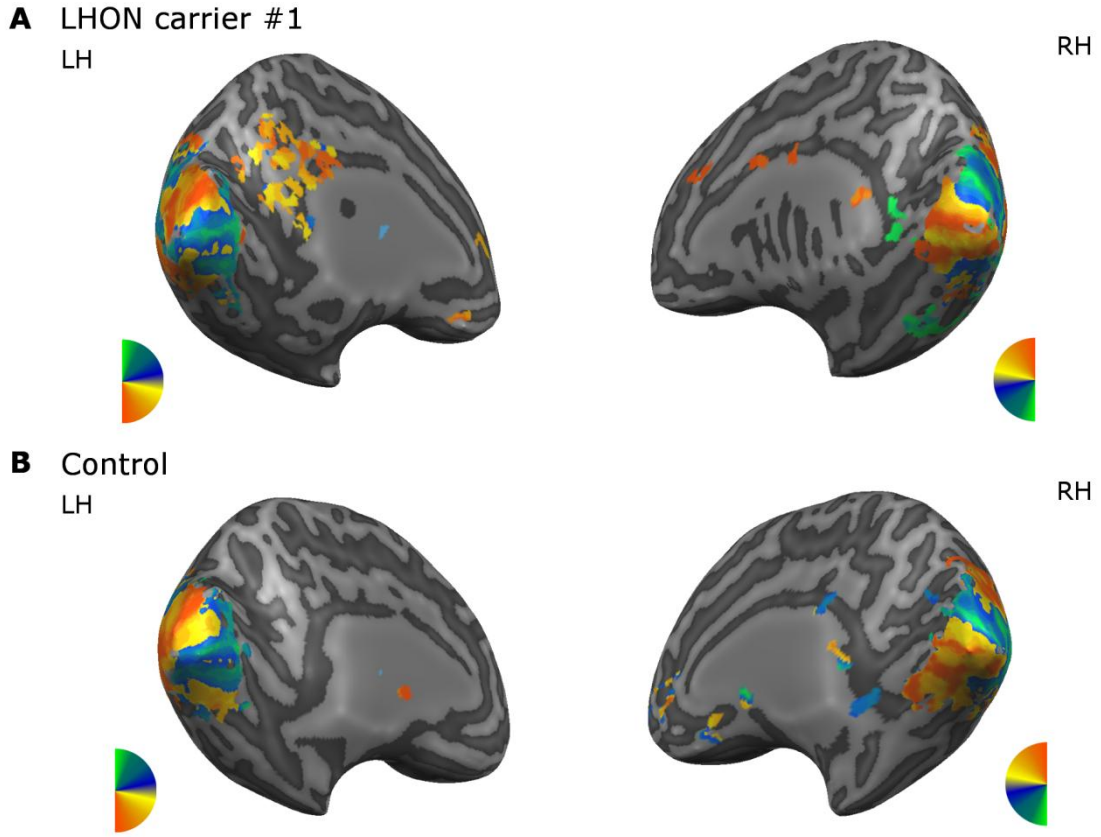

Figure 4.9. Representative functional retinotopic data of a LHON carrier #1 (A) and a control subject (B). These data show that retinotopic maps are intact despite the relative peripheral visual loss (LH, left hemisphere; RH, right hemisphere).

Correlation analyses for LHON carriers group

Significant correlations between retinal and cortical measures were found for asymptomatic LHON group: Macular RNFL thickness (ring 3) correlated positively with V2 (r=0.712, p=0.0075) and V3 (r=0.706, p=0.0083). These specific correlation patterns were not found in controls and were not observed for other measures.

Although we have not found a significant correlation between visual field measures and cortical data, we found a correspondence between the visual fields that showed the lowest sensitivity values for the most peripheral ring and highest cortical thickness values of extrastriate visual areas. We tested the consistency of this finding, by using median separation criteria, whether relative peripheral visual field loss was associated with increased extrastriate thickness. The proportion of concordant pairs was significantly larger than discordant pairs (p=0.004, binomial test).

We also found that the central ring of visual field correlated positively with the central ring of global macular thickness (r=0.601, p=0.0160) and with the central ring of ORL thickness (r=0.604, p=0.0360).

ROC Curve – Sensitivity/Specificity analysis

ROC sensitivity curves were generated for all included tests. At approximately 80% specificity, the highest sensitivities were found for OCT macular RNFL ring 3 (83%; cut-off: 46.25 µm); OCT outer retinal layer (75% for all rings; cut-off ring 1: 200.5 µm, ring 2: 180.25 µm, ring 3: 162 µm); OCT peripapillary RNFL inferior quadrant (73%; cut-off: 141.5 µm) and also for CCT Protan (69%; cut-off: 50.2 u'v' units) (for more details see Table 4.2).

Classification accuracy of the mutation carrier state by Areas Under the ROC Curve (AUC)

The AUC is an important measure that summarizes the diagnostic accuracy of each parameter. An AUC equal to 1 represents a perfect discrimination between healthy and mutation carrier groups, whereas an AUC of 0.5 represents chance discrimination. In our study, we found AUCs up to 0.903 (Table 4.2). The parameters that showed higher AUC value were macular RNFL ring 3 (AUC=0.903, p<0.0001), outer retinal

layer ring 1 (AUC=0.854, p=0.0001), CCT Protan (AUC=0.823, p<0.0001) and peripapillary RNFL inferior quadrant measures (AUC=0.800, p=0.0007).

Table 4.2. Areas under the receiver operating characteristic (ROC) curve (AUC) and associated 95% confidence interval (CI) are presented for CCT, PERG, OCT and MRI parameters. Sensitivities obtained for each parameter at approximately 80% specificity, and criterion values used for that specificity are also presented.

Parameters	**AUC**	**95% CI**	**p_value**	**Sensitivity/ Specificity (%)**	**Criteria for 80% Specificity**
CCT					
Protan	0.823	0.633, 0.940	<0.0001	69/80	50.2
Deutan	0.774	0.578, 0.909	0.0023	38/80	59.5
Tritan	0.792	0.598, 0.921	0.0012	38/80	76.95
PERG					
P-50 amp	0.710	0.512, 0.862	0.0325	53/82	3.48
N-95 amp	0.743	0.548, 0.886	0.0111	53/82	4.93
N-95/P-50 ratio	0.595	0.398, 0.772	n.s.	40/83	1.56
P-50 IT	0.510	0.318, 0.699	n.s.	13/83	52
N-95 IT	0.564	0.369, 0.746	n.s.	27/79	96
OCT					
Peripapillary RNFL sup	0.597	0.392, 0.780	n.s.	47/83	128.5
Peripapillary RNFL inf	0.800	0.602, 0.928	0.0007	73/83	141.5
Peripapillary RNFL nasal	0.694	0.489, 0.856	n.s.	40/83	85
Peripapillary RNFL temp	0.789	0.590, 0.921	0.0021	67/83	75.5
RT ring 1	0.775	0.574, 0.912	0.0026	67/83	272.5
RT ring 2	0.744	0.541, 0.891	0.0137	67/83	336.5
RT ring 3	0.508	0.310, 0.704	n.s.	27/83	290.13
RT sup	0.589	0.384, 0.773	n.s.	33/83	316.75
RT inf	0.606	0.400, 0.787	n.s.	47/83	312.5
RT nasal	0.656	0.449, 0.826	n.s.	47/83	325.5
RT temp	0.697	0.491, 0.858	n.s.	60/83	302.75
IRL ring 1	0.635	0.394, 0.835	n.s.	42/85	67
IRL ring 2	0.729	0.487, 0.900	n.s.	58/85	155
IRL ring 3	0.573	0.336, 0.788	n.s.	42/85	145.5
ORL ring 1	0.854	0.626, 0.970	0.0001	75/85	200.5
ORL ring 2	0.786	0.548, 0.935	0.0099	75/85	180.25
ORL ring 3	0.781	0.543, 0.932	0.0174	75/85	162
Macular RNFL ring 1	0.507	0.266, 0.746	n.s.	50/83	5
Macular RNFL ring 2	0.583	0.332, 0.806	n.s.	42/83	29.5
Macular RNFL ring 3	0.903	0.671, 0.990	<0.0001	83/83	46.25

MRI					
V1	0.608	0.462, 0.740	n.s.	40/82	2.40
V2	0.673	0.529, 0.796	0.0308	30/82	2.53
V3	0.706	0.563, 0.824	0.0136	33/82	2.49

Note: CCT = cambridge color test; PERG = pattern electroretinogram; OCT = optical coherence tomography; MRI = magnetic resonance imaging; RNFL = retinal nerve fiber layer; RT = retinal thickness; IRL = inner retinal layer; ORL = outer retinal layer; amp = amplitude; IT = implicit time; sup = superior; inf = inferior; temp = temporal; n.s. = not significant.

4.5 DISCUSSION

In this study, we established for the first time, a link between early RGC impairment at the axonal level (RNFL) in unaffected LHON carriers (mtDNA 11778G>A point mutation) and cortical compensatory plasticity in extrastriate cortex. Although we found cortical thickness changes specifically in extrastriate areas V2/V3, primary visual cortex actually tend to follow the same trend, but with a much smaller effect size. The novelty of our work is therefore that plasticity can occur even during clinically silent degeneration of RGC, and importantly, in the presence of relative peripheral visual loss, although retinotopic maps are intact. Interestingly, retinal and cortical biological markers can determine the presence of LHON carrier status, as measured by ROC analysis, suggesting that they are tightly coupled.

LHON carriers showed the expected RNFL swelling that is a pathophysiological marker of early damage in this condition, in particular for temporal and inferior quadrants (Savini et al., 2005). Since these patients show absence of leakage around the disk on fluorescein angiography (Smith et al., 1973; Nikoskelainen et al., 1996; Newman, 2005), the RNFL swelling corresponds to a pseudoedema. This pseudoedematous RNFL swelling is probably a consequence of impaired axoplasmic transport and compensatory increase of mitochondrial biogenesis (Barboni et al., 2010). Our findings are consistent with vulnerability of small axons of papillomacular bundle in a pre-clinical stage of this disease (Sadun et al., 2000). Taking into account that the thin RGC related papillomacular bundle is the anatomical substrate for color vision (Sadun et al., 2000; Carelli et al., 2004), this is consistent with the observation that parvo and koniocellular impairment occurs even in asymptomatic carriers before the

massive death stage and conversion to the acute stage (Sadun et al., 2006; Ventura et al., 2007).

We also found that global macular thickness was decreased, at the cost of the surprising and significant decrease in the outer retinal layer, suggesting that damage at the pre-ganglion level also occurs in the LHON carrier status. Our functional neurophysiologic correlates of RGC function (PERG) showed surprising response augmentation that was independent from the changes in RGC related layers (RNFL and IRL). In a previous study (Laguna et al., 2013) in Down syndrome (DS) and a trisomic mouse model of DS (Ts65Dn), we found that abnormally high responses may occur in a retina with abnormal cellularity at the RGC level. A recent study (Guy et al., 2014) reported a progressive decrease of PERG amplitude in asymptomatic Leber subjects. Since the physiology of pre-clinical stages may widely differ from after disease onset, future evaluations of these patients should be conducted in order to assess the RGC function over preclinical period until conversion to clinical stage.

Notably, we found that significantly increased cortical thickness measures (in particular in extrastriate cortex) in asymptomatic carriers (d'Almeida et al., 2013), were correlated with swelling of the macular RGC axons at the most peripheral ring**.** In other words, compensatory cortical plasticity occurring in V2 and V3 may be predicted by afferent changes in the thickness of RGC axonal layer (as measured by the segmented macular RNFL). This suggests that early retinal changes are reflected in retinotopically specific plasticity, as assessed by cortical thickness, which is a well established method to study structural plasticity (Kolb and Whishaw, 1998; Jiang et al., 2009; Engvig et al., 2010; Lövdén et al., 2013). Our findings are specific and other cortical regions show unchanged thickness.

It is relevant to point out that RNFL thickness was among the most sensitive classifiers of the mutation status (and with larger area under the ROC curve) further suggesting an important role in pre-clinical phases. Furthermore, our cortical measures were at least as discriminative as some of the retinal outcomes, suggesting that visual cortical plastic changes and reorganization (d'Almeida et al., 2013) go well in parallel with subtle axonal pathology. Although the link of RNFL status with cortical plasticity was assessed by correlation analysis, given that information flows unidirectionally from the retina to the cortex we argue that this link is likely causal.

We conclude that RGC impairment at the axonal level in Leber Optic Neuropathy carriers may trigger cortical compensatory plasticity in extrastriate cortex.

CHAPTER 5

A NEW APPROACH TO ASSESS EARLY PROGRESSIVE LOSS ACROSS MULTIPLE VISUAL CHANNELS IN THE NATURAL HISTORY OF GLAUCOMA

5.1 SUMMARY

Glaucoma is a progressive optic neuropathy characterized by death of RGC with subsequent visual loss and visual field defect. In this study, distinct subsets of RGC populations were tested using three novel two-alternative forced choice psychophysical discrimination tests between two separated peripheral, small moving single dots at four distinct meridians.

We aimed to evaluate the ability of new psychophysical tests, based on readily available hardware, to probe motion, achromatic and chromatic L, M and S cone contrast sensitivities, across the natural history of glaucoma. We assessed the sensitivity of these tests to detect functional damage at ocular hypertension stage, using ROC analysis. We also explored if eccentricity-related patterns of damage change with disease progression.

We studied a cohort of 43 participants, recruited from the glaucoma consultation of the University Hospital of Coimbra, which were divided across different groups: ocular hypertension (n = 16 eyes; mean age [SD] = 65.24 [7.01] years; IOP $\geq$ 21 mmHg, normal visual field and optic disc), glaucoma suspects (n = 15; mean age [SD] = 65.72 [10.71] years; normal visual field and optic disc changes) and primary open-angle glaucoma (n = 12; mean age [SD] = 68.79 [11.34] years; glaucomatous visual field defects and optic disc changes). These patients were compared with an age-matched group of controls (n = 15 eyes; mean age [SD] = 64.81 [8.24] years).

All tests showed significant correlation with disease progression (mean Rho ± SD = 0.708 ± 0.075; $p<0.0001$) and had sufficient power to discriminated glaucoma subgroups. Most tests using this design had large sensitivity (above 90% for a specificity of at least 80%) to detect functional damage at the ocular hypertensive stage.

Disease related eccentricity-related patterns of damage were also found, matching the expected pattern of progression. So, we concluded that our new psychophysical discrimination tests are capable to probe disease progression and to detect functional damage at ocular hypertension stage. It is therefore possible to customize psychophysical test software to detect early changes and monitor disease progression, including progressive loss of functional reserve, using relatively simple hardware.

5.2 INTRODUCTION

Glaucoma comprises a group of optic neuropathies related to the death or dysfunction of RGC leading to progressive visual loss. It was estimated that, in 2010, 60.5 million people had glaucoma, a figure which is expected to increase to 79.6 million in 2020 (Quigley and Broman, 2006).

The diagnosis and evaluation of progression in glaucoma is classically based upon the identification of structural defects - caused by RGC death (Harwerth and Carter-Dawson, 1999; Yücel et al., 2003), namely the thinning of the retinal nerve fiber layer and the cupping of the optic nerve head – as well as functional defects (Harwerth et al., 2010). These range from *de facto* visual field loss, classically assessed by SAP, to decreases in visual performance that are recognized to occur even at a pre-SAP loss stage (Johnson et al., 1993; Maddess et al., 1999; Bagga et al., 2006).

Such early functional defects depend on the relative degree of damage across the different central visual pathways for which two alternative hypotheses have been proposed. The preferential damage hypothesis states that glaucoma mainly targets large-fiber RGC (Quigley et al., 1987; Quigley et al., 1988) which mainly belong to the magnocellular pathway (Maddess and Henry, 1992; Maddess et al., 1999; Shabana et al., 2003; McKendrick et al., 2010). However, there is now histological evidence of damage in all three major visual pathways (Yücel et al., 2003) – magnocellular, parvocellular and koniocellular – as well as psychophysical evidence of early damage in red-green and blue-yellow channel processing, which are related to the parvocellular and koniocellular pathways (Pearson et al., 2001; Castelo-Branco et al., 2004). These findings support the reduced redundancy hypothesis (Johnson, 1994). This postulates

that the increased sensitivity of certain tests (Sample and Weinreb, 1990; Castelo-Branco et al., 2004; Fogagnolo et al., 2008) is explained by the stimulation of specific and therefore sparse subsets of ganglion cells, without the redundancy afforded by the other cell types. In other words, if a specific stimulus isolates a specific subset of ganglion cells, dysfunction of these cells will not be compensated due to lack of sufficient coverage. Therefore, even relative functional isolation of these ganglion cells types unmasks their smaller functional reserve (Anderson, 2006). Functional reserve is here defined as the amount of anatomical redundancy in terms of ganglion cell density in the retina and dendritic field overlap. Moreover, cell redundancy is also dependent on visual eccentricity, being lower in the periphery for all pathways (Silveira and Perry, 1991; Carelli et al., 2004). Taking these physiopathological concepts into account, we developed new psychophysical paradigms that try to provide some degree of relative functional isolation of specific ganglion cell populations, by testing independent visual functions, in order to attempt to relate glaucomatous neural losses with the natural history of the disease, from early to late stages. To this purpose we created discrimination tests that use small, moving and peripheral pairs of single dots which are targets for independent motion, achromatic contrast and chromatic contrast discrimination tests.

In summary, we aimed to evaluate the potential ability of novel tests to probe disease progression. We also assessed if these tests could detect functional damage at ocular hypertension stages, using sensitivity analysis. Finally, we also explored the putative relation between eccentricity and patterns of disease progression.

5.3 METHODS

5.3.1 PARTICIPANTS

Forty-three patients recruited from the glaucoma consultation of the University Hospital of Coimbra were included in the study and were compared with an age-matched group of controls (n = 15 eyes; mean age ± SD = 64.81 ± 8.24 years).

The clinical study sample consisted in 43 individuals in different stages of primary open-angle glaucoma (European Glaucoma Society, 2008): ocular hypertension (HT; n = 16 eyes; mean age ± SD = 65.24 ± 7.01 years; VA = 0.81 ± 0.16; SAP MD = -1.09 ± 0.84; C/D diameter = 0.36 ± 0.07), glaucoma suspects (GS; n = 15 eyes; mean age ± SD = 65.72 ± 10.71 years; VA = 0.83 ± 0.13; SAP MD = -1.01 ± 1.00; C/D = 0.62 ± 0.08) and primary open-angle glaucoma (G; n = 12 eyes; mean age ± SD = 68.79 ± 11.34 years; VA = 0.85 ± 0.12; SAP MD = -4.62 ± 0.66; C/D = 0.68 ± 0.06). Only the dominant eye of each subject was tested. ANOVA showed no significant age difference between groups.

Patients with primary open-angle glaucoma fulfilled the following criteria: C/D vertical diameter of 0.5 or more, MD visual field global index less than -2 dB (or <5% of confidence interval). Glaucoma suspects had C/D of 0.5 or more and normal visual fields (MD more than -2 dB or >5%, of confidence interval). Patients with HT showed an elevated IOP of 21 mmHg or more (on at least two occasions), without glaucomatous visual field defects (MD more than -2 dB or >5%, of confidence interval) or optic disc changes (C/D less than 0.5).

All participants underwent a complete ophthalmic examination, including best corrected VA obtained with Snellen chart, Goldmann applanation tonometry (IOP measurement), slit lamp examination of the anterior segment, gonioscopy, retinal examination and optic disc evaluation. All individuals were also submitted to a visual field examination (white-on-white SAP) using the 30-2 standard program of Humphrey automated field analyzer (SITA-Fast strategy; HFA II, Carl Zeiss Meditec, Dublin, CA) (*for details see Chapter 3 – Methodological overview*).

Exclusion criteria included the following: neuro-ophthalmologic diseases, retinal diseases, diabetes even in the absence of retinopathy, VA less than 0.6, known color vision disorders, pseudophakic and aphakic eyes, significant media opacities that preclude fundus examination, central corneal thickness outside normal range [540 ± 30 µm (European Glaucoma Society, 2008)], and high ammetropy (sphere > ±4D; cylinder > ±2D).

Informed consent was obtained from all subjects, in strict accordance with the institutional guidelines and approval of our local ethics committee and after explanation of the objectives of the study. The research was conducted in accordance with the tenets of the Declaration of Helsinki.

5.3.2 PSYCHOPHYSICAL METHODS

We developed three novel 2AFC psychophysical tests that required the comparison and discrimination of a visual features (motion, achromatic contrast and chromatic contrast) between two separated moving single dots (a reference dot and a target dot, which were presented in opposite hemifields).

For detailed psychophysical methods (set-up, general test features, staircase, motion discrimination test, achromatic contrast discrimination test and chromatic contrast discrimination test) see Chapter 3 – Methodological overview.

5.3.3 STATISTICAL ANALYSIS

Statistical analysis was performed using SPSS (IBM SPSS Statistics 21, IBM Corporation, NY, USA). After verifying the normality of the data across the study groups (Kolmogorov-Smirnov normality test), we used a parametric analysis (ANOVA between-group effects) for overall means comparison and Tukey HSD post-hoc test for multiple comparisons across groups. To study the effect of eccentricity within the same task performance, we used repeated measures ANOVA, with both main effects and linear trends adjusted to the least significant difference (LSD). We have also used a standard statistical measure of effect size (partial eta-squared, η_p^2) (Cohen, 1992). Spearman coefficient was used to correlate psychophysical thresholds and ordered subject grouping categories.

The Receiver Operating Characteristic (ROC) curve analyses were performed using MedCalc version 12.2.1.0 (MedCalc Software, Mariakerke, Belgium) to determine sensitivities at a fixed specificity (approximately 80%) for all tested parameters. The relative diagnostic accuracies of psychophysical tests were assessed by comparing areas under the ROC curves (AUC). Results with $p<0.05$ were considered statistically significant.

5.4 RESULTS

Correlation of Psychophysical Performance with Stage

We found that all of our new experimental measures strongly correlate with disease progression along stage defined by our study groups. Using Spearman Rank Correlation, a significant correlation between each and every psychophysical threshold and ordered subject grouping categories was found (mean Rho ± SD = 0.708 ± 0.075; $p<0.0001$ for all tests), revealing a distinct progressive visual performance profiling throughout the disease's natural history. Figure 5.1, which shows percentile distributions of measured threshold and their progressive ranking across our study groups, exemplifies these results using one meridian (90º) as an example from each test. Similar results were observed for the other meridians. The highest correlation coefficient originated from the M-cone test at meridian 45º / 15º of eccentricity (Rho = 0.820), while the lowest originated from the achromatic contrast test at meridian 0º / 7.5º of eccentricity (Rho = 0.553).

Despite our relatively small sample size, our effect sizes were large enough to perform group mean comparisons using ANOVA that revealed an overall significant difference between groups for every conducted test ($p<0.0001$ for every test except M-cone test at meridians 90º and 135º, with $p=0.014$). We conducted a post-hoc analysis for pair-wise comparisons using Tukey HSD post-hoc test, which showed significant differences ($p<0.05$) for all tests at every meridian between the control group and each patient group, except for achromatic contrast [meridian 0º and meridian 45º: control vs ocular hypertensive and control vs glaucoma suspect; meridian 135º: control vs ocular hypertensive comparison] and chromatic contrast M-cone test [meridians 45º and 135º: control vs ocular hypertensive comparison was marginally significant]. Overall, these results further reinforce the strength of our new paradigms to distinguish between control and patient groups. In particular the general differences between control and ocular hypertensive groups are noteworthy.

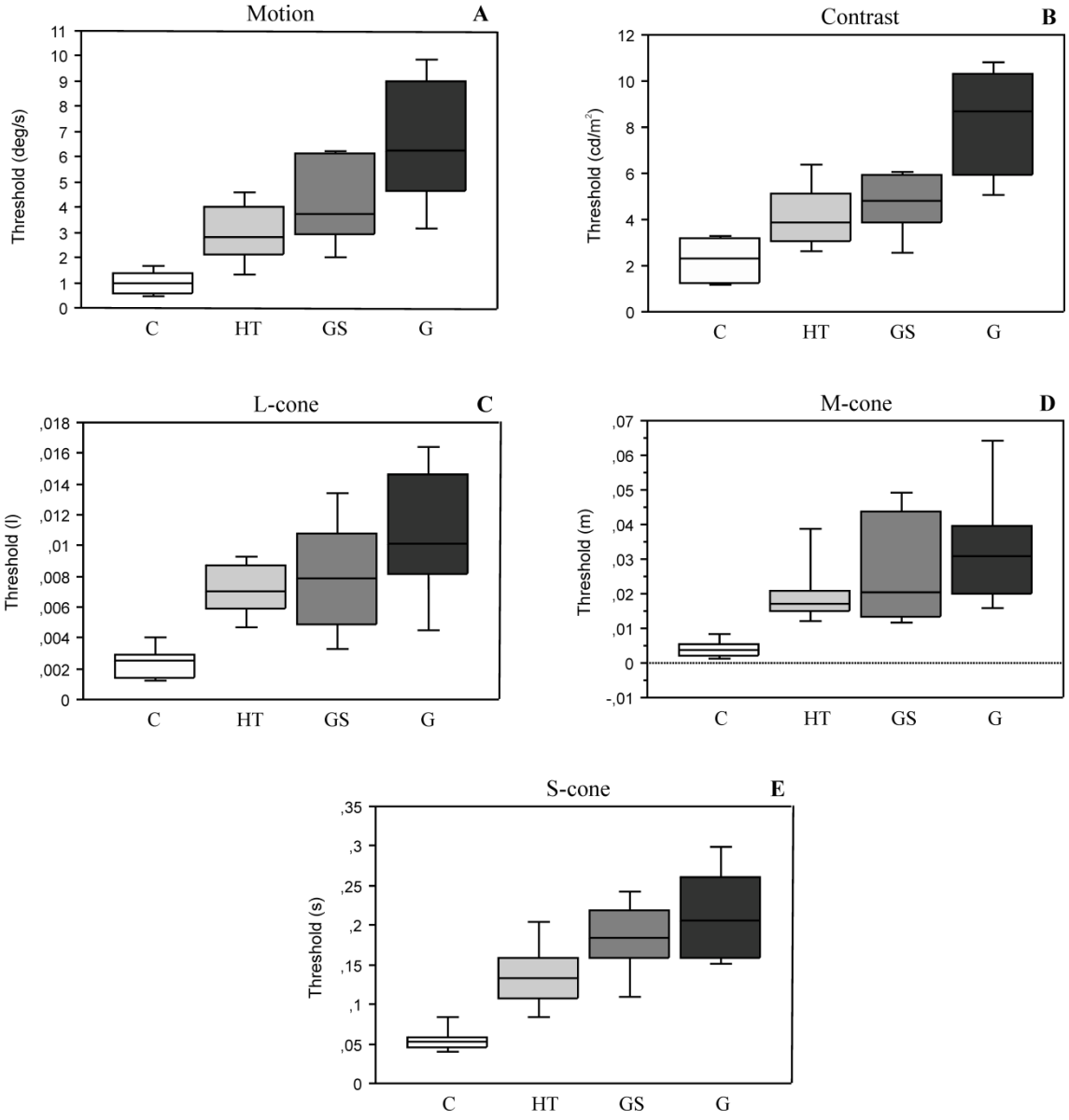

Figure 5.1. Representative examples of percentile box plots obtained for study groups (control, C; ocular hypertensive, HT; glaucoma suspect, GS; and glaucoma, G). Only the meridian 90º is presented (similar results are observed for the others). Bars depict 10th and 90th percentiles, the *top* and *bottom borders* of the boxes represent the 25th and 75th percentiles, and the *line* segment *inside* the boxes depicts the median. Box plots show a clear visual performance ranking along the disease progression stages, represented by each study group. All correlations in the presented tests between psychophysical thresholds and stage defining study groups were significant with $p<0.0001$: (A) Rho=0.785, (B) Rho=0.672, (C) Rho=0.626, (D) Rho=0.768 and (E) Rho=0.756.

The Effect of Eccentricity in Task Performance

Building on the fact that we repeated each test at different eccentricities, we also studied the effect of eccentricity on task performance. To this purpose, we used Repeated Measures ANOVA to assess if there were group related asymmetries of visual performance with increasing eccentricity and whether these asymmetries varied in a linear way. We studied this effect on the control, ocular hypertensive and glaucoma study groups and thresholds obtained at the 45º and 135º meridians (same eccentricity) were averaged.

First of all, under the conditions of our tests there were no significant eccentricity dependent differences in task performance in the control group for every test (motion test – p=0.324; achromatic contrast test – p=0.880; L-Cone test – p=0.426; M-Cone test – p=0.332; S-Cone test – p=0.079). Nonetheless, we observed a subtle, though not significant, increase in mean thresholds for the control group in the S-Cone test, which could suggest differential eccentricity-related performance within the physiological range.

Regarding the motion test, an interesting pattern was found. Ocular hypertensive subjects showed significantly varying performance with eccentricity (p=0.001). Moreover, this variation occurs in a linear fashion (p=0.001, partial eta-squared, η_p^2=0.605) meaning that visual performance is progressively impaired from the center to the periphery. However, in glaucoma subjects, there is a striking loss of significance in both mean differences (p=0.781) and linear trend (p=0.765) (see visual performance across eccentricities in Figure 5.2).

In the achromatic contrast test, as in the motion test, a significant mean difference across eccentricities was only found in the ocular hypertensive group (p=0.049), yet the linear trend was only marginally significant (p=0.051, η_p^2=0.231) (eccentricity effect in Figure 5.2).

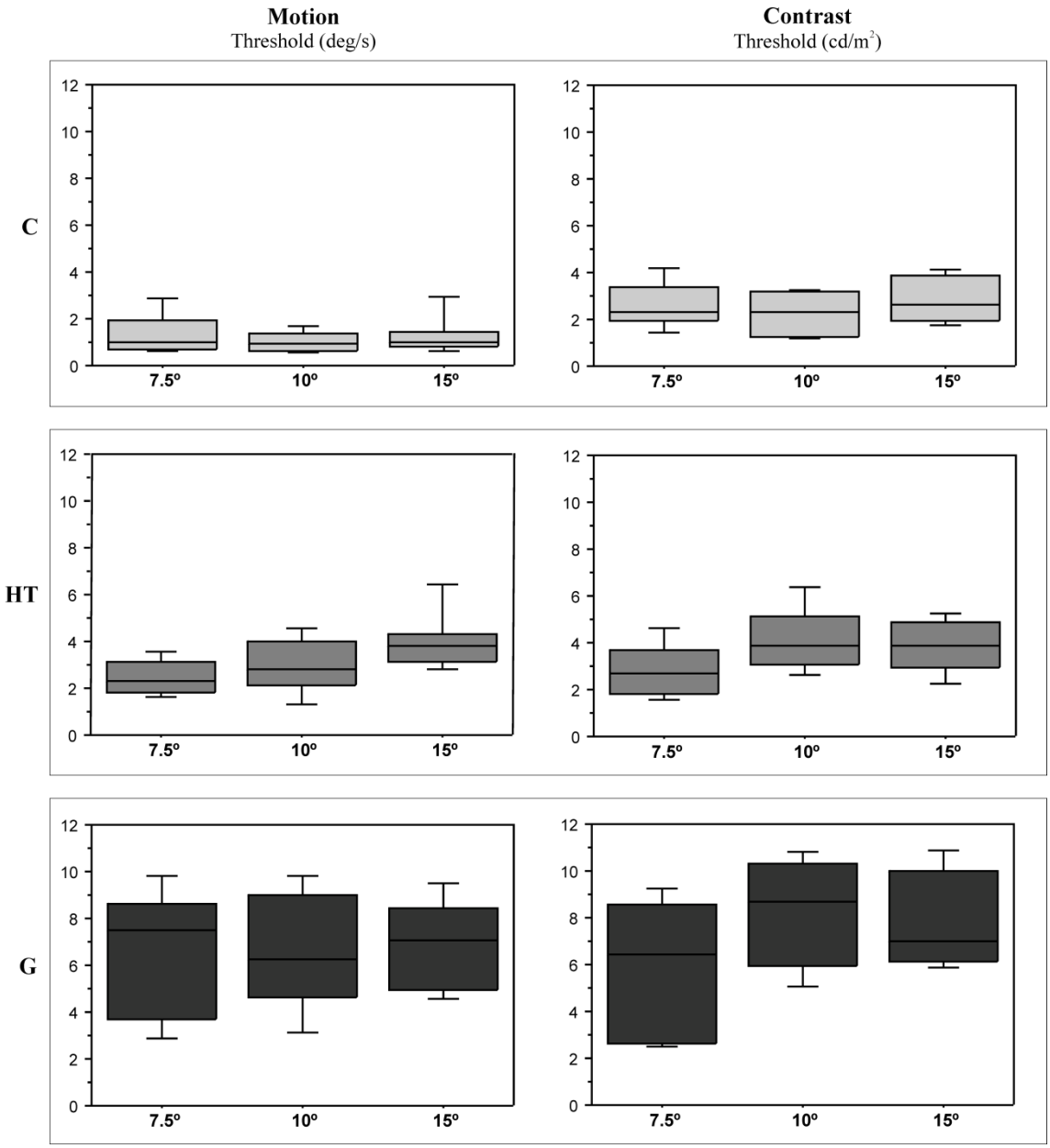

Figure 5.2. Visual performance across eccentricities (control, C; ocular hypertensive, HT; and glaucoma, G) for motion and achromatic contrast tests. A significant change across eccentricities was only found in the ocular hypertensive group for both tests with a linear trend clear and significant for motion tests and marginally significant for the achromatic contrast test, implying progressively more impaired visual performance from the center to the periphery.

Concerning the L-Cone, M-Cone and S-Cone tests, significant mean differences were found in ocular hypertensive subjects (p=0.031, p=0.001 and p=0.009, respectively) and it was true for linear trends (L-Cone: p=0.009, η_p^2=0.371; M-Cone: p=0.001, η_p^2=0.601; S-Cone: p=0.003, η_p^2=0.467). The glaucoma group showed

significant mean difference across eccentricities only for L-Cone and S-Cone tests (p=0.004 and p=0.049, respectively) with a linear pattern (p=0.001, η_p^2=0.716 and p=0.014, η_p^2=0.504, respectively) (see Figure 5.3, task performance across different eccentricities).

Given that none of the tests are comparing up vs down or left vs right (because reference and target and randomly swapped up and down or left right, in opposite hemifields), we do believe that meridian effects could only moderate the eccentricity effects into a small extent.

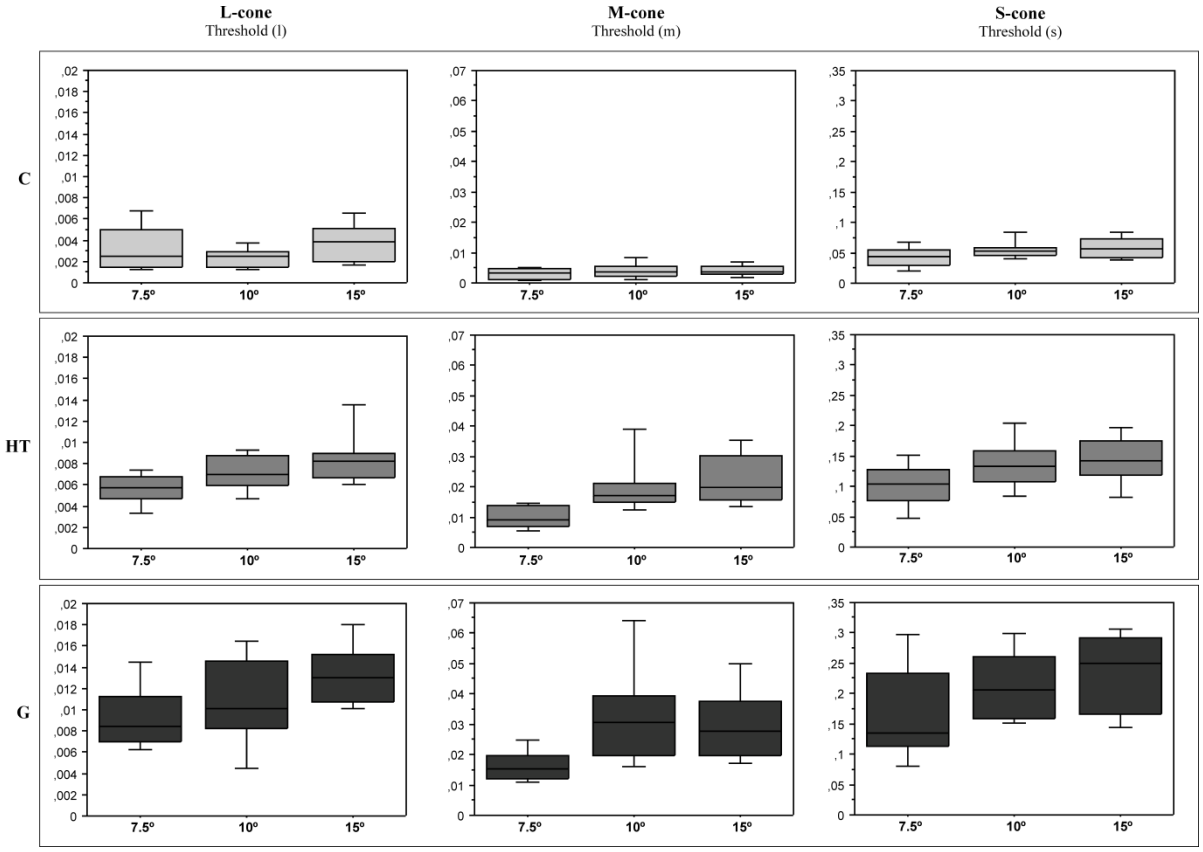

Figure 5.3. Task performance across eccentricities (control, C; ocular hypertensive, HT; and glaucoma, G) for the L, M and S-cone tests. A significant mean difference and linear trend across eccentricities were found for both the ocular hypertensive and glaucoma groups in the L and S-cone tests and only for the ocular hypertensive group in the M-cone test.

ROC Curve – Sensitivity/Specificity analysis

ROC curves were generated for all included tests, allowing to compare sensitivities at a fixed specificity. For *control vs ocular hypertensive* analysis, at 80% specificity, the highest sensitivity values (100%) were found for motion test at meridian 135º, L-cone test at meridian 90º, M-cone test at meridians 45º and 135º, and S-cone test at meridian 90º (for more details see Table 5.1A). Achromatic contrast tests showed the lowest sensitivity values. In analysis by meridians, we found that meridian 0º (7.5º of eccentricity) showed, as expected, the lowest sensitivity values for all tests.

For *control vs glaucoma* analysis, at 80% specificity, all tests reached 100% sensitivity, except for contrast test at meridian 0º (70% sensitivity). Whereas for *ocular hypertensive vs glaucoma* analysis, at 80% specificity, the highest sensitivity values (reaching 100%) were found for motion test at meridian 135º and contrast test at meridian 45º (for more details see Table 5.1B).

Table 5.1. Areas under the receiver operating characteristic (ROC) curve (AUC) and associated 95% confidence interval (CI) are presented for motion, achromatic contrast and chromatic contrast (L-cone, M-cone, S-cone) tests. Sensitivities obtained for each parameter at ~80% specificity, and criterion values used for that specificity are also presented for *control vs ocular hypertensive* (A) and *ocular hypertensive vs gaucoma* analysis (B).

(A)

Parameters	AUC	95% CI	p_value	Sensitivity/ Specificity (%)	Criteria for 80% Specificity
Motion test					
Meridian 0º	0.781	0.597, 0.909	0.0016	56/80	2.0052
Meridian 90º	0.925	0.771, 0.988	<0.0001	87/80	1.3967
Meridian 45º	0.965	0.828, 0.999	<0.0001	93/80	2.4319
Meridian 135º	0.915	0.757, 0.984	<0.0001	100/80	1.6783
Contrast test					
Meridian 0º	0.560	0.372, 0.737	n.s.	25/80	3.6252
Meridian 90º	0.798	0.616, 0.920	0.0006	68/80	3.2027
Meridian 45º	0.633	0.442, 0.798	n.s.	50/80	3.4585
Meridian 135º	0.702	0.512, 0.852	0.0408	43/80	3.8624
L-cone test					
Meridian 0º	0.794	0.611, 0.917	0.0004	62/80	0.0050
Meridian 90º	0.898	0.736, 0.977	<0.0001	100/80	0.0031
Meridian 45º	0.927	0.774, 0.989	<0.0001	93/80	0.0055
Meridian 135º	0.904	0.744, 0.980	<0.0001	93/80	0.0056

M-cone test					
Meridian 0º	0.933	0.783, 0.991	<0.0001	93/80	0.0049
Meridian 90º	0.948	0.803, 0.996	<0.0001	93/80	0.0056
Meridian 45º	0.987	0.865, 1.000	<0.0001	100/80	0.0056
Meridian 135º	0.992	0.872, 1.000	<0.0001	100/80	0.0054
S-cone test					
Meridian 0º	0.904	0.744, 0.980	<0.0001	87/80	0.0557
Meridian 90º	0.887	0.722, 0.972	<0.0001	100/80	0.0693
Meridian 45º	0.929	0.777, 0.990	<0.0001	93/80	0.0707
Meridian 135º	0.946	0.800, 0.995	<0.0001	87/80	0.0728

(B)

Parameters	**AUC**	**95% CI**	**p_value**	**Sensitivity/ Specificity (%)**	**Criteria for 80% Specificity**
Motion test					
Meridian 0º	0.931	0.760, 0.993	<0.0001	90/81	3.3387
Meridian 90º	0.869	0.679, 0.968	<0.0001	80/81	4.0955
Meridian 45º	0.847	0.652, 0.957	<0.0001	60/81	5.8459
Meridian 135º	0.931	0.760, 0.993	<0.0001	100/81	4.6336
Contrast test					
Meridian 0º	0.800	0.598, 0.930	0.0018	70/81	3.7594
Meridian 90º	0.925	0.751, 0.991	<0.0001	90/81	5.4287
Meridian 45º	0.978	0.830, 1.000	<0.0001	100/81	3.8624
Meridian 135º	0.825	0.626, 0.945	0.0001	40/81	6.4971
L-cone test					
Meridian 0º	0.869	0.679, 0.968	<0.0001	60/81	0.0074
Meridian 90º	0.737	0.529, 0.889	0.0509	60/81	0.0087
Meridian 45º	0.816	0.616, 0.939	0.0002	60/81	0.0095
Meridian 135º	0.841	0.645, 0.953	0.0001	80/81	0.0095
M-cone test					
Meridian 0º	0.844	0.648, 0.955	<0.0001	60/81	0.0134
Meridian 90º	0.869	0.679, 0.968	<0.0001	80/81	0.0159
Meridian 45º	0.894	0.710, 0.980	<0.0001	90/81	0.0159
Meridian 135º	0.784	0.580, 0.920	0.0028	60/81	0.021
S-cone test					
Meridian 0º	0.750	0.543, 0.897	0.0164	50/81	0.1338
Meridian 90º	0.884	0.698, 0.975	<0.0001	70/81	0.1632
Meridian 45º	0.869	0.679, 0.968	<0.0001	70/81	0.1932
Meridian 135º	0.831	0.634, 0.948	0.0002	70/81	0.171

Diagnostic accuracy by Areas Under the ROC Curve

The AUC is an important measure that summarizes the diagnostic accuracy of each parameter. An AUC equal to 1 represents a perfect discrimination between groups, whereas an AUC of 0.5 represents chance discrimination.

In *control vs ocular hypertensive* analysis, we found AUCs between 0.992 and 0.560 (Table 5.1A; see also a representative example of ROC curve in Figure 5.4A). The parameters that showed higher AUC values ($p<0.0001$) were M-cone test at meridians 135º (AUC = 0.992), 45º (AUC = 0.987) and 90º (AUC = 0.948) and motion test at meridian 45º (AUC = 0.965).

On the other hand, in *ocular hypertensive vs glaucoma* analysis (see a representative example of ROC curve in Figure 5.4B), we found AUCs between 0.978 and 0.737. Motion test at meridians 0º (AUC = 0.931) and 135º (AUC = 0.931) and contrast test at meridians 90º (AUC = 0.925) and 45º (AUC = 0.978) showed the higher AUC values ($p<0.0001$) (see Table 5.1B). Whereas the AUC values were always higher than 0.900 for all tests, for *control vs glaucoma* analysis.

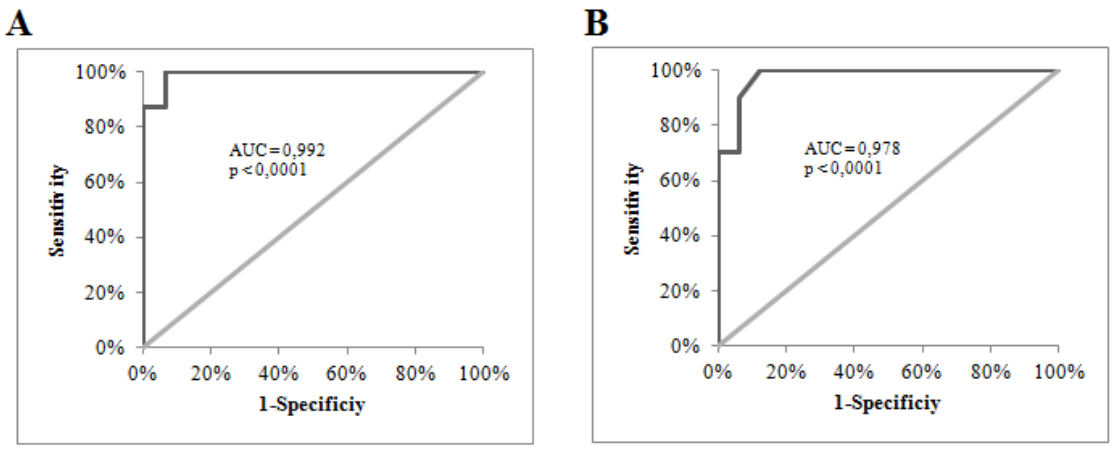

Figure 5.4. ROC curves. *Control vs ocular hypertensive* (A) and *ocular hypertensive vs glaucoma* analysis (B) are represented by the test/meridian with higher AUC value: M-cone test at meridian 135º (A) and contrast test at meridian 45º (B). Sensitivity is plotted on the y-axis and "1-specificity" on the x-axis.

5.5 DISCUSSION

This study addressed patterns of damage in different stages along the natural history of glaucoma, as measured by L -, M -, S - cone contrast thresholds, motion discrimination and achromatic CS. For this purpose, we have used discrimination (in the sense of comparison across two locations) instead of detection tasks. However, since in the chromatic tasks a color signal had to be detected in one of the locations, it was in this sense a detection task (which was desired given the standard hardware used).

Peripheral pairs of single dots, which were targets for motion, achromatic contrast and chromatic contrast discriminations, were used in order to isolate specific ganglion cell populations with a relatively small degree of redundancy (Wilson, 1970). Dots had constant local motion (except for direction and when speed was the dependent variable). Overall, this design optimized task difficulty, facilitated paradigm matching across tasks, and allowed us to test the visual system under low available information conditions (low redundancy).

We have reasons to believe that our motion test also embed directional judgments. This is because if a 24 deg/s dot moves 9.6 degrees in the 400 ms trial, it will change direction about 4 times (since it is on a 2 degrees path moving back), whereas the reference dot (5 deg/s) will travel 2 degrees and therefore will not change direction. So, in addition to the speed discrimination, the detection of how often the dot changes direction is also informative.

We found that impairment is concomitantly identified along all stages in motion, achromatic and chromatic channels. Moreover, sensitivity analysis showed that all tests discriminate well between early ocular hypertensive and the normal state, which is in line with our hypothesis that a smaller degree of test redundancy across pathways might allow for a greater diagnostic accuracy (Sample and Weinreb, 1990; Castelo-Branco et al., 2004; Fogagnolo et al., 2008). Concerning sensitivity analysis, and among the used psychophysical tests, motion (meridian 135º), L-cone (meridian 90º), M-cone (meridians 45º and 135º) and S-cone (meridian 90º) tests were quite sensitive to detect subtle damage at an early disease stage (ocular hypertension); unlike the achromatic contrast test, which showed the lowest sensitivity values and also the lowest diagnostic accuracy as measures by the area under the ROC curve. It is important to note that luminance noise used in chromatic S-, M- and L-cone tests ensured that the

measurement conditions were not biased (Castelo-Branco et al., 2004). On the other hand, the high discriminative power between the normal and hypertensive state is intriguing, given the fact that not all patients with well established ocular hypertension progress to the glaucomatous state (European Glaucoma Society, 2008). In fact, the conversion rate from untreated HT to glaucoma is only about 1% per year (Bach et al., 2006). So, future studies using these psychophysical tests are necessary to get insight on the role of these methods as potential predictors of conversion of ocular hypertension to the glaucoma state, allowing treat only the future converters, preferably well before the glaucomatous field defects develop and avoiding unnecessary side effects and expenditure from treatment of nonconverters.

Further, we found that psychophysical measures correlated significantly and strongly with the stage of the natural history of the disease, which suggest that each test at each meridian could be a potential marker of disease progression. Under the conditions of our test, differences across patient groups were surprisingly larger when compared with differences found in other studies (Silva et al., 2010).

On the other hand, since cell density redundancy is lower in the periphery for all pathways (Silveira and Perry, 1991), was expected that functional loss was more evident in the periphery, especially in early stages, such as in ocular hypertension. In fact, the eccentricity related patterns of damage with a significant linear trend for center versus peripheral decay were conspicuously observed in ocular hypertension and varied in a systematic manner across the natural history of the disease. This was particularly evident in the motion, achromatic contrast and M-cone tests that reveal clear a loss of these trends when progressing from the ocular hypertensive to the glaucoma stage. This finding is grounded on the hypothesis that with disease progression (in particular from ocular hypertension to glaucoma) there is a loss of central redundancy, weaning out the eccentricity-related asymmetries that were found on the ocular hypertensive group. This is particularly identifiable if visual tests are sufficiently sensitive. The model presented in Figure 5.5 attempts to explain the performance pattern found in motion, achromatic contrast and M-cone tests.

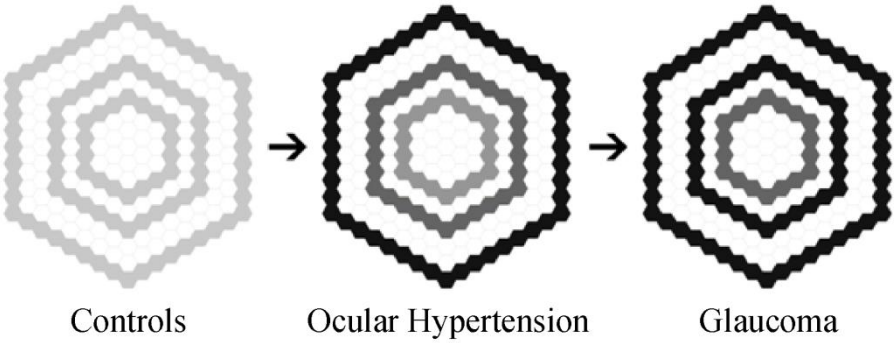

Figure 5.5. A theoretical model to explain visual performance asymmetries across disease stages, detected with sensitive testing conditions. The inner ring represents 7.5º of eccentricity, the middle ring 10º and the outer ring 15º. With disease progression, visual performance is progressively impaired from the periphery (smaller redundancy) to the center (larger redundancy), thereby maximizing eccentricity related asymmetries in the ocular hypertension stage. In glaucoma, the loss of central redundancy weans out this asymmetry.

Interestingly, concerning the L and S-cone tests, the linear trends found on the ocular hypertensive group were maintained in the glaucoma group. A possible explanation for these differences between the eccentricity related impairment patterns might be that with our tests we recruit different ganglion cells subsets from different visual channels, therefore probing visual performance at varying degrees of redundancy.

In summary, our work proves that disease mechanisms evolve similarly in color, motion and achromatic pathways in the natural history of glaucoma. The promising sensitivity of test measures identified through ROC analysis and their diagnostic potential should be confirmed and generalized in future studies with larger samples. Eccentricity related patterns of damage across the natural history of the disease and the clear early peripheral decay pattern for ocular hypertension, suggests that a progressive pattern of loss of functional reserve (globally defined as the available pool of cells within a channel) can be measured along the natural history of glaucoma.

CHAPTER 6

COMPARISON OF THE SENSITIVITY BETWEEN PSYCHOPHYSICAL, ELECTROPHYSIOLOGICAL AND STRUCTURAL TESTS IN ORDER TO DETECT EARLY DAMAGE IN OCULAR HYPERTENSION AND MONITOR GLAUCOMA PROGRESSION

6.1 SUMMARY

In this study we aimed to characterize early visual impairment of patients with HT, using psychophysical, electrophysiological and structural methods. We assessed the diagnostic accuracy of each test and compared their sensitivity for a fixed specificity. We also aimed to compare the sensitivity of these methods with three novel psychophysical discrimination tests designed by our group. The ability of these methods to probe disease progression was also analyzed.

Visual function was assessed in a cohort of 52 participants recruited from the glaucoma consultation: 18 patients with HT, 15 glaucoma suspects and 19 with primary open-angle glaucoma. Quantitative psychophysical methods were used to assess magno (FDT), parvo and koniocellular pathways (CCT), and RGC function was assessed by PERG. Ganglion cells axonal layer thickness was also obtained using OCT. These patients were compared with an age-matched group of controls (n=20).

An impairment in mean achromatic CS ($p=0.0298$) was found in patients with HT, as well as a reduced PERG N-95 wave amplitude ($p=0.0499$). Chromatic thresholds were significantly increased for protan, deutan and tritan axes ($p<0.03$) in these patients when compared with the control group. At approximately 80% specificity, the FDT showed the highest sensitivity to detect early functional damage (superior nasal quadrant, 66% sensitivity). We found a significant correlation between each test and ordered levels of disease progression ($0.487<Rho<0.706$, $p<0.0001$). The pattern of disease progression decline is approximately linear for all tests, but is more severe in OCT, namely RNFL thickness ($R_a^2 = 0.47$).

We found a relative damage of magno, parvo and koniocellular retinocortical pathways since the initial stage of the disease. The sensitivity of the currently available tests used is this study is lower comparing with our novel psychophysical discrimination tools (sensitivity above 90% for 80% specificity), suggesting that their smaller degree of test redundancy leads to a great ability to detect early glaucomatous damage. Finally, all these tests are potential markers of disease progression, since their measures correlate moderately with the ordered levels corresponding to natural course of glaucoma, especially in which concerns the structural test since its the pattern of decline is more pronounced.

6.2 INTRODUCTION

Glaucoma is a progressive optic neuropathy characterized by gradual death or dysfunction of RGC with subsequent vision loss (Weinreb and Khaw, 2004; Anderson, 2006). Traditional diagnostic approaches include criteria such as elevated IOP, visual field loss and optic nerve head atrophy. The elevated IOP is typically the dominant risk factor of the disease and current therapeutic strategies usually aim to reduce IOP as a way to slow vision loss, however many patients show a normal IOP and even when the IOP is well-controlled, disease progress may not be hindered (European Glaucoma Society, 2008). On the other hand, visual field loss does not appear at an early stage of the disease, meaning that when clinical features become evident in visual field testing (SAP), RGC loss can be as high as 50-60% (Harwerth et al., 1999; Harwerth and Quigley, 2006).

Taking this into account, current diagnostic techniques do not allow an early diagnosis, therefore jeopardizing treatment success. Thus, due to the irreversible RGC loss in glaucoma, it is particularly important that new tests are introduced into clinical practice that enable detection of early defects at a pre-SAP stage. Some studies performed in patients with ocular hypertension, involving psychophysical and electrophysiological tasks have been conducted in this direction, in order to test their potential ability to detect early damage (Casson et al., 1993; Johnson et al., 1993;

Brusini and Brusatto, 1998; Landers et al., 2000; Sample et al., 2000; Castelo-Branco et al., 2004; Monhart, 2007; Cellini et al., 2012).

To our knowledge, there are very few studies conducted in patients with ocular hypertension to evaluate the diagnostic accuracy of electrophysiological, psychophysical and structural tests simultaneously and their sensitivity to detect early changes (Bach et al., 2006). On the other hand, the ability of those functional and structural tests to monitor disease progression is often overlooked.

We attempted to address this issue using a cohort of patients with ocular hypertension, the most recognized risk factor for developing glaucomatous damage (Bahrami, 2006; Coleman and Miglior, 2008; Kwon et al., 2009). We aim to characterized early visual impairment in these patients, by means of functional (psychophysical and electrophysiological) and structural methods, using sensitivity analysis. We also aimed to assess the ability of these methods to probe disease progression. Visual performance in the different stages of the disease within multiple visual channels (magno, parvo and koniocellular pathways), using computerized psychophysical tests that access the function of visual pathways in an independent manner was therefore also analysed. Finally, we wanted to compare the sensitivity/specificity of these methods with three novel two-alternative-forced-choice psychophysical discrimination tests (motion, achromatic and chromatic L, M and S cone contrasts) designed by our group, which probe distinct subsets of retinal ganglion cell populations.

For this purpose, we used achromatic CS task using gratings with low spatial/ high temporal frequencies (probing magnocellular pathway) (Mateus et al., 2013; Silva et al., 2008), chromatic CS task using a static pattern of circles with a superimposed chromatic C-shaped ring (probing parvo and koniocellular pathways) (Castelo-Branco et al., 2004; Reis et al., 2012), an electrophysiological task assessing retinal ganglion cell (RGC) function (Reis et al., 2012) and optical coherence tomography to detect structural changes in peripapillary RCG axonal layer.

6.3 METHODS

6.3.1 PARTICIPANTS

The clinical sample consisted in 52 individuals recruited from the glaucoma consultation of the University Hospital of Coimbra: 18 patients diagnosed with ocular hypertension (HT; n = 18 eyes; mean age ± SD = 62.94 ± 7.38 years; VA = 0.83 ± 0.16; SAP MD = -1.00 ± 0.80; C/D diameter = 0.37 ± 0.08), 15 patients were glaucoma suspects (GS; n = 15 eyes; mean age ± SD = 65.36 ± 10.85 years; VA = 0.84 ± 0.14; SAP MD = -1.09 ± 0.89; C/D = 0.63 ± 0.07) and 19 patients with primary open-angle glaucoma (G; n = 19 eyes; mean age ± SD = 71.58 ± 11.48 years; VA = 0.74 ± 0.23; SAP MD = -10.07 ± 7.14; C/D = 0.71 ± 0.09). Patients were compared with an age-matched group of controls (n = 20 eyes; mean age ± SD = 64.45 ± 8.41 years). Only the dominant eye of each subject was tested. ANOVA showed no significant age difference between groups.

Patients with primary open-angle glaucoma fulfilled the following criteria: C/D vertical diameter of 0.5 or more, MD visual field global index less than -2 dB (or <5% of confidence interval). Glaucoma suspects had C/D of 0.5 or more and normal visual fields (MD more than -2 dB or >5%, of confidence interval). Patients with ocular hypertension showed an elevated IOP of 21 mmHg or more (on at least two occasions), without glaucomatous visual field defects (MD more than -2 dB or >5%, of confidence interval) or optic disc changes (C/D less than 0.5).

All participants underwent a complete ophthalmic examination, including best corrected VA obtained with Snellen chart, Goldmann applanation tonometry (IOP measurement), slit lamp examination of the anterior segment, gonioscopy, retinal examination and optic disc evaluation. All individuals were also submitted to a visual field examination (white-on-white SAP) using the 30-2 standard program of Humphrey automated field analyzer (SITA-Fast strategy; HFA II, Carl Zeiss Meditec, Dublin, CA).

Exclusion criteria included the following: neuro-ophthalmologic diseases, retinal diseases, diabetes even in the absence of retinopathy, VA less than 0.6, known color vision disorders, pseudophakic and aphakic eyes, significant media opacities that preclude fundus examination, central corneal thickness outside normal range (540 ± 30 µm), and high ammetropy (sphere > ±4D; cylinder > ±2D).

Informed consent was obtained from all subjects, in strict accordance with the institutional guidelines and approval of our local ethics committee and after explanation of the objectives of the study. The research was conducted in accordance with the tenets of the Declaration of Helsinki.

6.3.2 FUNCTIONAL ASSESSMENT

In this study, participants performed the following psychophysical and electrophysiological methods:

- Standard automated perimetry (Humphrey automated field analyzer, HFA II, Carl Zeiss Meditec, Dublin, CA);
- Achromatic contrast sensitivity perimetry (FDT; Humphrey Matrix perimeter, Welch Allyn, Skaneateles, NY; Zeiss – Humphrey, Dublin, CA);
- Chromatic contrast sensitivity psychophysical test (CCT; Cambridge Research Systems Lda., CRS, Rochester, UK);
- Pattern electroretinogram (PERG; RETIport32, Roland Consult, Germany).

6.3.3 STRUCTURAL ASSESSMENT

We have used a Spectralis SD-OCT software version 5.3.2 (Heidelberg Engineering, Heidelberg, Germany) to obtain peripapillary RNFL measurements.

For detailed methods see Chapter 3 – Methodological overview.

6.3.4 STATISTICAL ANALYSIS

Statistical analysis was performed using SPSS statistical software package (IBM SPSS Statistics 21, IBM Corporation, NY, USA). After verifying the normality of the data across the study groups (Kolmogorov-Smirnov normality test and Levene homogeneity test), we applied a parametric analysis for overall means comparisons [multivariate analysis of variance (ANOVA)] and Fisher HSD post-hoc test for multiple comparisons. Spearman coefficient was used to correlate each quantitative test parameter and ordered subject grouping categories. When applicable, functional and structural data was fit with linear regression model and the adjusted coefficient of determination (R_a^2) was used as an indicator of goodness of fit.

To study the effect of eccentricity across achromatic contrast sensitivity channel, we used repeated measures ANOVA, with both main effects and linear trends adjusted to the least significant difference (LSD). We have also used a standard statistical measure of effect size (partial eta-squared, η_p^2).

The ROC curve analyses were performed using MedCalc version 12.2.1.0 (MedCalc Software, Mariakerke, Belgium) to determine sensitivities at a fixed specificity (approximately 80%). Since the classification of patients was based on the results of SAP and optic nerve head excavation, these two parameters were not used to compare sensitivities.

The relative diagnostic accuracies were assessed by comparing areas under the ROC curves (AUC). Results with $p<0.05$ were considered statistically significant.

6.4 RESULTS

Achromatic contrast sensitivity to probe Magnocellular pathway

We found a significant group effect on mean contrast sensitivity [$F_{(3,75)} = 23.86$, $p<0.0001$], mean deviation [$F_{(3,75)} = 20.22$, $p<0.0001$] and pattern standard deviation [$F_{(3,75)} = 12.23$, $p<0.0001$]. For MS and MD, post-hoc tests (corrected for multiple comparisons) revealed significant differences between all groups ($p<0.04$), except for HT vs GS (see Figure 6.1 and Figure 6.2A for a representative example); for PSD, post-

hoc tests showed only significant differences between C and G ($p<0.0001$), HT and G ($p<0.0001$), GS and G ($p=0.0001$).

Furthermore, a moderate correlation between MS and ordered subject grouping categories was found (MS: Rho = -0.542, $p<0.0001$), whereby CS performance declines with ordered levels of glaucoma progression. We also found moderate correlations between MD/PSD and clinical stages (MD: Rho = -0.585, $p<0.0001$; PSD: Rho = 0.510, $p<0.0001$). Then, we applied a linear regression to data to investigate the presence of linear trends and using this approximation found that mean CS decreases linearly 3.26 dB per clinical stage [MS: *y=33.26-3.26*clinical stage*, $F(1,77) = 52.87$, $\mathbf{R_a^2} = 0.40$, $p<0.0001$; MD: *y=9.37-4.56*clinical stage*, $F(1,77) = 33.14$, $\mathbf{R_a^2} = 0.39$, $p<0.0001$; PSD: *y=2.41+0.97*clinical stage*, $F(1,77) = 26.87$, $\mathbf{R_a^2} = 0.25$, $p<0.0001$].

We also studied the effect of disease progression in terms of eccentricity and its loss was around 3.41/3.58 dB per clinical stage for the most central locations [Zone 1: *y=35.95-3.41*clinical stage*, $F(1,77) = 39.25$, $\mathbf{R_a^2} = 0.33$, $p<0.0001$; Zone 2: *y=34.89-3.58*clinical stage*, $F(1,77) = 50.53$, $\mathbf{R_a^2} = 0.39$, $p<0.0001$] and was less pronounced in the most peripheral location, around 3.16 dB [Zone 3: *y=32.60-3.16*clinical stage*, $F(1,77) = 48.95$, $\mathbf{R_a^2} = 0.39$, $p<0.0001$]. Along visual field quadrants, CS decreases between 2.94 dB and 3.77 dB per clinical stage [ST: *y=33.65-3.77*clinical stage*, $F(1,77) = 61.19$, $\mathbf{R_a^2} = 0.44$; SN: *y=33.01-3.33*clinical stage*, $F(1,77) = 35.74$, $\mathbf{R_a^2} = 0.31$; IN: *y=32.69-3.02*clinical stage*, $F(1,77) = 39.54$, $\mathbf{R_a^2} = 0.33$; IT: *y=33.22-2.94*clinical stage*, $F(1,77) = 37.40$, $\mathbf{R_a^2} = 0.32$; $p<0.0001$ for all cases].

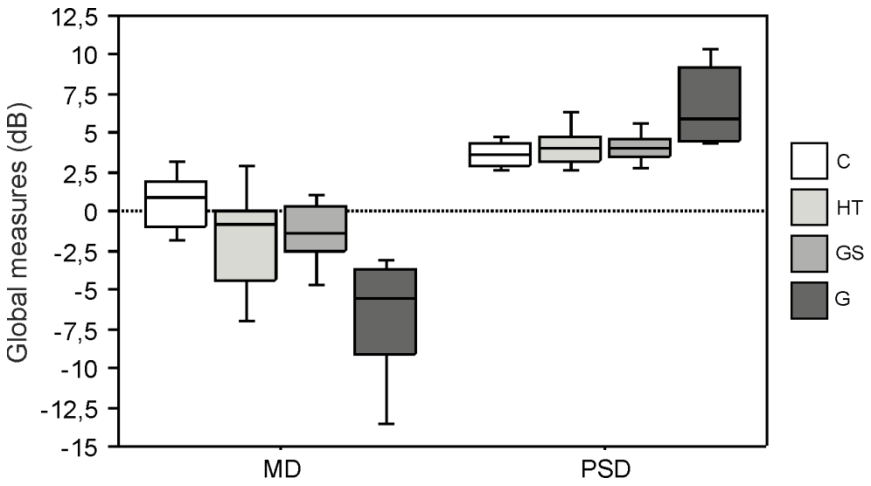

Figure 6.1. Achromatic contrast sensitivity, expressed in FDT global measures (MD – mean deviation; PSD – pattern standard deviation), along the disease progression stages (control, C; ocular hypertensive, HT; glaucoma suspect, GS; and glaucoma, G). Bars depict 10th and 90th percentiles, the *top* and *bottom borders* of the boxes represent the 25th and 75th percentiles, and the *line* segment *inside* the boxes depicts the median.

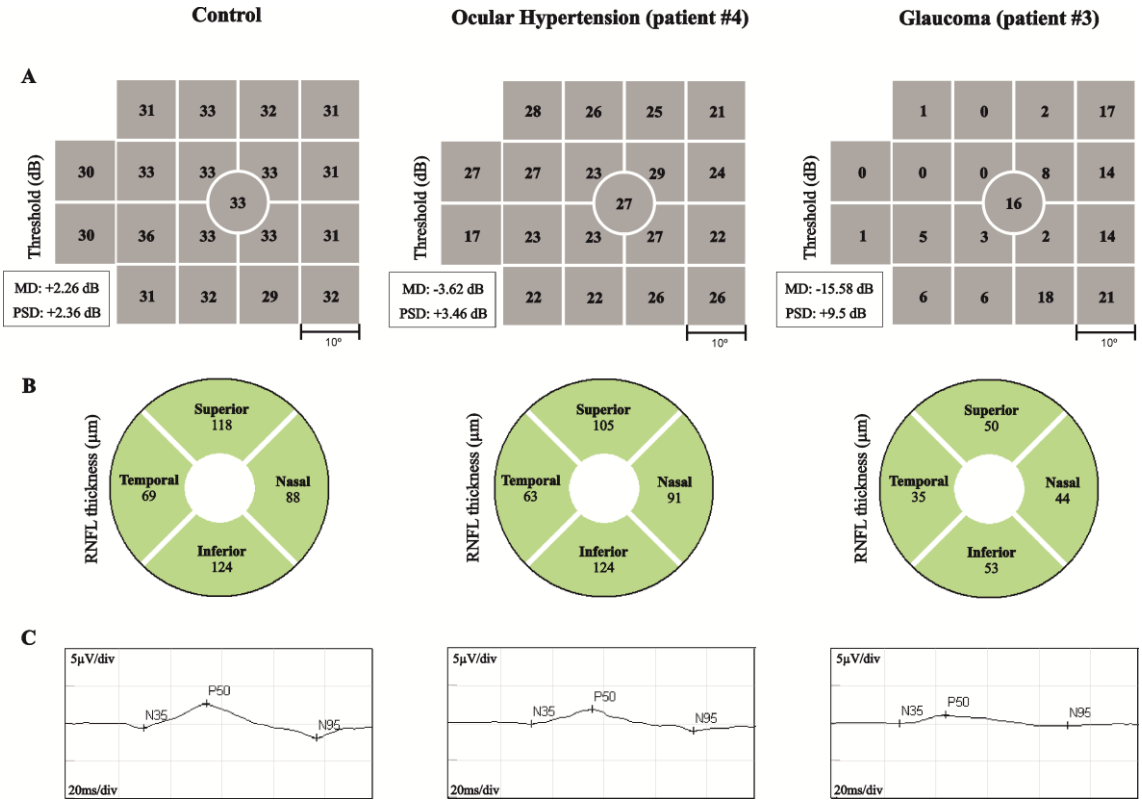

Figure 6.2. FDT perimetry output (A), OCT – peripapillary RNFL thickness map (B) and PERG plots (C) of representative control, ocular hypertensive (#4) and glaucoma (#3) cases. Note the progressive impairment in all measures with disease progression, except for peripapillary RNFL thickness that showed no differences between the control subject and ocular hypertensive patient.

Chromatic contrast sensitivity to assess Parvo and Koniocellular pathways

We found a significant group effect on chromatic CS for protan (red) [$F_{(3,72)}$ = 4.485, p=0.0061], deutan (green) [$F_{(3,72)}$ = 4.401, p=0.0067] and tritan (blue) [$F_{(3,72)}$ = 7.055, p=0.0003] cone confusion axes. Concerning post-hoc tests, we found significant differences between C and HT (p<0.03), C and G (p<0.001), HT and G (p<0.008), GS and G (p<0.02), for all chromatic axes (Figure 6.3).

Using Spearman correlation analysis, a significant correlation between chromatic thresholds and ordered subject grouping categories was found (protan: Rho = 0.598; deutan: Rho = 0.594; tritan: Rho = 0.658; p<0.0001). This means that chromatic thresholds increase with disease progression. Note that high chromatic thresholds relate to low CS. In this sense, through the linear regression analysis we found that chromatic thresholds increase linearly (corresponding to a contrast sensitivity decline) 37.86, 38.96 and 51.63 u'v' units per clinical stage, for protan, deutan and tritan axes, respectively [Protan: *y=-3.84+37.86*clinical stage*, F(1,74) = 10.22, R_a^2 = 0.11, p=0.002; Deutan: *y=-5.27+38.96*clinical stage*, F(1,74) = 10.61, R_a^2 = 0.11, p=0.0017; Tritan: *y=4.31+51.63*clinical stage*, F(1,74) = 18.10, R_a^2 = 0.19, p<0.0001].

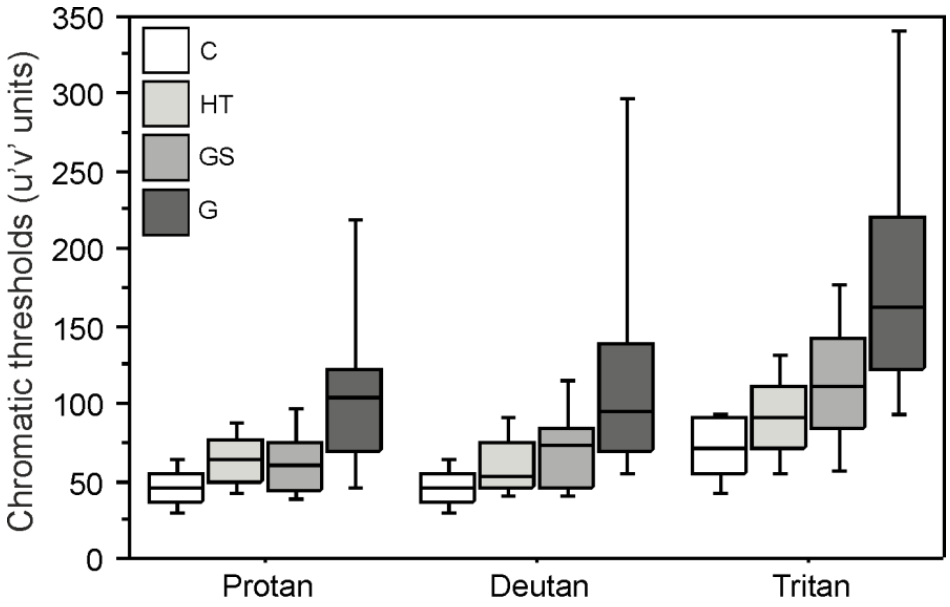

Figure 6.3. Chromatic contrast sensitivity performance over clinical stages (control, C; ocular hypertensive, HT; glaucoma suspect, GS; and glaucoma, G). Note that higher chromatic thresholds are related to lower contrast sensitivity.

Objective analysis of RGC axonal damage using Optical Coherence Tomography

We found a significant effect of group on peripapillary RNFL thickness for superior [$F_{(3,75)}$ = 23.73, p<0.0001], inferior [$F_{(3,75)}$ = 23.25, p<0.0001], nasal [$F_{(3,75)}$ = 12.59, p<0.0001] and temporal [$F_{(3,75)}$ = 19.97, p<0.0001] quadrants. Post-hoc tests showed significant differences between all clinical stages (p<0.04), except for C vs HT (p>0.05), for all tested RNFL quadrants (Figure 6.4; see also a representative example in Figure 6.2B).

We also found a significant correlation between RNFL thickness and ordered subject grouping categories (superior: Rho = -0.706; inferior: Rho = -0.649; nasal: Rho = -0.515; temporal: Rho = -0.655; p<0.0001), which means that peripapillary RNFL thickness decreases with the glaucoma progression. Thus, RNFL thickness decreases linearly with disease progression around 13.14 µm per clinical stage for superior quadrant [*y=137.29-13.14*clinical stage*, F(1,77) = 69.69, $\mathbf{R_a^2}$ = 0.47, p<0.0001], 15.06 µm for inferior [*y=152.09-15.06*clinical stage*, F(1,77) = 64.48, $\mathbf{R_a^2}$ = 0.45, p<0.0001], 7.11 µm for nasal [*y=85.83-7.11*clinical stage*, F(1,77) = 29.61, $\mathbf{R_a^2}$ = 0.27, p<0.0001] and 6.92 µm for temporal quadrants [*y=78.70-6.92*clinical stage*, F(1,77) = 54.59, $\mathbf{R_a^2}$ = 0.41, p<0.0001].

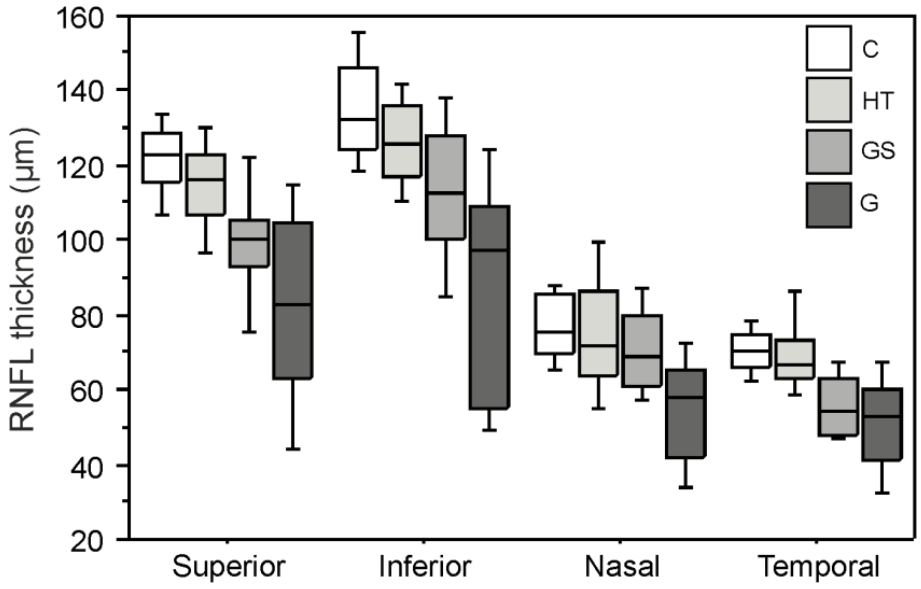

Figure 6.4. Peripapillary RNFL thickness assessed by SD-OCT across disease progression stages (control, C; ocular hypertensive, HT; glaucoma suspect, GS; and glaucoma, G).

Macular ganglion cell function assessed by Pattern Electroretinogram

We found a significant group effect on amplitudes of P-50 [$F_{(3,67)}$ = 7.67, p=0.0002] and N-95 [$F_{(3,67)}$ = 10.57, p<0.0001] waves. This effect was not verified for the implicit time of both waves, as well as N-95/P-50 ratio. Post-hoc tests for multiple comparisons revealed the following significant differences: $P\text{-}50_{amplitude}$ – C vs GS (p=0.0233), C vs G (p<0.0001), HT vs G (p=0.0025), GS vs G (p=0.0541); and for $N\text{-}95_{amplitude}$ – C vs HT (p=0.0499), C vs GS (p=0.0005), C vs G (p<0.0001), HT vs G (p=0.0019) (see Figure 6.5 and a representative example in Figure 6.2C).

Spearman correlation analysis showed that P-50 and N-95 waves amplitudes decrease moderately with the disease progression (P-50 wave: Rho = -0.487; N-95 wave: Rho = -0.524; p<0.0001). This amplitude decrease occurs in a linear fashion around 0.29 µV per clinical stage for the P-50 wave and 0.487 µV for the N-95 wave [P-50: *y=2.71-0.29*clinical stage*, F(1,69) = 23.20, R^2_a = 0.24, p<0.0001; N-95: *y=3.75-0.49*clinical stage*, F(1,69) = 32.35, R^2_a = 0.31, p<0.0001].

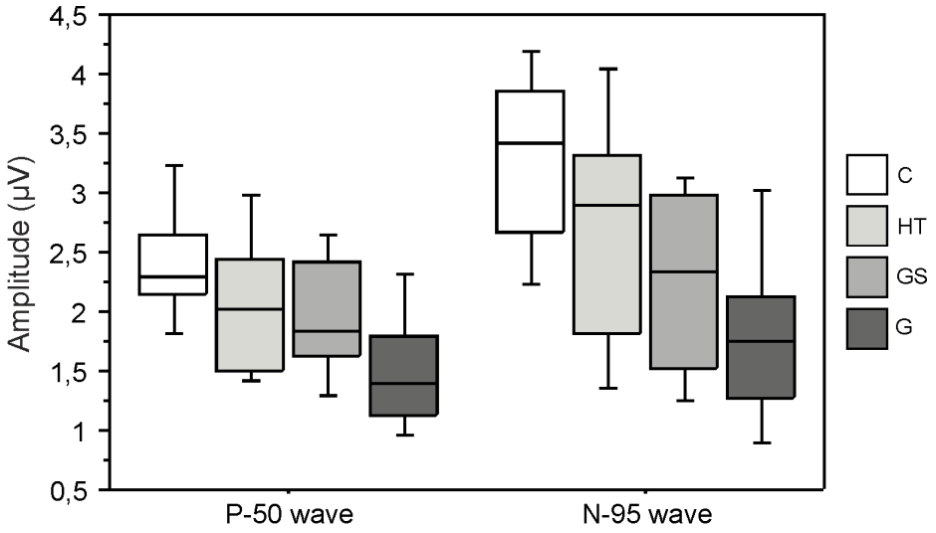

Figure 6.5. Amplitude of P-50 and N-95 waves of pattern ERG over clinical stages (control, C; ocular hypertensive, HT; glaucoma suspect, GS; and glaucoma, G).

Correlation analysis

We found significant correlations between structural and functional measures specifically for the *glaucoma group*: 1) Peripapillary RNFL thickness (superior

quadrant) correlated positively with PERG N-95 wave amplitude (r=0.560, p=0.0115), FDT MD (r=0.640, p=0.0086), FDT Ring 1 (r=0.588, p=0.0195) and FDT Ring 2 (r=0.547, p=0.0333); 2) Peripapillary RNFL thickness (inferior quadrant) correlated positively with FDT MD (r=0.514, p=0.0492) and FDT Ring 1 (r=0.537, p=0.0376). We also found a positive correlation between PERG N-95 wave amplitude and FDT in the inferior temporal quadrant (r=0.528, p=0.0419). These correlation patterns were not found in HT, GS and control groups.

ROC Curve – Sensitivity/Specificity analysis

ROC curves were generated for all tests in order to compare sensitivities at approximately 80% specificity. For *control vs ocular hypertensive* analysis, the highest sensitivity value was found for FDT SN quadrant (66%; cut-off: 26.6 dB), followed by CCT Protan (56%; cut-off: 59 u'v' units) (for more details see Table 6.1A).

Concerning *ocular hypertensive vs glaucoma* analysis, the highest sensitivity values were found for FDT ST quadrant (93%; cut-off: 22.75 dB), FDT Zone 2 (87%; cut-off: 23 dB) and CCT Tritan (84%; cut-off: 115 u'v' units) (see Table 6.1B). On the other hand, for *control vs glaucoma* analysis, we found sensitivities higher than 80% (at approximately 80% specificity) for all parameters, except for PERG waves implicit time and ratio (around 20-30%).

Diagnostic accuracy by Areas Under the ROC Curve

In *control vs ocular hypertensive* analysis, we found AUC values between 0.777 and 0.519. The higher AUC values correspond to CCT Protan (AUC = 0.777, p=0.0002), CCT Tritan (AUC = 0.729, p=0.0054) and also FDT IN quadrant (AUC = 0.700, p=0.0190) (Table 6.1A).

On the other hand, in *ocular hypertensive vs glaucoma* analysis we found AUC values between 0.924 and 0.506. In this sense, FDT ST quadrant (AUC = 0.924), OCT RNFL inferior (AUC = 0.901) and OCT RNFL superior (AUC = 0.883) showed the higher AUC values (p<0.0001) (see Table 6.1B). Concerning *control vs glaucoma* analysis, the parameter that showed the higher AUC was FDT MD (AUC = 0.971, p<0.0001). The AUC values were higher than 0.892 for all parameters (p<0.0001), except for PERG waves implicit time and ratio that represent only a change discrimination between groups (AUC values between 0.514 and 0.504).

Table 6.1. Areas under the receiver operating characteristic (ROC) curve (AUC) and associated 95% confidence interval (CI) are presented for psychophysical, electrophysiological and structural tests. Sensitivities obtained for each parameter at ~80% specificity, and criterion values used for that specificity are also presented [(A) Control vs Ocular hypertensive analysis; (B) Ocular hypertensive vs Glaucoma analysis].

(A)

Parameters	AUC	95% CI	p_value	Sensitivity/ Specificity (%)	Criteria for 80% Specificity
FDT perimetry					
MS	0.684	0.537, 0.808	0.0307	44/81	26.63
MD	0.694	0.547, 0.816	0.0253	50/81	-1.08
PSD	0.597	0.449, 0.733	n.s.	28/81	4.34
Zone 1	0.635	0.486, 0.766	n.s.	39/81	29
Zone 2	0.629	0.481, 0.762	n.s.	39/81	27.25
Zone 3	0.693	0.546, 0.815	0.0231	44/81	26.21
ST quadrant	0.615	0.467, 0.750	n.s.	50/81	26.75
SN quadrant	0.677	0.530, 0.802	0.0416	66/81	26.6
IN quadrant	0.700	0.554, 0.821	0.0190	44/81	27
IT quadrant	0.633	0.485, 0.765	n.s.	33/81	26.5
Cambridge color test					
Protan	0.777	0.624, 0.889	0.0002	56/80	59
Deutan	0.676	0.516, 0.810	0.0355	44/80	55.1
Tritan	0.729	0.572, 0.853	0.0054	50/80	91.9
OCT – RNFL thickness					
Superior	0.642	0.489, 0.770	n.s.	34/82	114
Inferior	0.653	0.498, 0.787	n.s.	28/82	121
Nasal	0.569	0.415, 0.714	n.s.	33/79	66
Temporal	0.620	0.465, 0.759	n.s.	33/82	63
PERG					
P-50 amplitude	0.663	0.491, 0.807	n.s	39/80	2.05
N-95 amplitude	0.671	0.500, 0.814	0.0509	45/80	2.39
P-50 implicit time	0.547	0.378, 0.709	n.s.	28/80	53
N-95 implicit time	0.607	0.436, 0.761	n.s.	39/80	93
N-95/P-50 ratio	0.519	0.352, 0.684	n.s.	22/80	1.06

(B)

Parameters	AUC	95% CI	p_value	Sensitivity/ Specificity (%)	Criteria for 80% Specificity
FDT perimetry					
MS	0.841	0.672, 0.944	<0.0001	73/83	21.16
MD	0.807	0.633, 0.923	0.0001	60/83	-5.09
PSD	0.837	0.667, 0.942	<0.0001	67/83	4.85
Zone 1	0.844	0.676, 0.947	<0.0001	80/83	26
Zone 2	0.870	0.708, 0.961	<0.0001	87/83	23
Zone 3	0.824	0.652, 0.934	<0.0001	67/83	20.29
ST quadrante	0.924	0.777, 0.987	<0.0001	93/83	22.75
SN quadrante	0.783	0.606, 0.907	0.0005	60/83	21.2
IN quadrante	0.785	0.608, 0.908	0.0004	53/83	20
IT quadrante	0.833	0.663, 0.940	<0.0001	73/83	23
Cambridge color test					
Protan	0.814	0.652, 0.923	<0.0001	74/83	77
Deutan	0.835	0.676, 0.936	<0.0001	68/83	79
Tritan	0.857	0.702, 0.950	<0.0001	84/83	115
OCT – RNFL thickness					
Superior	0.883	0.735, 0.965	<0.0001	74/83	102
Inferior	0.901	0.757, 0.974	<0.0001	79/83	114
Nasal	0.832	0.673, 0.934	<0.0001	68/83	61
Temporal	0.851	0.695, 0.946	<0.0001	79/83	60
PERG					
P-50 amplitude	0.754	0.585, 0.881	0.0017	53/83	1.14
N-95 amplitude	0.754	0.585, 0.881	0.0018	53/83	1.74
P-50 implicit time	0.506	0.337, 0.674	n.s.	37/83	56
N-95 implicit time	0.601	0.427, 0.758	n.s.	26/83	96
N-95/P-50 ratio	0.596	0.423, 0.754	n.s.	32/83	0.934

Note: FDT = frequency doubling technology; MS = mean sensitivity; MD = mean deviation; PSD = pattern standard deviation; ST = superior temporal; SN = superior nasal; IN = inferior nasal; IT = inferior temporal; OCT = optical coherence tomography; RNFL = retinal nerve fiber layer; PERG = pattern electroretinogram; n.s. = not significant.

6.5 DISCUSSION

In this study we have characterized the early visual impairment of patients with ocular hypertension, using psychophysical, electrophysiological and structural methods. We found changes in achromatic and chromatic contrast sensitivities and also in RGC function in the early stage of glaucomatous disease, corroborating the notion that functional damage may precede structural damage (Ventura et al., 2006). According, a significant correlation between structural and functional damage was found, but only in the later stages of the disease. Thus, a correspondence between structural and functional assessment may allow to establish with relative certainty the glaucomatous status.

In this sense, visual performance seems to be impaired even before the appearance of visual field defects in standard automated perimetry (SAP) and also structural changes in optic nerve head and RNFL. This evidence is consistent with some previous studies in ocular hypertension, which use functional methods to indirectly assess specific RGC populations (Casson et al., 1993; Johnson et al., 1993; Brusini and Brusatto, 1998; Landers et al., 2000; Castelo-Branco et al., 2004; Bach et al., 2006; Cellini et al., 2012).

We also found that functional and structural measures correlated significantly and moderately with the stage of the ordered clinical categories corresponding to the natural history of the disease, making these tests potential markers of disease progression. In general, the pattern of decline is approximately linear and is more pronounced for structural tests, namely RNFL thickness. About 47% of variability in RNFL thickness is explained by disease progression (R_a^2 = 0.47), showing the role of this test in monitoring the progression of glaucoma.

Visual performance within multiple visual channels was tested using a computerized chromatic contrast sensitivity test to probe parvo and koniocellular pathways and a FDT perimetry to probe magnocellular pathway (Silva et al., 2005; Ribeiro et al., 2012; Mateus et al., 2013). We found a relative damage of all retinocortical pathways since the initial hypertensive stage of the disease, proving that glaucoma is not restricted to impairment of M-cells (Kalloniatis et al., 1993; Felius et al., 1995; Greenstein et al., 1996; Alvarez et al., 1997; Castelo-Branco et al., 2004).

Concerning ROC curve analyses, we found that FDT (superior nasal quadrant) showed the highest sensitivity value (66%) for 80% specificity. This perimetry uses

high temporal/ low spatial frequency stimuli, which functionally isolated a specific subgroup of magnocellular ganglion cells (My cells) (Quigley, 1998), increasing its sensitivity to detect glaucomatous defects before SAP. On the other hand, PERG waves amplitude showed a low sensitivity to detect early functional damage, which do not exceed 45% for 80% specificity, possibly due to this test study macular function, whereas the initial glaucomatous impairment appears in the peripheral visual field (Quigley, 2011).

Interestingly, most of our novel psychophysical discrimination tests (*see Chapter 3 – 3.1.1.4 Novel psychophysical motion, achromatic contrast and chromatic contrast discrimination tests*), which were applied to a subgroup of glaucoma patients, showed a larger sensitivity to detect functional damage at the ocular hypertensive stage (above 90% for 80% specificity, reaching 100% in some cases). These novel tests exhibit a higher sensitivity when compared with the FDT, PERG and CCT, suggesting that a test with a smaller degree of redundancy across pathways enable for a greater diagnostic accuracy.

In summary, the development of methodological approaches that can be used to detect glaucoma at an early stage of the disease is critical to prevent permanent structural damage and irreversible vision loss, not forgetting the fact that RGC dysfunction may precede their death. FDT and CCT Protan performed well in detecting early glaucomatous damage in a cohort of patients with ocular hypertension, whereas longitudinal analysis of the ganglion cells axonal layer appears to be a good method to monitor the progression of the glaucomatous disease.

PART IV

FINAL REMARKS

CHAPTER 7

DISCUSSION AND CONCLUSIONS

7.1 NOVEL BIOMARKERS OF PATHOPHYSIOLOGICAL IMPAIRMENT IN ACQUIRED AND GENETIC DISEASES OF RETINAL GANGLION CELL DYSFUNCTION: ANALYSIS BETWEEN AND WITHIN CONDITIONS

In this study, we attempted to identify novel biomarkers of pathophysiological impairment in two distinct disease models of RGC dysfunction. For this purpose, we addressed an acquired and an inherited disease, namely glaucomatous optic neuropathy and LHON, respectively. While in glaucomatous optic neuropathy functional tests seem to have a higher sensitivity (and larger area under the ROC curve) in detecting changes the initial stage of the pathology (ocular hypertension stage), in Leber optic neuropathy we found that structural tests were more sensitive in determining the presence of LHON carriers status.

For both optic neuropathies, the CCT protan seems to be the chromatic axis that best discriminate between normal and pathological status, as demonstrated by the higher AUC and higher sensitivity for 80% specificity when compared with deutan and tritan axes.

On the other hand, PERG showed a higher diagnostic accuracy in LHON carriers as compared with patients with ocular hypertension, albeit still showing in general lower performance than the other low-level tests. This evidence is consistent with the fact that electrophysiological test allow to assess the macular function, whereas the initial glaucomatous damage appears in the peripheral visual field and our LHON carriers showed a constant pattern of a paracentral defect in visual field with a preserved sensitivity of the central locations.

Concerning acquired optic neuropathy model, ROC curve analysis showed that FDT perimetry, which uses sinusoidal grating stimulus with high temporal and low

spatial frequencies optimized to activate the magnocellular pathway, exhibited the highest sensitivity value for a 80% specificity level. Indeed, we found that FDT perimetry can detect functional deficits even before visual field defects arise in standard white/white perimetry and optic nerve changes become evident, showing the important role of this psychophysical test in the early stage of glaucomatous disease.

Comparing currently available psychophysical and electrophysiological tests with the three novel psychophysical tools developed by our group, we found that the novel tests showed a larger sensitivity to detect functional damage at the ocular hypertensive stage, proving that a smaller degree of functional test redundancy across pathways might allow for a greater diagnostic accuracy. The novel 2AFC psychophysical tests required the comparison and discrimination of a visual feature (motion, achromatic contrast and chromatic contrast) between two separated moving single dots, which were presented in opposite hemifields. We found that these novel discrimination tests reach near 100% sensitivity for 80% specificity in some cases, namely motion (meridian 135º), L-cone (meridian 90º), M-cone (oblique meridians) and S-cones (meridian 90º) tests. The parameter that showed lower sensitivity values was the achromatic contrast test, however still within the same performance level as the currently available tests.

Further, we found that functional and structural measures correlated significantly and strongly with the ordered stages of the natural history of the disease, which suggest that each test could be a potential marker of disease progression.

The fact that we have applied a significant range of psychophysical chromatic, achromatic and motion tests allowed us to study independent visual information processing across magno, parvo and koniocellular pathways. We found a relative damage of all retinocortical channels since the early stages of glaucomatous disease.

Regarding the ROC curve analysis for the genetic optic neuropathy model, we found that the most peripheral ring of macular RNFL thickness showed the larger AUC value and was the most sensitive classifier of the mutation status, suggesting an important role in pre-clinical phases. This is consistent with the known vulnerability of small axons of papillomacular bundle in the asymptomatic stage of this disease. The preferential involvement of the papillomacular bundle is probably due to the particularly disadvantageous energetic conditions intrinsic to the small and less myelinated axons that constitute the macular RGC.

We also found that cortical measures (especially extrastriate) discriminate well between healthy and mutation carriers, at the performance level of some of the retinal outcomes, suggesting that cortical and retinal markers are highly coupled in the determination of LHON carrier status.

Interestingly we found a link between the most discriminative feature of RGC impairment (macular RNFL) and cortical reorganization in LHON carriers, as assessed by cortical thickness measures in retinotopically mapped visual cortical areas. This is consistent with the idea that structural plasticity can occur even during clinically silent degeneration of RGC, and importantly, in the presence of relative peripheral visual loss, although retinotopic maps are still intact.

7.2 FUTURE WORK

Since only a small percentage of patients with ocular hypertension progress to a more advanced stage of the disease, future studies with larger samples are necessary to get insight on the role of these methods as potential predictors of conversion of ocular hypertensive to the glaucoma state. In this way, we might also avoid unnecessarily treatment of patients who would never convert to glaucoma stage. On the other hand, it would be possible focus our attention on patients who actually require treatment, allowing to treat future converters before a significant number of RGC being irreversibly damage.

Concerning LHON carriers, a follow-up of these patients should be done periodically to check how the structure and function of RGC behave along the preclinical phase until conversion to the symptomatic cell death stage. It would be also interesting to follow the changes in cortical thickness in these patients over preclinical period until conversion to clinical stage, since this approach has never been done before in LHON groups.

REFERENCES

Aaker GD, Myung JS, Ehrlich JR, Mohammed M, Henchcliffe C, Kiss S (2010) Detection of retinal changes in Parkinson's disease with spectral-domain optical coherence tomography. Clin Ophthalmol 4:1427-1432.

Ahnelt PK (1998) The photoreceptor mosaic. Eye; 12: 531-540.

Alvarez S, Pierce G, Vingrys A, Benes S, Weber P, King-Smith P (1997) Comparison of red-green, blue-yellow and achromatic losses in glaucoma. Vision Res; 37: 2295-2301.

Alward WL, Fingert JH, Coote MA, Johnson AT, Lerner SF, Junqua D, Durcan FJ, McCartney PJ, Mackey DA, Sheffield VC, Stone EM (1998) Clinical features associated with mutations in the chromosome 1 open-angle glaucoma gene (GLC1A). N Engl J Med; 338: 1022-1027.

Anderson RS (2006) The psychophysics of glaucoma: improving the structure/function relationship. Prog Retin Eye Res; 25: 79-97.

Archibald NK, Clarke MP, Mosimann UP, Burn DJ (2009) The retina in Parkinson's disease. Brain; 132; 1128-1145.

Artes PH, Chauhan BC (2005) Longitudinal changes in the visual field and optic disc in glaucoma. Prog Retin Eye Res; 24: 333-354.

Bach M, Unsoeld AS, Philippin H, Staubach F, Maier P, Walter HS, Bomer TG, Funk J (2006) Pattern ERG as an early glaucoma indicator in ocular hypertension: a long-term, prospective study. Invest Ophthalmol Vis Sci; 47: 4881-4887.

Bach M, Brigell MG, Hawlina M, Holder GE, Johnson MA, McCulloch DL, Meigen T, Viswanathan S (2013) ISCEV standard for clinical pattern electroretinography (PERG): 2012 update. Doc Ophthalmol 126:1-7.

Bagga H, Feuer WJ, Greenfield DS (2006) Detection of psychophysical and structural injury in eyes with glaucomatous optic neuropathy and normal standard automated perimetry. Arch Ophthalmol; 124: 169-176.

Bahrami H (2006) Causal inference in primary open angle glaucoma: specific discussion on intraocular pressure. Ophthalmic Epidemiol; 13: 283-289.

Barbiroli B, Montagna P, Cortelli P, Iotti S, Lodi R, Barboni P, Monari L, Lugaresi E, Frassineti C, Zaniol P (1995) Defective brain and muscle energy metabolismo shown by in vivo 31P magnetic resonance spectroscopy in nonaffected carriers of 11778 mtDNA mutation. Neurology; 45: 1364-1369.

Barboni P, Savini G, Valentino ML, Montagna P, Cortelli P, De Negri AM, Sadun F, Bianchi S, Longanesi L, Zanini M, De Vivo A, Carelli V (2005) Retinal nerve fiber layer evaluation by optical coherence tomography in Leber's hereditary optic neuropathy. Ophthalmology; 112: 120-126.

Barboni P, Carbonelli M, Savini G, Ramos CV, Carta A, Berezovsky A, Salomao SR, Carelli V, Sadun AA (2010) Natural history of Leber's hereditary optic neuropathy: longitudinal analysis of the retinal nerve fiber layer by optical coherence tomography. Ophthalmology; 117: 623-627.

Barbur JL, Harlow AJ, Plant GT (1994) Insights into the different exploits of colour in the visual cortex. Proc R Soc Lond B Biol Sci; 258: 327-334.

Barcella V, Rocca MA, Bianchi-Marzoli S, Milesi J, Melzi L, Falini A, Pierro L, Filippi M (2010) Evidence for retrochiasmatic tissue loss in Leber's hereditary optic neuropathy. Hum Brain Mapp; 31: 1900-1906.

Behbehani R (2007) Clinical approach to optic neuropathies. Clin Ophthalmol; 1: 233-246.

Brainard DH (1997) The psychophysics toolbox. Spat Vis; 10: 433-436.

Brainard DH, Pelli DG, Robson T. Display characterization. J Hornak. *Encyclopedia of imaging science and technology*: Wiley-Interscience; 2002: 172-188.

Brusini P, Busatto P (1998) Frequency doubling perimetry in glaucoma early diagnosis. Acta Ophthalmol Scand Suppl; 23-24.

Burr JM, Mowatt G, Hernández R, Siddiqui MA, Cook J, Lourenco T, Ramsay C, Vale L, Fraser C, Azuara-Blanco A, Deeks J, Cairns J, Wormald R, McPherson S, Rabindranath K, Grant A (2007) The clinical effectiveness and cost-effectiveness of screening for open angle glaucoma: a systematic review andeconomic evaluation. Health Technol Assess; 11: 1-190.

Callaway EM (2005) Structure and function of parallel pathways in the primate early visual system. J Physiol; 566: 13-19.

Caprioli J (1991) Automated perimetry in glaucoma. Am J Ophthalmol; 111: 235-239.

Carelli V, Ross-Cisneros FN, Sadun AA (2002) Optic nerve degeneration and mitochondrial dysfunction: genetic and acquired optic neuropathies. Neurochem Int; 40: 573-584.

Carelli V, Ross-Cisneros FN, Sadun AA (2004) Mitochondrial dysfunction as a cause of optic neuropathies. Prog Retin Eye Res; 23: 53-89.

Carelli V, La Morgia C, Iommarini L, Carroccia R, Mattiazzi M, Sangiorgi S, Farne' S, Maresca A, Foscarini B, Lanzi L, Amadori M, Bellan M, Valentino ML (2007) Mitochondrial optic neuropathies: how two genomes may kill the same cell type? Biosci Rep; 27: 173-184.

Carelli V, La Morgia C, Valentino ML, Barboni P, Ross-Cisneros FN, Sadun AA (2009) Retinal ganglion cell neurodegeneration in mitochondrial inherited disorders. Biochim Biophys Acta; 1787: 518-528.

Casson EJ, Johnson CA, Shapiro LR (1993) Longitudinal comparison of temporal-modulation perimetry with white-on-white and blue-on-yellow perimetry in ocular hypertension and early glaucoma. J Opt Soc Am A Opt Image Sci Vis; 10: 1792-1806.

Castelo-Branco M, Formisano E, Backes W, Zanella F, Neuenschwander S, Singer W, Goebel R (2002) Activity patterns in human motion-sensitive areas depend on the interpretation of global motion. Proc Natl Acad Sci USA; 99: 13914-13919.

Castelo-Branco M, Faria P, Forjaz V, Kozak LR, Azevedo H (2004) Simultaneous comparison of relative damage to chromatic pathways in ocular hypertension and glaucoma: correlation with clinical measures. Invest Ophthalmol Vis Sci; 45: 499-505.

Cellini M, Toschi PG, Strobbe E, Balducci N, Campos EC (2012) Frequency doubling technology, optical coherence technology and pattern electroretinogram in ocular hypertension. BMC Ophthalmol; 12: 33.

Cello KE, Nelson-Quigg JM, Johnson CA (2000) Frequency doubling technology perimetry for detection of glaucomatous visual field loss. Am J Ophthalmol; 129: 314-322.

Chauhan BC, Hutchison DM, LeBlanc RP, Artes PH, Nicolela MT (2005) Central corneal thickness and progression of the visual field and optic disc in glaucoma. Br J Ophthalmol; 89: 1008-1012.

Chinnery PF, Johnson MA, Wardell TM, Singh-Kler R, Hayes C, Brown DT, Taylor RW, Bindoff LA, Turnbull DM (2000) The epidemiology of pathogenic mitochondrial DNA mutations. Ann Neurol; 48: 188-193.

Chinnery PF, Andrews RM, Turnbull DM, Howell NN (2001) Leber hereditary optic neuropathy: does heteroplasmy influence the inheritance and expression of the G11778A mitochondrial DNA mutation? Am J Med Genet; 98: 235-243.

Clement CI, Goldberg I, Healey PR, Grahams (2009) Humphrey matrix frequency doubling perimetry for detection of visual-field defects in open-angle glaucoma. Br J Opthalmol; 93: 582-588.

Cohen J (1992) A power primer. Psychol Bull; 112: 155-159.

Coleman AL, Miglior S (2008) Risk factors for glaucoma onset and progression. Surv Ophthalmol; 53: S3-S10.

Cortelli P, Montagna P, Avoni P, Sangiorgi S, Bresolin N, Moggio M, Zaniol P, Mantovani V, Barboni P, Barbiroli B, et al (1991) Leber's hereditary optic neuropathy: genetic, biochemical, and phosphorus magnetic resonance spectroscopy study in an Italian family. Neurology; 41: 1211-1215.

Curcio CA, Sloan KR, Packer O, Hendrickson AE, Kalina R (1987) Distribution of cones in human and monkey retina: individual variability and radial asymmetry. Science; 236: 579-582.

Curcio CA, Sloan KR, Kalina RE, Hendrickson AE (1990) Human photoreceptor topography. J Comp Neurol; 292: 497-523.

Curcio CA, Millican CL, Allen KA, Kalina RE (1993) Aging of the human photoreceptor mosaic: Evidence for selective vulnerability of rods in central retina. Invest Ophthalmol Vis Sci; 34: 3278-3296.

Dacey DM (1994) Physiology, morphology and spatial densities of identified ganglion cell types in primate retina. Ciba Found Symp; 184: 12-28; discussion 28-34, 63-70.

Dacey DM, Lee BB (1994) The "blue-on" opponent pathway in primate retina originates from a distinct bistratified ganglion cell type. Nature; 367: 731-735.

Dacey DM (2000) Parallel pathways for spectral coding in primate retina. Annu Rev Neurosci; 23: 743-775.

Dai H, Morelli JN, Ai F, Yin D, Hu C, Xu D, Li Y (2013) Resting-state functional MRI: functional connectivity analysis of the visual cortex in primary open-angle glaucoma patients. Hum Brain Mapp; 34: 2455-2463.

d'Almeida OC, Mateus C, Reis A, Grazina MM, Castelo-Branco M (2013) Long term cortical plasticity in visual retinotopic areas in humans with silent retinal ganglion cell loss. Neuroimage 81:222-230.

DeLong ER, DeLong DM, Clarke-Pearson DL (1988) Comparing the areas under two or more correlated receiver operating characteristic curves: a nonparametric approach. Biometrics; 44: 837-845.

Derrington AM, Lennie P (1984) Spatial and temporal contrast sensitivities of neurones in lateral geniculate nucleus of macaque. J Physiol; 357: 219-240.

Duncan RO, Sample PA, Weinreb RN, Bowd C, Zangwill LM (2007a) Retinotopic organization of primary visual cortex in glaucoma: comparing fMRI measurements of cortical function with visual field loss. Prog Retin Eye Res; 26: 38-56.

Duncan RO, Sample PA, Weinreb RN, Bowd C, Zangwill LM (2007b) Retinotopic organization of primary visual cortex in glaucoma: a method for comparing cortical function with damage to the optic disk. Invest Ophthalmol Vis Sci; 48: 733-744.

Engvig A, Fjell AM, Westlye LT, Moberget T, Sundseth O, Larsen VA, Walhovd KB (2010) Effects of memory training on cortical thickness in the elderly. Neuroimage 52: 1667–1676.

Ernest JT (1975) Pathogenesis of glaucomatous optic nerve disease. Trans Am Ophthalmol Soc; 73: 366-388.

European Glaucoma Prevention Study Group (2007) Central corneal thickness in the European Glaucoma Prevention Study. Ophthalmology; 114: 454-459.

European Glaucoma Society. *Terminology and guidelines for glaucoma.* 3rd ed. Italy: Editrice Dogma; 2008.

Falkenberg HK, Bex PJ (2007) Sources of motion-sensitivity loss in glaucoma. Invest Ophthalmol Vis Sci; 48: 2913-2921.

Fechtner RD, Weinreb RN (1994) Mechanisms of optic nerve damage in primary open angle glaucoma. Surv Ophthalmol; 39: 23-42.

Felius J, deJong LAMS, van den Berg TJTP, Greve EL (1995) Functional characteristics of blue-on-yellow perimetric thresholds in glaucoma. Invest Ophthalmol Vis Sci; 36: 1665-1674.

Fingert JH, Héon E, Liebmann JM, Yamamoto T, Craig JE, Rait J, Kawase K, Hoh ST, Buys YM, Dickinson J, Hockey RR, Williams-Lyn D, Trope G, Kitazawa Y, Ritch R, Mackey DA, Alward WL, Sheffield VC, Stone EM (1999) Analysis of myocilin mutations in 1703 glaucoma patients from five different populations. Hum Mol Genet; 8: 899-905.

Fingert JH, Stone EM, Sheffield VC, Alward WL (2002) Myocilin Glaucoma. Surv Ophthalmol; 47: 547-561.

Fogagnolo P, Rossetti L, Ranno S, Ferreras A, Orzalesi N (2008) Short-wavelength automated perimetry and frequency-doubling technology perimetry in glaucoma. Prog Brain Res; 173: 101-124.

Gegenfurtner KR, Kiper DC (2003) Color vision. Annu Rev Neurosci; 26: 181-206.

Goodale MA, Milner AD (1992) Separate visual pathways for perception and action. Trends Neurosci; 15: 20-25.

Graewe B, Lemos R, Ferreira C, Santana I, Farivar R, De Weerd P, Castelo-Branco (2013) Impaired processing of 3D motion-defined faces in MCI and healthy ageing: an fMRI study. Cereb Cortex; 23: 2489-2499.

Gray LS, Heron G, Cassidy D, Clark GM, Cowley GR, Gourlay DM, Ross FM (1995) Comparison of age-related changes in short-wavelength-sensitive cone thresholds between normals and patients with primary open-angle glaucoma. Optom Vis Sci; 72: 205-209.

Greenstein VC, Halevy D, Zaidi Q, Koenig KL, Ritch RH (1996) Chromatic and luminance system deficits in glaucoma. Vision Res; 36: 621-629.

Guy J, Feuer WJ, Porciatti V, Schiffman J, Abukhalil F, Vandenbroucke R, Rosa PR, Lam BL (2014) Retinal ganglion cell dysfunction in asymptomatic G11778A: Leber hereditary optic neuropathy. Invest Ophthalmol Vis Sci 55:841-848.

Harding AE, Sweeney MG, Govan GG, Riordan-Eva P (1995) Pedigree analysis in Leber hereditary optic neuropathy families with a pathogenic mtDNA mutation. Am J Hum Genet; 57: 77-86.

Harwerth RS, Quigley HA (2006) Visual field defects and retinal ganglion cell losses in patients with glaucoma. Arch Ophthalmol; 124: 853-859.

Harwerth RS, Carter-Dawson L (1999) Ganglion cell losses underlying visual field defects from experimental glaucoma. Invest Ophthalmol Vis Sci; 40: 2242-2250.

Harwerth RS, Carter-Dawson L, Shen F, Smith EL 3rd, Crawford ML (1999) Ganglion cell losses underlying visual field defects from experimental glaucoma. Invest Ophthalmol Vis Sci; 40: 2242-2250.

Harwerth RS, Wheat JL, Fredette MJ, Anderson DR (2010) Linking structure and function in glaucoma. Prog Retin Eye Res; 29: 249-271.

Hernowo AT, Boucard CC, Jansonius NM, Hooymans JM, Cornelissen FW (2011) Automated morphometry of the visual pathway in primary open-angle glaucoma. Invest Ophthalmol Vis Sci; 52: 2758-2766.

Heron G, Erskine NA, Farquharson E, Moore AT, White H (1994) Colour vision screening in glaucoma: the Tritan Album and other simple tests. Ophthalmic Physiol Opt; 14: 233-238.

Hicks TP, Lee BB, Vidyasagar TR (1983) The responses of cells in macaque lateral geniculate nucleus to sinusoidal grating. J Physiol; 337: 183-200.

Jacobson N, Andrews M, Shepard AR, Nishimura D, Searby C, Fingert JH, Hageman G, Mullins R, Davidson BL, Kwon YH, Alward WL, Stone EM, Clark AF, Sheffield VC (2001) Non-secretion of mutant proteins of the glaucoma gene myocilin in cultured trabecular meshwork cells and in aqueous humor. Hum Mol Genet; 10: 117-125.

Jiang J, Zhu W, Shi F, Liu Y, Li J, Qin W, Li K, Yu C, Jiang T (2009) Thick visual cortex in the early blind. J Neurosci; 29: 2205-2211.

Johnson CA, Adams AJ, Casson EJ, Brandt JD (1993) Blue-on-yellow perimetry can predict the development of glaucomatous visual field loss. Arch Ophthalmol; 111: 645-650.

Johnson CA (1994) Selective versus nonselective losses in glaucoma. J Glaucoma; 3 Suppl 1: S32-44.

Johnson CA, Samuels SJ (1997) Screening for glaucoma visual field loss with frequency-doubling perimetry. Invest Ophthalmol Vis Sci; 38: 413-425.

Johnson CA, Sample PA, Cioffi GA, Liebmann JR, Weinreb RN (2003) Structure and function evaluation (SAFE): II. Comparison of optic disk and visual field characteristics. Am J Ophthalmol; 135: 148-154.

Jones SE, Buchbinder BR, Aharon I (2000) Three-dimensional mapping of cortical thickness using Laplace's equation. Hum Brain Mapp 11:12-32.

Kalloniatis M, Harwerth RS, Smith EL, De Santis L (1993) Colour vision anomalies following experimental glaucoma in monkeys. Ophthalmic Physiol Opt; 13: 56-67.

Kaplan E (2004) The M, P and K pathways of the primate visual system. In: L.M. Chalupa & J.S. Werner (Eds.), *The Visual Neurosciences*, Vol. 1 (pp. 481-493). Cambridge: MIT press.

Kermode AG, Moseley IF, Kendall BE, Miller DH, MacManus DG, McDonald WI (1989) Magnetic resonance imaging in Leber's optic neuropathy. J Neurol Neurosurg Psychiatry; 52: 671-674.

Kerrigan-Baumrind LA, Quigley HA, Pease ME, Kerrigan DF, Mitchell RS (2000) Number of ganglion cells in glaucoma eyes compared with threshold visual field tests in the same persons. Invest Ophthalmol Vis Sci; 41: 741-748.

Kingman S (2004) Glaucoma is second leading cause of blindness globally. Bull World Health Organ; 82: 887-888.

Kleiner M, Brainard DH, Pelli DG (2007) What's new in Psychtoolbox-3? Perception; 36: ECVP Abstr Suppl.

Ko ML, Peng PH, Ma MC, Ritch R, Chen CF (2005) Dynamic changes in reactive oxygen species and antioxidant levels in retinas in experimental glaucoma. Free Radic Biol Med; 39: 365-373.

Kolb B, Whishaw IQ (1998) Brain plasticity and behaviour. Annu Rev Psychol; 49: 43-64.

Kolb H, Linberg KA, Fisher SK (1992) Neurons of the human retina: a Golgi study. J Comp Neurol; 318: 147-187.

Kwon YH, Fingert JH, Kuehn MH, Alward WL (2009) Primary open-angle glaucoma. N Engl J Med; 360: 1113-1124.

Laguna A, Barallobre MJ, Marchena MA, Mateus C, Ramírez E, Martínez-Cue C, Delabar JM, Castelo-Branco M, de la Villa P, Arbonés ML (2013) Triplication of DYRK1A causes structural and functional retina alterations in Down syndrome. Hum Mol Genet 22:2775-2784.

Lam B (2005) Maturation, aging and testing in infants. In: Electrophysiology of vision: Clinical testing and applications. Boca Raton, FL: Taylor & Francis Group. pp. 151-173.

Landers J, Goldberg I, Graham S (2000) A comparison of short wavelength automated perimetry with frequency doubling perimetry for early detection of visual field loss in ocular hypertension. Clin Experiment Ophthalmol; 28: 248-252.

Lemos R, Figueiredo P, Santana I, Simões MR, Castelo-Branco M (2012) Temporal integration of 3D coherent motion cues defining visual objects of unknown orientation is impaired in amnestic Mild Cognitive Impairment and Alzheimer's Disease. J Alzheimers Dis; 28: 885-896.

Leske MC, Connell AM, Wu SY, Nemesure B, Li X, Schachat A, Hennis A (2001) Incident of open-angle glaucoma: the Barbados Eye Studies. The Barbados Eye Studies Group. Arch Ophthalmol; 119: 89-95.

Levy NS, Crapps EE, Bonney RC (1981) Displacement of the optic nerve head. Response to acute intraocular pressure in primate eyes. Arch Ophthalmol; 99: 2166-2174.

Liu Y, Vollrath D (2004) Reversal of mutant myocilin non-secretion and cell killing: implications for glaucoma. Hum Mol Genet; 13: 1193-1204.

Lodi R, Carelli V, Cortelli P, Iotti S, Valentino ML, Barboni P, Pallotti F, Montagna P, Barbiroli B (2002) Phosphorus MR spectroscopy shows a tissue specific in vivo distribution of biochemical expression of the G3460A mutation in Leber's hereditary optic neuropathy. J Neurol Neurosurg Psychiatry; 72: 805-807.

Lövdén M, Bäckman L, Lindenberger U, Schaefer S, Schmiedek F (2010) A theoretical framework for the study of adult cognitive plasticity. Psychol Bull 136:659-676.

Lövdén M, Wenger E, Mårtensson J, Lindenberger U, Bäckman L (2013) Structural brain plasticity in adult learning and development. Neurosci Biobehav Rev 37:2296-2310.

Lynch JJ, Silveira LC, Perry VH, Merigan WH (1992) Visual effects of damage to P ganglion cells in macaques. Vis Neurosci; 8:575-583.

Mackey DA, Oostra RJ, Rosenberg T, Nikoskelainen E, Bront-Stewart J, Poulton J, Harding AE, Govan G, Bolhuis PA, Norby S (1996) Primary pathogenic mtDNA mutations in multigeneration pedigrees with Leber hereditary optic neuropathy. Am J Hum Genet; 59: 481-485.

Maddess T, Henry GH (1992) Performance of nonlinear visual units in ocular hypertension and glaucoma. Clin Vis Sci; 7: 371-383.

Maddess T, Goldberg I, Dobinson J, Wine S, Welsh AH, James AC (1999) Testing for glaucoma with the spatial frequency doubling illusion. Vision Res; 39: 4258-4273.

Maia-Lopes S, Silva ED, Silva MF, Reis A, Faria P, Castelo-Branco M (2008) Evidence of widespread retinal dysfunction in patients with stargardt disease and morphologically unaffected carrier relatives. Invest Ophthalmol Vis Sci; 49: 1191-1199.

Man PY, Turnbull DM, Chinnery PF (2002) Leber hereditary optic neuropathy. J Med Genet; 39: 162-169.

Mateus C, Lemos R, Silva MF, Reis A, Fonseca P, Oliveiros B, Castelo-Branco M (2013) Aging of low and high level vision: from chromatic and achromatic contrast sensitivity to local and 3D object motion perception. PLoS One 8:e55348.

McKendrick AM, Sampson GP, Walland MJ, Badcock DR (2010) Impairments of contrast discrimination and contrast adaptation in glaucoma. Invest Ophthalmol Vis Sci; 51: 920-927.

Merigan WH, Maunsell JH (1993) How parallel are the primate visual pathways? Annu Rev Neurosci; 16: 369-402.

Monhart M (2007) What are the options of psychophysical approaches in glaucoma? Surv Ophthalmol; 52: S127-S133.

Morales J, Weitzman ML, Gonzáles de la Rosa M (2000) Comparison between Tendency-Oriented Perimetry (TOP) and octopus threshold perimetry. Opthalmology; 107: 134-142.

Morrissey SP, Borruat FX, Miller DH, Moseley IF, Sweeney MG, Govan GG, Kelly MA, Francis DA, Harding AE, McDonald WI (1995) Bilateral simultaneous optic neuropathy in adults: Clinical, imaging, serological, and genetic studies. J Neurol Neurosurg Psychiatry; 58: 70-74.

Mozaffarieh M, Grieshaber MC, Flammer J (2008) Oxygen and blood flow: players in the pathogenesis of glaucoma. Mol Vis; 14: 224-233.

Newman NJ, Lott MT, Wallace DC (1991) The clinical characteristics of pedigrees of Leber's hereditary optic neuropathy with the 11778 mutation. Am J Ophthalmol; 111: 750-762.

Newman NJ (1996) Optic neuropathy. Neurology; 46: 315-322.

Newman NJ, Biousse V (2004) Hereditary optic neuropathies. Eye; 18: 1144-1160.

Newman NJ (2005) Hereditary optic neuropathies: from the mitochondria to the optic nerve. Am J Ophthalmol; 140: 517-523.

Nikoskelainen EK, Huoponen K, Juvonen V, Lamminen T, Nummelin K, Savontaus ML (1996) Ophthalmologic findings in Leber hereditary optic neuropathy, with special reference to mtDNA mutations. Ophthalmology; 103: 504-514.

O'Neill EC, Danesh-Meyer HV, Kong GX, Hewitt AW, Coote MA, Mackey DA, Crowston JG; Optic Nerve Study Group (2011) Optic disc evaluation in optic neuropathies: the optic disc assessment project. Ophthalmology; 118: 964-970.

Oostra RJ, Bolhuis PA, Wijburg FA, Zorn-Ende G, Bleeker-Wagemakers EM (1994) Leber's hereditary optic neuropathy: correlations between mitochondrial genotype and visual outcome. J Med Genet; 31: 280-286.

Owsley C (2011) Aging and vision. Vision Res; 51: 1610-1622.

Pacheco-Cutillas M, Edgar DF, Sahraie A (1999) Acquired colour vision defects in glaucoma-their detection and clinical significance. Br J Ophthalmol; 83: 1396-1402.

Pearson P, Swanson WH, Fellman RL (2001) Chromatic and achromatic defects in patients with progressing glaucoma. Vision Res; 41: 1215-1227.

Pelli DG (1997) The videoToolbox software for visual psychophysics: transforming numbers into movies. Spat Vis; 10: 437-442.

Perry VH, Oehler R, Cowey A (1984) Retinal ganglion cells that project to the dorsal lateral geniculate nucleus in the macaque monkey. Neuroscience; 12: 1101-1123.

Pezzi PP, De Negri AM, Sadun F, Carelli V, Leuzzi V (1998) Childhood Leber's hereditary optic neuropathy (ND1/3460) with visual recovery. Pediatr Neurol; 19: 308-312.

Pokorny J, Smith VC, Lutze M (1987) Aging of the human lens. Appl Opt; 26: 1437-1440.

Qing G, Zhang S, Wang B, Wang N (2010) Functional MRI signal changes in primary visual cortex corresponding to the central normal visual field of patients with primary open-angle glaucoma. Invest Ophthalmol Vis Sci; 51: 4627-4634.

Quigley HA, Addicks EM (1981) Regional differences in the structure of the lamina cribrosa and their relation to glaucomatous optic nerve damage. Arch Ophthalmol; 99: 137-143.

Quigley HA, Sanchez RM, Dunkelberger GR, L'Hernault NL, Baginski TA (1987) Chronic glaucoma selectively damages large optic nerve fibers. Invest Ophthalmol Vis Sci; 28: 913-920.

Quigley HA, Dunkelberger GR, Green WR (1988) Chronic human glaucoma causing selectively greater loss of large optic nerve fibers. Ophthalmology; 95: 357-363.

Quigley HA, Dunkelberger GR, Green WR (1989) Retinal ganglion cell atrophy correlated with automated perimetry in human eyes with glaucoma. Am J Ophthalmol; 107: 453-464.

Quigley HA (1998) Identification of glaucoma-related visual field abnormality with screening protocol of frequency doubling technology. Am J Ophthalmol; 125: 819-829.

Quigley HA (1999) Neuronal death in glaucoma. Prog Retin Eye Res; 18: 39-57.

Quigley HA, McKinnon SJ, Zack DJ, Pease ME, Kerrigan-Baumrind LA, Kerrigan DF, Mitchell RS (2000) Retrograde axonal transport of BDNF in retinal ganglion cells is blocked by acute IOP elevation in rats. Invest Ophthalmol Vis Sci; 41: 3460-3466.

Quigley HA, Broman AT (2006) The number of people with glaucoma worldwide in 2010 and 2020. Br J Ophthalmol; 90: 262–267.

Quigley HA (2011) Glaucoma. Lancet; 377: 1367-1377.

Quiros PA, Torres RJ, Salomao S, Berezovsky A, Carelli V, Sherman J, Sadun F, De Negri A, Belfort R, Sadun AA (2006) Colour vision defects in asymptomatic carriers of the Leber's hereditary optic neuropathy (LHON) mtDNA 11778 mutation from a large Brazilian LHON pedigree: a case-control study. Br J Ophthalmol; 90: 150-153.

Ramon y Cajal S (1892) La rètine des vertèbrès. La Cellule; 9: 119-257.

Regan BC, Reffin JP, Mollon JD (1994) Luminance noise and the rapid determination of discrimination ellipses in colour deficiency. Vision Res; 34: 1279-1299.

Reis A, Mateus C, Macário MC, de Abreu JR, Castelo-Branco M (2011) Independent patterns of damage to retinocortical pathways in multiple sclerosis without a previous episode of optic neuritis. J Neurol; 258: 1695-1704.

Reis A, Mateus C, Viegas T, Florijn R, Bergen A, Silva E, Castelo-Branco M (2013) Physiological evidence for impairment in autosomal dominant optic atrophy at the pre-ganglion level. Graefes Arch Clin Exp Ophthalmol 251:221-234.

Resch ZT, Fautsch MP (2009) Glaucoma-associated myocilin: a better understanding but much more to learn. Exp Eye Res; 88: 704-712.

Resnikoff S, Pascolini D, Etya'ale D, Kocur I, Pararajasegaram R, Pokharel GP, Mariotti SP (2004) Global data on visual impairment in 2002. Bull World Health Organ; 82: 844-851.

Ribeiro MJ, Violante IR, Bernardino I, Ramos F, Saraiva J, Reviriego P, Upadhyaya M, Silva ED, Castelo-Branco M (2012) Abnormal achromatic and chromatic contrast sensitivity in neurofibromatosis type 1. Invest Ophthalmol Vis Sci; 53: 287-293.

Sadun AA (1998) Acquired mitochondrial impairment as a cause of optic nerve disease. Trans Am Ophthalmol Soc; 46: 881-923.

Sadun AA, Win PH, Ross-Cisneros FN, Walker SO, Carelli V (2000) Leber's hereditary optic neuropathy differentially affects smaller axons in the optic nerve. Trans Am Ophthalmol Soc; 98: 223-232.

Sadun AA, Salomao SR, Berezovsky A, Sadun F, DeNegri AM, Quiros PA, Chicani F, Ventura D, Barboni P, Sherman J, Sutter E, Belfort R Jr, Carelli V (2006) Subclinical carriers and conversions in Leber hereditary optic neuropathy: a prospective psychophysical study. Trans Am Ophthalmol Soc; 104: 51-61.

Sample PA, Weinreb RN (1990) Color perimetry for assessment of primary open-angle glaucoma. Invest Ophthalmol Vis Sci; 31: 1869-1875.

Sample P, Bosworth C, Weinreb R (1997) Short-wavelength automated perimetry and motion automated perimetry in patients with glaucoma. Arch Ophthalmol; 115: 1129-1133.

Sample PA, Bosworth CF, Blumenthal EZ, Girkin C, Weinreb RN (2000) Visual function-specific perimetry for indirect comparison of different ganglion cell populations in glaucoma. Invest Ophthalmol Vis Sci; 41: 1783-1790.

Savini G, Barboni P, Valentino ML, Montagna P, Cortelli P, De Negri AM, Sadun F, Bianchi S, Longanesi L, Zanini M, Carelli V (2005) Retinal nerve fiber layer evaluation by optical coherence tomography in unaffected carriers with Leber's hereditary optic neuropathy mutations. Ophthalmology; 112: 127–131.

Schiller PH, Logothetis NK, Charles ER (1990) Role of the color-opponent and broad-band channels in vision. Vis Neurosci; 5: 321-346.

Schiller PH, Logothetis NK, Charles ER (1991) Parallel pathways in the visual system: their role in perception at isoluminance. Neuropsychologia; 29:433-441.

Sekuler R, Blake R (1994) *Perception.* (3rd edition), New York: McGraw Hill.

Sereno MI, McDonald CT, Allman JM (1994) Analysis of retinotopic maps in extrastriate cortex. Cereb Cortex 4:601-620.

Shabana N, Pérès VC, Carkeet A, Chew PT (2003) Motion perception in glaucoma patients: a review. Surv Ophthalmol; 48:92-106.

Sharma P, Sample PA, Zangwill LM, Schuman JS (2008) Diagnostic tools for glaucoma detection and management. Surv Ophthalmol; 53: S17-S32.

Shepard AR, Jacobson N, Millar JC, Pang IH, Steely HT, Searby CC, Sheffield VC, Stone EM, Clark AF (2007) Glaucoma-causing myocilin mutants require the peroxisomal targeting signal-1 receptor (PTS1R) to elevate intraocular pressure. Hum Mol Genet; 16: 609-617.

Shimizu S, Lichter PR, Johnson AT, Zhou Z, Higashi M, Gottfredsdottir M, Othman M, Moroi SE, Rozsa FW, Schertzer RM, Clarke MS, Schwartz AL, Downs CA, Vollrath D, Richards JE (2000) Age-dependent prevalence of mutations at the GLC1A locus in primary open-angle glaucoma. Am J Ophthalmol; 130: 165-177.

Silva MF, Faria P, Regateiro FS, Forjaz V, Januário C, Freire A, Castelo-Branco M (2005) Independent patterns of damage within magno-, parvo- and koniocellular pathways in Parkinson's disease. Brain 128:2260-2271.

Silva MF, Maia-Lopes S, Mateus C, Guerreiro M, Sampaio J, Faria P, Castelo-Branco M (2008) Retinal and cortical patterns of spatial anisotropy in contrast sensitivity tasks. Vision Res; 48: 127-135.

Silva MF, Mateus C, Reis A, Nunes S, Fonseca P, Castelo-Branco M (2010) Asymmetry of visual sensory mechanisms: electrophysiological, structural, and psychophysical evidences. J Vis; 10: 26.

Silveira LC, Perry VH (1991) The topography of magnocellular projecting ganglion cells (M-ganglion cells) in the primate retina. Neuroscience; 40: 217-237.

Smith JL, Hoyt WF, Susac JO (1973) Ocular fundus in acute Leber optic neuropathy. Arch Ophthalmol; 90: 349-354.

Sommer A, Katz J, Quigley HA, Miller NR, Robin AL, Richter RC, Witt KA (1991) Clinically detectable nerve fiber atrophy precedes the onset of glaucomatous fiels loss. Arch Ophthalmol; 109: 77-83.

Spry PG, Johnson CA, Mansberger SL, Cioffi GA (2005) Psychophysical investigation of ganglion cell loss in early glaucoma. J Glaucoma; 14: 11-19.

Stockman A, Sharpe LT (2000) The spectral sensitivities of the middle- and long-wavelength-sensitive cones derived from measurements in observers of known genotype. Vision Res; 40: 1711-1737.

Stone EM, Newman NJ, Miller NR, Johns DR, Lott MT, Wallace DC (1992) Visual recovery in patients with Leber's hereditary optic neuropathy and the 11778 mutation. J Clin Neuroophthalmol; 12: 10-14.

Stone EM, Fingert JH, Alward WL, Nguyen TD, Polansky JR, Sunden SL, Nishimura D, Clark AF, Nystuen A, Nichols BE, Mackey DA, Ritch R, Kalenak JW, Craven ER, Sheffield VC (1997) Identification of a gene that causes primary open angle glaucoma. Science; 275: 668-670.

Tielsch JM, Sommer A, Katz J, Royall RM, Quigley HA, Javitt J (1991) Racial variations in the prevalence of primary open-angle glaucoma. The Baltimore Eye Survey. JAMA; 266: 369-374.

Turpin A, McKendrick A, Johnson C, Vingrys A (2002a) Performance of efficient test procedures for frequency-doubling technology perimetry in normal and glaucomatous eyes. Invest Ophthalmol Vis Sci; 43: 709-715.

Turpin A, McKendrick A, Johnson C, Vingrys A (2002b) Development of efficient threshold strategies for frequency doubling technology perimetry using computer simulation. Invest Ophthalmol Vis Sci; 43: 322-331.

Ungerleider LG, Haxby JV (1994) 'What' and 'where' in the human brain. Curr Opin Neurobiol; 4:157-165.

van der Boomen C, van der Smagt MJ, Kemner C (2012) Keep your eyes on development: the behavioral and neurophysiological development of visual mechanisms underlying form processing. Front Psychiatry; 3: 1-20.

Ventura LM, Sorokac N, De Los Santos R, Feuer WJ, Porciatti V (2006) The relationship between retinal ganglion cell function and retinal nerve fiber thickness in early glaucoma. Invest Ophthalmol Vis Sci; 47: 3904-3911.

Ventura DF, Gualtiere M, Oliveira AG, Costa MF, Quiros P, Sadun F, de Negri AM, Salomão SR, Berezovsky A, Sherman J, Sadun AA, Carelli V (2007) Male prevalence of acquired color vision defects in asymptomatic carriers of Leber's hereditary optic neuropathy. Invest Ophthalmol Vis Sci; 48: 2362-2370.

Votruba M, Aijaz S, Moore T (2003) A review of primary hereditary optic neuropathies. J Inherit Metab Dis; 26: 209-227.

Votruba M (2004) Molecular genetic basis of primary inherited optic neuropathies. Eye; 18: 1126-1132.

Watanabe M, Rodieck RM (1989) Parasol and midget ganglion cells of the primate retina. J Comp Neurol; 289: 434-454.

Weinreb RN, Khaw PT (2004) Primary open-angle glaucoma. Lancet; 363: 1711-1720.

Wentz-Hunter K, Kubota R, Shen X, Yue BY (2004) Extracellular myocilin affects activity of human trabecular meshwork cells. J Cell Physiol; 200: 45-52.

Werblin FS, Dowling JE (1969) Organization of the retina of the mudpuppy, *Necturus maculosus*. II. Intracellular recording. J Neurophysiol; 32: 339-355.

Wilson ME (1970) Invariant features of spatial summation with changing locus in the visual field. J Physiol; 207: 611-622.

Wolfs RC, Klaver CC, Ramrattan RS, van Duijn CM, Hofman A, de Jong PT (1998) Genetic risk of primary open-angle glaucoma. Population-based familial aggregation study. Arch Ophthalmol; 116: 1640-1645.

Yamada ES, Silveira LC, Perry VH (1996) Morphology, dendritic field size, somal size, density, and coverage of M and P retinal ganglion cells of dichromatic Cebus monkeys. Vis Neurosci; 13: 1011-1029.

Yoonessi A, Yoonessi A (2011) Functional assessment of magno, parvo and konio-cellular pathways; current state and future clinical applications. J Ophthalmic Vis Res; 6: 119-126.

Yücel YH, Zhang Q, Weinreb RN, Kaufman PL, Neeru G (2003) Effects of retinal ganglion cell loss on magno-, parvo-, koniocellular pathways in the lateral geniculate nucleus and visual cortex in glaucoma. Prog Retin Eye Res; 22: 465-481.

Yu Wai Man CY, Chinnery PF, Griffiths PG (2005) Optic neuropathies – importance of spatial distribution of mitochondria as well as function. Med Hypotheses; 65: 1038-1042.

Yu-Wai-Man P, Griffiths PG, Hudson G, Chinnery PF (2009) Inherited mitochondrial optic neuropathies. J Med Genet; 46: 145-158.

Zeimer RC, Ogura Y (1989) The relation between glaucomatous damage and optic nerve head mechanical compliance. Arch Ophthalmol; 107: 1232-1234.